ATMOSPHERIC-PRESSURE PLASMA-DROPLET TREATMENT SYSTEM: FOCUS ON AEROSOLISED BACTERIA AND REMOTE DELIVERY OF REACTIVE SPECIES

Thesis submitted to

the Faculty of Engineering

at Ulster University for the degree of

Doctor of Philosophy by

David Colin Ernest Rutherford BSc. (Hons)

Awarded: AUGUST 2017

In memory of Laurence Rutherford

"the molecular world must necessarily remain entirely beyond the powers of our imagination"

de Duve, C. (1984) A Guided Tour of the Living Cell, vol. 2, p. 293. New York: W. H. Freeman and Company. ISBN-10: 071675006

TABLE OF CONTENTS

List of Figures

Declaration

I confirm that the word count of this thesis is less than 100,000 excluding the title page, contents acknowledgements, summary or abstract, abbreviations, footnotes, diagrams, maps, illustrations, tables, appendices, and references or bibliography.

I hereby declare that with effect from the date on which the thesis is deposited in Research Student Administration of Ulster University, I permit:

1. the Librarian of the University to allow the thesis to be copied in whole or in part without reference to me on the understanding that such authority applies to the provision of single copies made for study purposes or for inclusion within the stock of another library.

2. the thesis to be made available through the Ulster Institutional Repository and/or EThOS under the terms of the Ulster eTheses Deposit Agreement which I have signed.*

IT IS A CONDITION OF USE OF THIS THESIS THAT ANYONE WHO CONSULTS IT MUST RECOGNISE THAT THE COPYRIGHT RESTS WITH THE AUTHOR AND THAT NO QUOTATION FROM THE THESIS AND NO INFORMATION DERIVED FROM IT MAY BE PUBLISHED UNLESS THE SOURCE IS PROPERLY ACKNOWLEDGED.

Acknowledgements

The aim of this section is to pay recognition to all the people that have helped and supported me throughout my thesis without sounding like an acceptance speech at an awards ceremony. Firstly, I would like to thank my supervisors, Professor Paul Maguire, Professor David McDowell and Professor Davide Mariotti, for the opportunity to be part of a research project. I have thoroughly enjoyed the experience and their valued guidance. Some in-depth discussions were at a level of detail I hadn't previously thought at, and it will undoubtedly have a lasting effect on my future career. Working alongside Dr. Charlie Mahony in the laboratory was the best training an early-stage researcher could hope for. He was an invaluable source of information during my thesis and his tutorship on plasma gave me understanding and confidence in an entirely new science that I was a complete novice in. I would also like to thank Dr. Sarah Spence for her valuable assistance in the use of the main analytical equipment used in this study and general bacteria discussions. Special thanks must also be reserved for Dr. Fatima Perez-Martin, Dr. Colin Kelsey, Dr. Mark Tweedie, Julie Dhiersat, and Bernard Blair. An experimental investigation requires adequate laboratory space and equipment, therefore I must thank Dr. Patrick Dunlop, Dr. Jeremy Hamilton and Dr. George Burke for their help in this regard. My PhD was made less daunting and arduous by being part of a supportive research group at NIBEC, namely Sadegh, Somak, Jenish, Dan, Manuel, Darragh, Dilli, Supriya, Neil, Conor, Calum, Ruairi, Bruno, Atta, and Gunisha. Special thanks must be given to NIBEC administration staff during my time at the institute, namely Ann Blair, Andrea Coard and Gillian Conlane. The vast majority of the materials used in this investigation were ordered by them and the results produced would not have been possible without their effort. The experimental studies were facilitated by the technical expertise of Brian McGrath and the maintenance of the computer systems by Damien McDonald enabled the efficient analysis of generated results.

My work colleagues in the molecular bacteriology department at the Agri-Food and Biosciences Institute (AFBI) were influential in my development as a scientific researcher before I started my thesis. It was here I was introduced to scientific research and was where I first truly thought about experiments and results. I cannot thank them enough for their patience and understanding upon my return and allowing me to use the Spoligotyping laboratory as an unofficial private study area during the final stages of my thesis write-up.

My family have been a constant source of support throughout my PhD. My mother ensured I had enough food in the fridge (and freezer and cupboards), and my sister, brother-in-law and nieces have been incredibly understanding and supportive during my studies. Although if it's any consolation, it has been beneficial to observe other people stressed outside of my own PhD bubble (or droplet). My mother-in-law and father-in-law have given advice, support and food as if I was their own kin and I hope to repay their kindness, culinary exploits and laundrette services ten-fold once I complete my thesis. I would not have attempted a doctorate if it wasn't for my wife, Catherine. You gave me the belief to pursue such a challenge and you have been a constant support throughout. Your mantra: "if anyone can do it, so can you" has served me well in some difficult times and I cannot thank you enough. And lastly, to my incredible friends who provided light-hearted relief, humour and horror in equal measure throughout my studies. I'm truly fortunate to have a group of friends like them.

I found some advice a colleague, Dr. Adrian Allen, gave me regarding his PhD most valuable during my thesis:

"it's fun, sometimes stressful and very frustrating…the key is to keep going!"

List of Abbreviations

$^1O_2$	singlet oxygen
A	adenine
Au	gold
AuNP	gold nanoparticle
AC	alternating current
APGD	atmospheric-pressure glow discharge
APPJ	atmospheric-pressure plasma jet
Ar	argon
C	cytosine
CPD	cyclobutane pyrimidine dimer
Cu	copper
dH_2O	deionised water
D_2O	deuterium oxide (‘heavy’ water)
DBD	dielectric-barrier discharge
DBGD	dielectric-barrier grating discharge
DC	direct current
DNA	deoxyribonucleic acid
DSB	double-strand (DNA) break
E. coli	*Escherichia coli*
EDTA	Ethylenediaminetetraacetic acid

EtBr	Ethidium bromide
Fe	iron
G	guanine
H	hydrogen
H^+	hydrogen cation (hydron)
H_2O	water
H_2O_2	hydrogen peroxide
He	helium
$^{\bullet}HO_2$	hydroperoxyl radical
I-V	current-voltage
I.D.	inner diameter
L-OO•	lipid hydroperoxide radical
LIF	laser-induced fluorescence
LP	lipid peroxidation
LPS	lipopolysaccharide
μ-APPJ	micro-scaled atmospheric-pressure plasma jet
MB	methylene blue
MD	molecular dynamics
MDA	malondialdehyde
MDR	multi-drug resistant
N	nitrogen

N_2	molecular nitrogen
NaCl	sodium chloride
Ne	neon
n_e	electron density
NIST	National Institute of Standards Technology
NTP	non-thermal plasma
O	oxygen atom
O_2	molecular oxygen
O_2^-	superoxide anion
$O_2^{\bullet -}$	superoxide radical
O_3	ozone
$^{\bullet}OH$	hydroxyl radical
OH^-	hydroxyl anion
OD	optical density
O.D.	outer diameter
OM	outer membrane
PAM	plasma-activated media
PBS	phosphate-buffered saline
PCR	polymerase chain reaction
PUFA	polyunsaturated fatty acid
Q	flow rate

qPCR	quantitative polymerase chain reaction
rf	radio-frequency
RCS	Ringer's solution with catalase
RNAse	Ribonuclease
RONS	reactive oxygen and nitrogen species
ROS	reactive oxygen species
RS	Ringer's solution
SOD	superoxide dismutase
SSB	single-strand (DNA) break
T	thymine
TA	terephlatic acid
TA-OH	2-hydroxyterephathalic acid
TBA	thiobarbituric acid
TBARS	thiobarbituric acid reactive substances
TE	Tris-EDTA buffer
T_e	electron temperature
T_{gas}	gas temperature
T_i	ion temperature
Ti-S	Titanium oxysulphate-Sulphuric acid
Tris	tris(hydroxymethyl)aminomethane
UHF	ultra-high (radio) frequency

U_m	transmembrane voltage
UFA	unsaturated fatty acid
UV	Ultra-violet
UV-vis	Ultra-violet-visible light spectroscopy
VNBC	viable but non-culturable

Units

Å	ångström
ºC	degrees celsius
cfu ml^{-1}	colony forming units per millilitre
cm	centimetre
cm^{-3}	cubic centimetre
eV	electron-volt
g	gram
g L^{-1}	grams per litre
g mol^{-1}	grams per mole
h	hour
K	kelvin
kHz	kilohertz
L	litre
M	Molar
m^{-3}	cubic metre

MHz	megahertz
µm	micrometer
µs	microsecond
µl	microliter
µg ml^{-1}	micrograms per millilitre
µmol L^{-1}	micromoles per litre
mg	milligram
ml	millilitre
mm	millimetre
mM	millimolar
mmol L^{-1}	millimoles per litre
min	minute
mol L^{-1}	moles per litre
ms	millisecond
nm	nanometre
nmol L^{-1}	nanomole per litre
ppm	parts per million
s	second
slm	standard litres per minute
V	volt
W	watt

Publications and Presentations

- **Controlled microdroplet transport in an atmospheric pressure microplasma**. P. D. Maguire, C. M. O. Mahony, C. P. Kelsey, A. J. Bingham, E. P. Montgomery, E. D. Bennet, H. E. Potts, **D. C. E. Rutherford**, D. A. McDowell, D. A. Diver and D. Mariotti. Appl. Phys. Lett. **106**, 224101 (2015); doi: http://dx.doi.org/10.1063/1.4922034
- **Continuous in-flight synthesis for on-demand delivery of ligand-free colloidal gold nanoparticles.** Paul Maguire, **David Rutherford**, Manuel Macias-Montero, Charles Mahony, Colin Kelsey, Mark Tweedie, Fátima Pérez-Martin, Harold McQuaid, Declan Diver, and Davide Mariotti. Nano Lett., 2017, 17 (3), pp 1336–1343; **DOI:** 10.1021/acs.nanolett.6b03440
- **Impact of plasma-induced liquid chemistry and charge on bacteria-loaded aerosol droplets.** '3rd Young Professionals Workshop on Plasma Medicine'. 18-20th September 2014. Zinnowitz, Germany. Oral Presentation: http://www.plasmatis.de/workshop_3young.html
- **Impact of plasma-induced liquid chemistry and charge on bacteria-loaded aerosol droplets.** 67th Gaseous Electronics Conference. 2nd – 7th November 2014. Raleigh, North Carolina, U.S.A. Oral Presentation: http://www.aps.org/meetings/meeting.cfm?name=GEC14
- **A new generation of atmospheric-pressure plasmas for instant detection of airborne bacteria.** Faculty of Computing and Engineering Research Awards Dinner 7th May 2015. Belfast, N. Ireland. Poster Presentation
- **A new generation of atmospheric-pressure plasmas for instant detection of airborne bacteria.*** Northern Ireland Biomedical Engineering Society Annual Symposium. Friday 5th June 2015. Oral Presentation; *awarded best presentation for 2nd-3rd year students
- **Uniform dose atmospheric pressure microplasma exposure of individual bacterial cells.** Bioplasmas and Plasma with Liquids Conference 13-16th September 2015, Bertinoro, Italy. Poster Presentation: http://www.cost-plasma-liquids.eu/Events/Joint-meeting-of-COST-Actions-CMST-TD1208-and-MPNS-MP1101_1
- **Uniform dose atmospheric pressure microplasma exposure of individual bacterial cells.** 68th Gaseous Electronics Conference. 12th – 16 th October, 2015. Honolulu, Hawaii, U.S.A. Oral Presentation: http://www.aps.org/meetings/meeting.cfm?name=GEC15

ABSTRACT

This thesis presents an experimental study of a novel non-thermal atmospheric-pressure gas plasma with controlled liquid droplet flow as an efficient source of reactive species that can influence fundamental chemistries in many applications. The electrical discharge is ignited within the confined geometry of a cylindrical quartz tube that allowed for small liquid droplets entrained in the gas flow to pass through the plasma region only once. Neon was used to generate the droplets from deionised water or a buffered solution and additional helium transported the droplets from the nebuliser through the plasma. A diffuse, glow-like discharge formed that remained ignited during droplet transport. Droplets that enter the plasma contribute to the formation of reactive species and survive the treatment without complete evaporation. This observation paved the way for attempts to expose bacteria-loaded droplets to the same treatment. When collected in the presence of a hydrogen peroxide scavenger, plasma treatment did not affect cell viability or growth kinetics. A biomarker of lipid peroxidation was detected, suggesting cell interaction with plasma-generated species delivered into the droplet over short timescales i.e. droplet transit time through the plasma region. Due to the omission of oxygen and nitrogen from the plasma, a vast proportion of RONS that are reported in the plasma-liquid literature cannot be generated, therefore simplifying the chemistry. Hydroxyl radical is thought to feature in the onset of cellular oxidative stress and the species is known to be generated from plasma-liquid interactions. The radical was detected in both the gas and liquid phases from the plasma treatment of droplets and remained chemically active far from the core plasma region. Hydrogen peroxide is a well-known biocide generated from plasma-liquid interactions and was detected in the plasma-treated droplet collection liquid. These results suggest the new technique can remotely apply reactive species contained in plasma-activated droplets or bulk liquid to a target that never comes in direct contact with the plasma itself. This has the potential to be able to influence biological systems in a controlled way by fine-tuning the chemistry generated from the interaction between non-equilibrium plasma and low volume liquid droplets.

Key words: atmospheric-pressure gas plasma, glow discharge, low-volume liquid droplets, hydroxyl radical, hydrogen peroxide, plasma medicine

1. PLASMA-DROPLET SYSTEM: RATIONALE & INVESTIGATION OUTLINE

1.1. Background

The application of gas plasma in the clinical environment has gained recent interest as a source of reactive species that can influence the chemistry of a number of important biochemical interactions. Wound-healing, blood coagulation, sterilisation of surfaces or medical equipment and cancer tumour treatment are examples where plasma treatment has shown potential [1, 2]. 'Plasma medicine' is the collective term used to describe this multi-disciplinary area of research that encompasses aspects of physics, engineering, biochemistry and life sciences. Since all cells are mostly composed of water and are generally surrounded by it, the plasma-liquid interface is an important focus of the research and the physical processes that govern biologically-relevant species generation. Plasma-induced liquid chemistry is known to inactivate bacteria cells, but due to the complexity of the reactive species generated the precise mechanism of inactivation, and which species are involved, are not clear.

Plasmas generated at atmospheric-pressure generally have a background gas temperature close to room temperature and, therefore, can be applied to a biological target without causing thermal ablation. These non-thermal plasmas (NTP) have electron energies many orders of magnitude greater than the background gas ion energies ($T_e >> T_{gas}$) and it is the energetic electrons that underpins NTP chemistry. Electron-induced generation of highly reactive chemical species, i.e. radicals, in the gas phase interact with surfaces, such as the top layer of bulk liquid. It is generally agreed that plasma-generated reactive species are the reason for the treatment's antibacterial effect, however the specific molecular pathways that induce a cell response are dependent on the experimental design of the plasma and target environment. The literature presents a wide range of electrical configurations which can ignite a gas plasma at atmospheric-pressure, each generating different mixtures of reactive species. Therefore, it is not uncommon to see conflicting reports in the literature that specify a particular species responsible for inactivation, even when the same cell model is used. For example, *E. coli* was inactivated using a single streamer Dielectric Barrier Discharge (DBD) operating in humid air and ozone was predominantly responsible [3]; yet inactivation of the same bacteria using a multi-gas atmospheric-pressure plasma jet (APPJ) array was mainly attributed to the hydroxyl radical ($^{\bullet}$OH) when nitrogen was used as the feed gas, and singlet oxygen when

carbon dioxide was used as the feed gas [4]. It is generally accepted that RONS, generated by plasma, are important effectors of the plasma-induced cell response thus one aspect of this thesis investigation is to limit RONS production by reducing O_2 and N_2 from the plasma feed gas and therefore hopefully simplify the plasma-generated chemistry and make the cell response to plasma treatment easier to elucidate.

The plasma-liquid interface is a highly reactive and turbulent region where mass and energy transfers between the gas and liquid phases. The interface between the gas-phase plasma and the liquid surface results in gas-phase species diffusion into the liquid, and vaporisation of the liquid into the gas-phase. The formation of a vapour layer above the bulk liquid surface during plasma exposure is essential in efficient reactive species generation (Figure 1.1). There is thought to be a rapid reduction in the concentration of highly-reactive species from the liquid surface to the liquid bulk [5], however experimental evidence to reinforce these simulations is lacking. Plasma-generated species in the liquid phase are the same chemical species that are involved in normal intracellular signalling pathways [6], [7]. Information on the lifetime and penetration of plasma-generated reactive species in liquid suggests that the short-lived radicals (e.g. $^{\bullet}OH$) are less likely to induce a direct cell response due to their limited penetration depth.

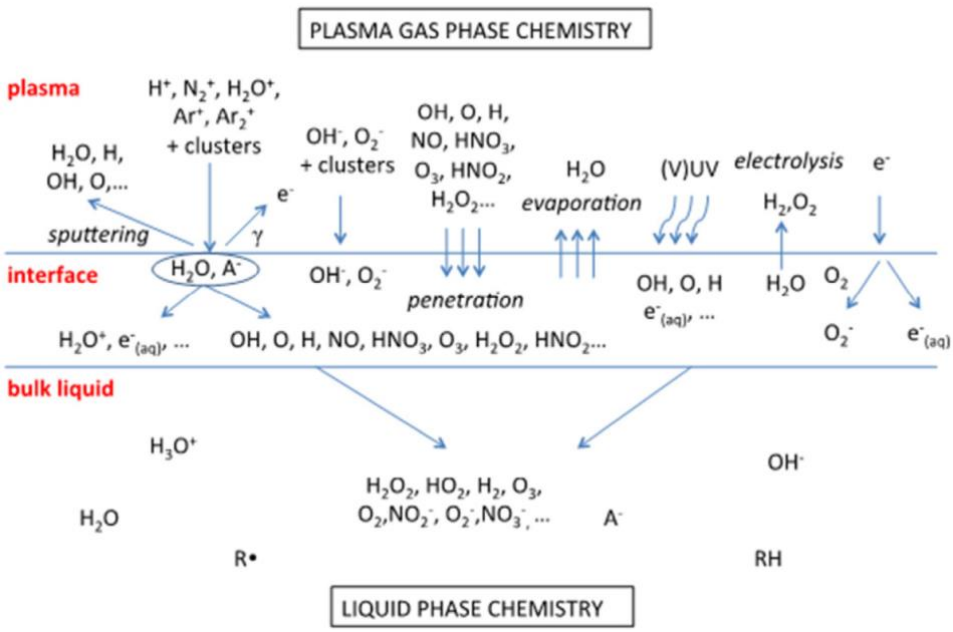

Figure 1.1 Schematic representation of reactive species that exist in a humid Ar plasma in contact with water [8]

The chemical pathways initiated by species generated at the plasma-liquid interface are complex; detection of plasma-generated species in the liquid phase and parallel measurement of the cell response are often used to attribute an observed cell effect to a particular reactive species. The schematic diagram above attempts to simplify the main reactive pathways produced from a humid Ar plasma interacting with static bulk liquid [8]. As mentioned previously, the species generated by plasma are also found in cell signalling pathways. Cells possess molecules that protect against elevated intracellular concentrations of reactive species i.e. anti-oxidants/scavengers. It is assumed that plasma-treatment of a cell suspension that contains a scavenger of a particular species negates that species from any observed cell effect. Recently, cells added to plasma-treated liquid exhibited similar losses in viability as cells subjected to plasma treatment. It is thought that the extended cytotoxicity and mutagenic effect was due to the generation of long-lived reactive species [9].

The interaction between NTP and cells is mediated through the liquid film which surrounds them; therefore plasma-liquid interfacial reactions are fundamental to the cell response. It is possible to standardise the liquid volume which surrounds a cell prior to plasma treatment by aerosolising the cell suspension. NTP treatment proved effective against aerosolised bacteria [10], [11], [12], [13], [14]. Each droplet becomes its own micro-producer of reactive species in close proximity to the encapsulated bacteria cell. This approach also presents individual cells, preventing protective shielding among cell clumps and ensures uniform exposure of each cell to the plasma-generated reactive species.

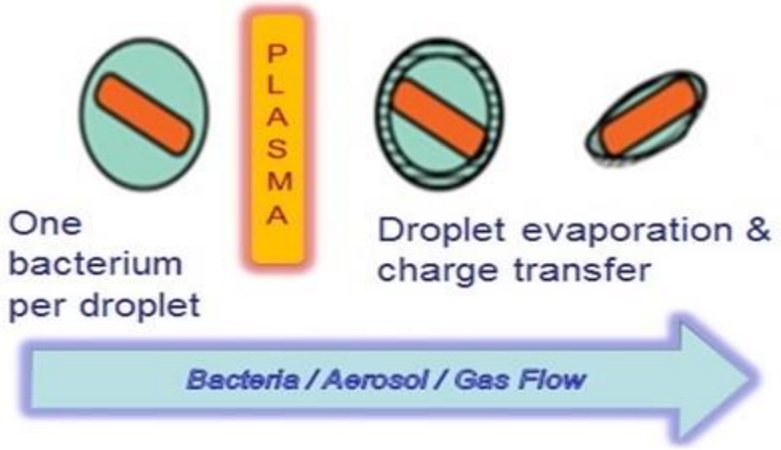

Figure 1.2 Schematic diagram of the non-thermal plasma exposure technique for isolated bacteria cells within a low volume liquid carrier droplet

The motivation for the research was to expose bacteria-loaded droplets to a single-pass NTP treatment, recover treated cells in a collection liquid, and to examine resultant cell viability and chemical reactivity. Encapsulation of the bacteria within droplets entrained in the feed gas flow ensured a relatively uniform exposure to the plasma i.e. droplet transit time through the plasma (Figure 1.2). This thesis attempted to improve the understanding of the plasma-liquid interface by delivering low volume liquid droplets through a low power rf discharge with noble feed gases. Optical emission spectroscopy (OES) of the plasma was used to detect reactive species in the gas phase and chemical indicators detected short and long-lived reactive species in the liquid phase. The discharge provides a source of reactive-species through which the droplet passes and remains intact after treatment. It is hoped that this technology might facilitate the development of tailored, controlled delivery of a defined concentration of reactive species to remotely induce a chemical response.

1.2. Thesis Structure

An experimental investigation into atmospheric-pressure non-thermal plasma interaction with low volume liquid droplets is presented. Following this introductory chapter, a brief overview of relevant literature is given (Chapter 2). Chapter 3 describes the materials and methods that were employed in the investigations. In Chapter 4, electrical and optical characteristics of the rf-driven glow discharge are reported, as well as the use of chemical indicators for short and long-lived reactive species detection. Chapter 5 details the anti-microbial effect of the plasma effluent on bacteria on agar and a coloured dye was used to visualise the droplet impaction zone on the surface. Analysis of bacteria-loaded droplet transport through the plasma is reported in Chapter 6 and the plasma treatment the gas flow-entrained droplet receives is uniform with respect to species concentration and exposure time. Finally, Chapter 7 will discuss the conclusions of the thesis and possible future work involving the plasma-droplet system and atmospheric-pressure plasma studies in general.

The custom-designed plasma-droplet system detailed in this study offers a unique insight into the interaction between a steady-state atmospheric-pressure plasma and low volume liquid droplets containing bacteria that survive exposure. Liquid carrier vessels could deliver biologically-active species remotely from the plasma source to a target. Bacteria-loaded droplets allow for uniform plasma exposure of isolated cells. The bulk liquid reservoir that contained the cells in conventional

plasma studies that treated a cell suspension was removed here, replaced with a micron-scale carrier droplet that standardised the liquid volume that encased the cell, plasma treatment time and exposure to the reactive species. Whilst this study predominantly focussed on exposing bacteria-loaded droplets to plasma, droplets without bacteria are no less interesting. Operation of the developed system allowed the investigation of droplet/plasma interactions, a less studied but interesting area of research.

2. LITERATURE REVIEW

This thesis is comprised of investigations into plasma-liquid-bacteria interactions, which result in cell damage and destruction. The interface between plasma and the cell is a complex matrix of bio-molecules in an aqueous phase i.e. the cell wall and cell membrane, and possible damage pathways initiated by plasma will be discussed. In this section, relevant cell structure and several known mechanisms of cell damage are outlined. Thereafter follows a brief introduction to plasma and its interaction with liquid. Concluding this section will be an overview of cell responses to plasma exposure, with particular focus given to bacteria.

2.1. Bacteria Cell Structure

Bacteria are a large domain of unicellular microorganisms with a prokaryotic cell configuration. Prokaryotes (etymology: 'pro' – before and 'karyote' – nut or kernel) lack any membrane-bound organelles or a nuclear membrane to house its genetic material. This is in part due to their small volume (*E. coli* ~ 1.5-2.5 μm^3) [15] and the intracellular space not being large enough to establish organelles for specific functions. Therefore, the surface layers of bacteria cells are critical for survival; permitting diffusion of nutrients into the cell and removal of waste products out, all the while maintaining cell shape and structure.

2.1.1. Cell Wall

Most bacteria can be classified into 2 general groups, depending on the Gram stain-retention properties of the cell surface, in particular the cell wall. An alcohol dehydration step in Gram Stain technique is crucial; it degrades the outer lipid membrane of 'Gram-negative' bacteria which facilitates primary stain loss through increased permeability whilst also constricting the peptidoglycan layer of 'Gram-positive' cells, ensuring primary stain retention. When viewed using a light microscope, fixed cells that retain the primary stain (usually crystal violet) are termed 'Gram-positive' and those that contain the secondary stain (usually safarin) are 'Gram-negative'. High resolution electron microscopy imaging of bacteria cell surface cross-sections has confirmed a difference in structure which can account for the variation observed in stain retention.

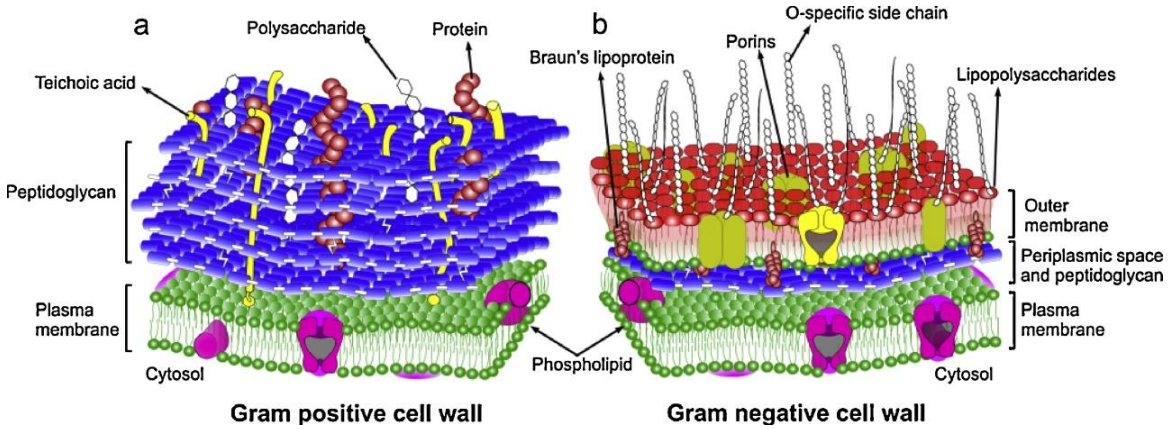

Figure 2.1 Schematic representation of the two general types of cell wall: (a) Gram-positive and (b) Gram-negative [16]

Figure 2.21 displays the complexity of the bacteria cell wall and highlights the differences between Gram-positive and Gram negative bacteria. The Gram-positive cell wall has a multi-layered peptidoglycan structure (thickness = 15-80 nm) [17] on top of the phospholipid-rich cytoplasmic membrane (i.e. cell membrane - discussed in more detail later). Teichoic acids are present throughout the peptidoglycan layers, adding to the structural integrity of the cell wall. Functional groups are present in peptidoglycan (carboxylic) and teichoic acid (phosphate) which contribute to the overall negative charge on the cell wall (excess anionic sites). The cell wall of a Gram-negative organism contains a much thinner layer of peptidoglycan (1-2 nm) [17] positioned in the periplasmic space, between two phospholipid bilayer membranes: the inner cytoplasmic membrane and an outer membrane (OM). In addition to a phospholipid bilayer, the OM consists of lipopolysaccharides (LPS), lipoproteins and aggregates of proteins (porins). The relative membrane permeability to small hydrophilic and hydrophobic molecules is attributed to the presence of Porins. The chemical structure of the OM contains LPS that are often unique to particular bacterial strains and which are responsible for many antigenic properties of Gram-negative strains. LPS is composed of three parts, namely the inner hydrophobic lipid A, the core oligosaccharide, and the outer O-antigen polysaccharide [18].

2.1.2. Cell Membrane

Lipids and proteins are essential components of membranes. The most abundant lipid in membranes is the phospholipid and its amphipathic nature causes structural alignment according to water interactions with the different charged regions of the molecule. Singer and Nicholson's Fluid

Mosaic Model [19] still best describes how lipids and proteins are arranged within the restrictions imposed by thermodynamics (Figure 2.2). The nonpolar ‘tails’ of the phospholipid are sequestered together away from the aqueous phase, maximising hydrophobic interactions. The hydrophobic hydrocarbon chain of the lipid is further characterised by the number of hydrogen molecules that are bound to each carbon i.e. a saturated fatty acid is one with the maximum possible amount of hydrogen bound; unsaturated chains contain at least one double bond between carbons and are ‘unsaturated’ with hydrogen. The polar ‘head’ of the molecules are in direct contact with the aqueous phase, maximising hydrophilic interactions [20]. The result is the formation of a ‘bilayer’; a mirror image of a monolayer of molecules arranged due to weak charge interactions and resultant hydrophilicity/hydrophobicity. Proteins are incorporated into the ‘fluid’ membrane structure in a ‘mosaic’ pattern. Chemical affinity of the polar (hydrophilic) end of the phospholipid and protein functional groups towards water creates a molecular arrangement that allows the formation of a ‘membrane’ to encapsulate important molecules.

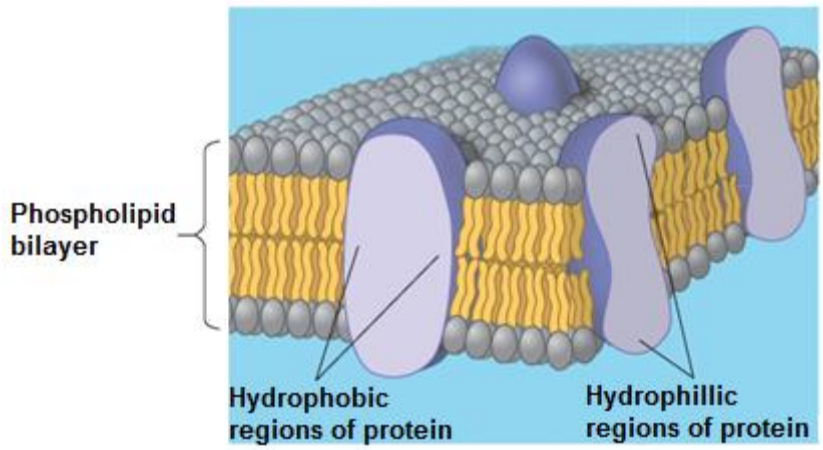

Figure 2.2 A schematic representation of Singer & Nicholson’s fluid model of cell surface structure [21]

2.1.3. Cell Damage and Response Mechanisms

2.1.3.1. Oxidative Stress

Oxidative stress is a physiological imbalance between the generation of highly reactive oxygen species (ROS) and the inherent anti-oxidant defence mechanisms e.g. enzymes capable of neutralising ROS [22]. *E. coli* possess superoxide dismutase (SOD) and catalase to remove ROS from within the cell, generating non-reactive/non-toxic products. In the presence of oxidising agents such as O_2 and ROS, *E. coli* produces, manganese-superoxide dismutase [23].

2.1.3.1.1. Lipid peroxidation

The first parts of bacterial cells subjected to external oxidative stress include the cell wall and cell membrane [24]. ROS can react with polyunsaturated fatty acids (PUFA) in the cell membrane that can initiate lipid peroxidation. This chemical cascade is often initiated by hydrogen (H) abstraction (Figure 2.3, reaction 1) from an unsaturated fatty acid to form a reactive lipid species, which further reacts with molecular oxygen to form fatty acid hydroperoxides (L-OO•) (Figure 2.3, reaction 2). L-OO• may react with PUFA, which feeds back into the reaction cascade, prolonging the effect (Figure 2.3, reaction 3) [25]. Lipid peroxidation products compromise membrane integrity as they are shorter than the membrane unsaturated fatty acid leading to loss of osmotic homeostasis that may cause the cell to rupture due to uncontrolled inward water diffusion [26].

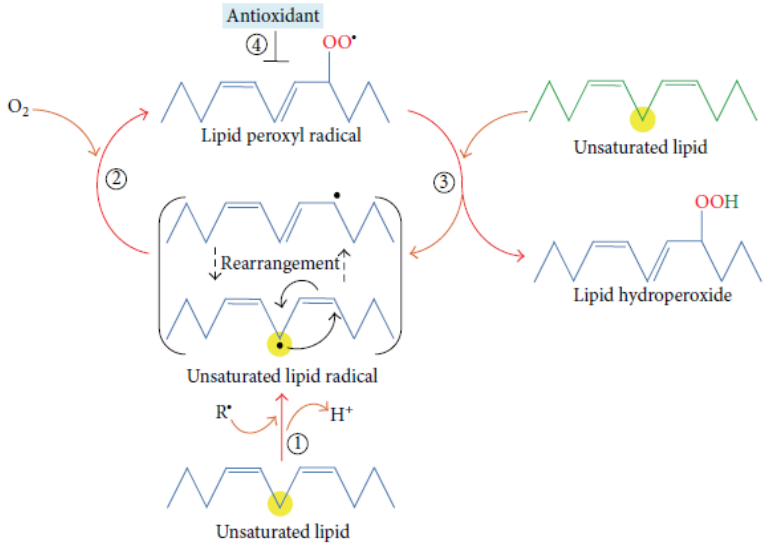

Figure 2.3 The lipid peroxidation cascade, from initiation (1), propagation (2), radical formation (3) and termination (4) [27]

2.1.3.1.2. Deoxyribonucleic acid (DNA) oxidation

DNA is composed of a double-stranded polymer of nucleotides with a deoxyribose-phosphate backbone and is an essential molecule governing inheritance [28]. It carries instructions contained within the specific sequence of nucleotides that encode for cell survival i.e. reproduction, growth, metabolism, and stress response mechanisms. There are four different nitrogen (N)-containing nucleotides that compose DNA: cytosine (C) thymine (T), adenine (A) and guanine (G). Under normal conditions, the molecular structure dictates that pyrimidine (C) can only forge a hydrogen bond with purine (G), and pyrimidine (T) with purine (A) i.e. complementary base pairing.

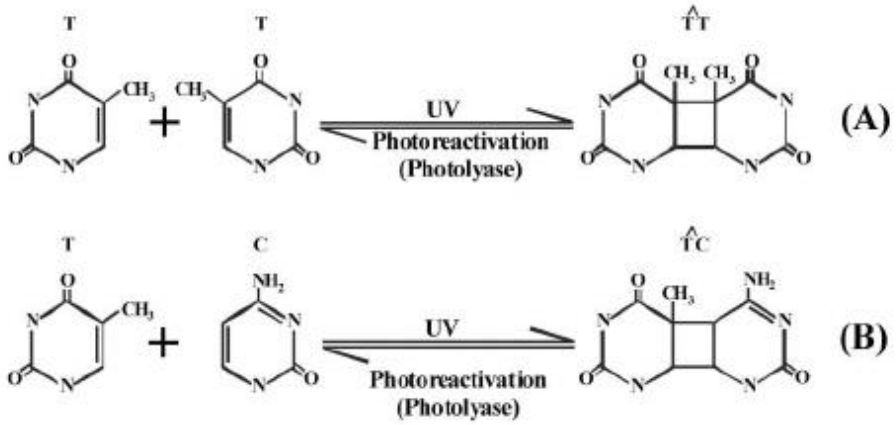

Figure 2.4 Molecular structural arrangements of cyclobutane-pyrimidine dimers as a result of UV exposure. Thymine-thymine cyclobutane dimer is shown in (A), and thymine-cytosine dimer is shown in (B) [29]

UV photon absorption by DNA causes the generation of photoproducts and the type produced is dependent on the wavelength i.e. energy [30]. The most prevalent are cyclobutane pyrimidine dimers (CBD) and these are formed by the cross-linkage of two adjacent pyrimidines (Figure 2.4 (a)). CBD formation results in a number of biological effects, such erythema (sunburn) and related inflammatory responses, immune function suppression and mutation induction which could eventually lead to the development of skin cancer [30]. DNA exposed to UV radiation can also result in mismatch base pairing during replication (Figure 2.4 (b)). Ultraviolet radiation (UV), in the form of solar energy, with a wavelength between 200-400 nm is 'absorbed' by the DNA molecule, causing 'direct' DNA damage. UV radiation can be categorised, based on the range of light wavelength: UV-C = 100-280 nm, UV-B = 280 – 315 nm, and UV-C = 315 – 400 nm. The majority of the most energetic solar radiation (i.e. shortest wavelength: UV-C) does not reach the surface of the Earth due to the ozone layer, therefore most of the DNA damage is caused by UV-B and UV-A. UV-C has been utilised for many bactericidal treatments and an optimal lethal effect for UV-C light is between 250-260 nm [31]. End products of lipid peroxidation e.g. malondialdehyde (MDA) have also been implicated in indirect DNA damage [32]. MDA reacts with nucleotides to form adducts which severely compromises DNA integrity. DNA damage is a chemical or physical alteration to the molecules structure and is a fairly common occurrence through aggressive environmental interactions.

Indirect DNA damage is often facilitated by highly reactive chemical species interacting with the DNA molecule. Oxidation of nucleotides can cause structural distortion and impairment of replication. The hydroxyl radical ($^{\bullet}OH$) has been implicated in the oxidation of all 4 types of nucleotide

[33]. Hydrogen peroxide (H_2O_2) is generally unreactive towards DNA but serves as an intermediary for $^{\bullet}OH$ production via 'Fenton's Reaction'. This reaction proceeds due to transition metals ability to occupy more than one oxidation state; unpaired electrons exist in the outer valance orbital and can become involved in one-electron redox reactions. Free iron (II) reacts with H_2O_2 and forms $^{\bullet}OH$. The Haber-Weiss Reaction is inextricably linked as it generates iron (II) from the reduction of iron (III) by superoxide ($O_2^{\bullet -}$) (Figure 2.5). OH generation using an Fe catalyst is biochemically important as Fe (II) can be found in close proximity to DNA.

$$Fe(II) + H_2O_2 \rightarrow Fe(III) + {}^{\bullet}OH + OH^- \qquad \textbf{(2.1)}$$

$$Fe(III) + {}^{\bullet}O_2^- \rightarrow Fe(II) + O + H^+ \qquad \textbf{(2.2)}$$

Adapted from [34]

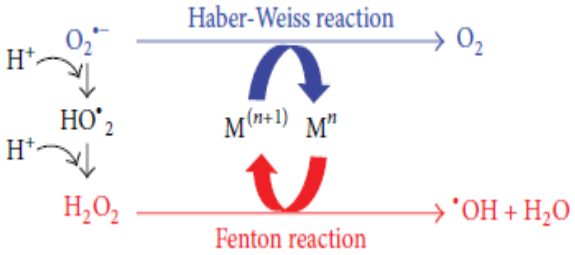

Figure 2.5 Schematic showing the interplay between the Fenton and Haber-Weiss reactions. Reduced transition metals react with H_2O_2 (Fenton Reaction), generating $^{\bullet}OH$. Superoxide radical reacts with oxidised form of transition metals, as determined by the Haber-Weiss reaction [27]

2.1.4. Electroporation

Electrostatic disruption of cells was proposed as a mechanism for the observed surface damage to *E. coli* (in liquid) exposed to an atmospheric pressure glow discharge [35]. Membrane conductivity and permeability can be manipulated by applying electrical pulses to cells in suspension or in tissue, termed 'electroporation' [36]. Short electrical pulses that increase the transmembrane voltage beyond a threshold (U_m ~ 0.2 V) cause a rapid and confined rearrangement of molecules within the membrane. Transient water-filled structures form to facilitate the transport of molecules across the bilayer, reducing membrane resistance without affecting the capacitance [37]. Figure 2.6 is a molecular dynamics simulation of the creation of an electropore. The small red and white spheres at the top and bottom of the panel are water oxygen and hydrogen atoms (a). Gold and blue spheres are head group phosphorus and nitrogen, respectively, and in the presence of an electric field of sufficient

strength a water intrusion appears (b), and extends across the bilayer (c). Hydrophillic head groups follow the water to form a hydrophilic pore (d). The pore formation sequence, from the initiation of the water bridge to the formation of the head-group-lined pore takes less than 5 ns. Upon cessation of the electrical pulse, the membrane can return to its normal molecular bilayer configuration. Biomedical applications of reversible electroporation include DNA transfection for cloning and to improve drug delivery into tissues. The major advantage for electrical manipulation of membranes is that it is universal across all cell types and non-cellular lipid bilayer models [38]. Increasing pulse duration or magnitude may cause gross membrane damage and the molecules cannot revert back to form a bilayer structure. The resulting loss of membrane integrity and uncontrolled permeability is irreversible electroporation.

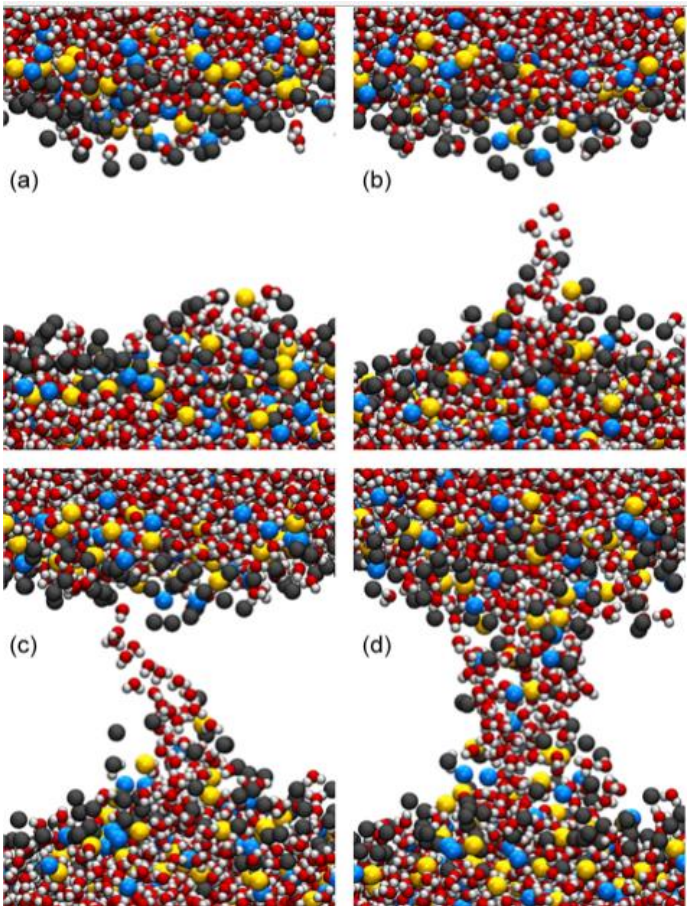

Figure 2.6 Screenshots from a molecular dynamics representation of an ‘electropore’ creation event [37]

2.1.5. Aerosolisation - Cell Isolation Technique

In principle, individual cells can be isolated from the rest of the population by encapsulation within a droplet. Aerosolisation techniques centred on the interaction of a liquid suspension containing

biological material and a gas flow are best adapted to bacteria, yeasts and viruses [39]. If the liquid suspension interacts where the kinetic energy is greatest i.e. centre of the gas flow, a higher proportion of small uniform droplets is produced [40]. A nebuliser (Burgener X-175) enables a bacteria suspension to interact with the central portion of the gas stream due to surface tension and a unique liquid 'spout' which covers the gas flow exit. The 'enhanced parallel path' design allows for separate liquid and gas delivery to the point of interaction i.e. the nebuliser tip.

Collection of aerosolised bacteria can be achieved by 2 main methods: Impaction and Impingement. Impaction is where a solid (e.g. glass slide) or semi-solid (e.g. agar) surface interacts with the cell in-flight; impingement is when a liquid medium is used. For relatively non-stressed bacteria, there was little difference in the collection efficiency between the two techniques [41]. The collection vessel for impingement must contain an adequate volume or the collection efficiency is greatly reduced [42].

2.2. Plasma

Plasma is a physical state of matter beyond the conditions that normally define in a gas [43], where gas atoms or molecules dissociate to form a mixture of neutral atoms, ions, electrons and charged particles [44]. In this electrically-conductive gaseous regime, charged ions (positive and negative) and electrons exist in a quasi-neutral state i.e. equal number of positive and negative charges [45]. Electrons with sufficient energy collide with gas atoms or molecules produce gas-phase ions and electrons [46]. Elastic and inelastic collisions between charged particles in the gas phase involves energy and mass transfer which results in the generation of short-lived yet chemically-active species [43]. Once charge carrier generation processes are balanced with charge carrier losses, a steady-state plasma develops [46].

Plasmas can be generated in the laboratory when a neutral gas interacts with an externally-applied electric field and the electrical energy contained within the electric field is transferred to the plasma by accelerating charged species [47]. Because of their small mass, electrons retain most of their energy in elastic collisions with the much larger gas atoms or molecules and primarily transfer their energy through inelastic collisions [46]. The energetic electrons collide with the heavier gas atoms causing secondary dissociation, excitation and ionisation in the gas phase [47]. The

fundamental process that underpins both plasma formation and the generation of chemically-active species is the electron kinetics (i.e. electron temperature (T_e) [47]. A vast array of electrical configurations exists for laboratory-generated plasmas, each one producing different compositions of reactive species which makes comparison difficult. This task can be simplified, somewhat, by categorising plasmas based on some fundamental parameters.

The number of charged particles is a parameter used to aid comparison between plasmas, in particular the electron density (n_e). Charged particle (species) density is a general indication of the reactivity of a plasma and the probability of collisions. The kinetic energy of the species, e.g. electron temperature (T_e), ion temperature (T_i), and gas temperature (T_{gas}) can be estimated by analysing emission spectra from the plasma. Species kinetics coupled with density estimation creates a fuller representation of the conditions within the discharge. Optical emission spectroscopy (OES) is a non-invasive technique that can be used to estimate species density and the gas temperature [48]. The composition of the gas directly influences the type and number of reactive species generated in the plasma i.e. the chemistry. Most plasmas use a mono-atomic gas (i.e. noble/halogen) such as He, Ar, or Ne to ignite and sustain the discharge; addition of molecular gases or vapours to the primary (feed) gas, either upstream or downstream from the discharge, alters the species produced. Diatomic/molecular gases make plasma stabilisation difficult since the intramolecular bond is more susceptible to excitation, leading to bond breakage and molecular fragmentation, rather than excitation/ionisation. Therefore, admixtures of O_2 and/or N_2 is usually limited to a few percent of the total gas volume [49] which is still sufficient to enhance the production of reactive oxygen and nitrogen species (RONS). Also, as a consequence of electrons interacting with O_2 in the feed gas, the available electron energy for background gas ionisation is lowered e.g. T_e reduced when O_2 was added to Ar feed gas, compared to Ar only plasma [50]. Water vapour can be added to the gas to act as a precursor for ROS formation. Plasma sustained in the presence of water vapour has different physical and chemical properties compared to without water vapour.

Plasmas are dynamic steady-state owing to the short lifetimes of the charged particles that compose them. Within the discharge exists a balance between the energy losses (sinks) due to the charged species and production (sources), requiring a constant flow of energy to sustain the steady

state [43]. The frequency at which the electrical energy is delivered into the discharge region impacts on the charged particle kinetics, and influences plasma properties.

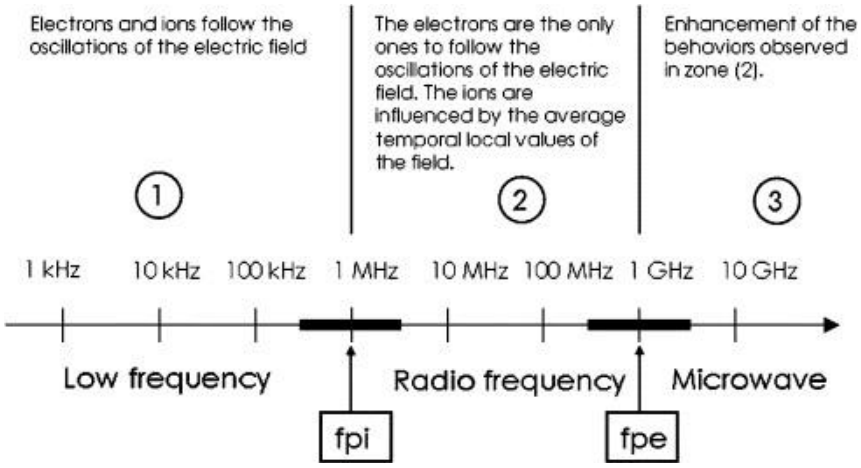

Figure 2.7 Frequency-dependant behaviour of electrons and ions in non-thermal plasma [51]

Figure 2.7 shows the impact of power frequency on the behaviour of the electrons and ions in a non-equilibrium plasma. At low frequency (e.g. DC & rf-kHz), both the electrons and ions are kept within the oscillations of the electric field [51]. At mid-frequency (e.g. rf & UHF), the electrons are confined within the electric field oscillations, whereas the heavier ions are relatively unaffected. Here, the electrons are the main drivers of the reactive species generation as they are lighter and are directly influenced by the electric field. Discharges ignited using microwaves generally enhance the electron and ion effects observed at rf [51]. In addition to the frequency, the amount of electrical energy, i.e. power, required to sustain a plasma can be varied to assess the effect on species density generation and the resultant chemistry. For stable, diffuse discharges, the input power is generally proportional to species density. Voltage and current probes can be directly coupled to the powered electrode, allowing for plasma power estimation [48]. Electrode positioning and structure also affect the discharge properties. Plasmas can be ignited between parallel-plate electrodes in direct contact with the gas or have a dielectric layer separating the electrode and gas. An electrode in direct contact with plasma may over time deteriorate due to etching and contaminate the discharge e.g. DC-driven discharges [49]. A dielectric material may be placed in between the electrode and the plasma region, acting as a physical barrier between the plasma and the electrode surface but still allowing the electric field to flow through it and interact with the gas (e.g. DBD). The breakdown voltage (i.e. the minimum voltage required to generate a plasma) is the product of the distance between the high-voltage

electrode and the grounded electrode, and the gas pressure within the electrode gap (Paschen's Law). Therefore, to maintain a stable discharge at atmospheric (high) pressure, the discharge length (i.e. electrode distance) must decrease [47].

2.2.1. Non-thermal microplasmas

Non-(thermal)-equilibrium plasmas have electron energies much greater than the gas temperature [50]. The electrons drive excitation and ionisation reactions that generate chemically-active species while the larger background gas ions are less responsive to the electric field which prevents the gas temperature from rising. At atmospheric-pressure, this non-equilibrium is enhanced as plasma size (i.e. distance between electrodes) is reduced [50]. These small-scale plasmas, termed 'microplasmas', are a potent source of reactive species. The relatively low gas temperature allows heat-sensitive surfaces to be exposed to the plasma, allowing for chemical modification without thermal damage. The core plasma region may be confined within the geometry of the electrodes, creating a definite reactive region i.e. diffuse/glow discharge. This can be achieved by exciting the gas in between parallel plate electrodes or by using ring electrodes placed around a dielectric capillary tube with an additional gas flow inside. Plasma-generated species entrained within the gas flow are transported beyond the core region may interact with ambient air, resulting in secondary excitation/species formation e.g. jet/pencil configuration. The interaction between the plasma effluent and ambient air can be turbulent [52], making the chemistry difficult to elucidate and even more difficult to control. Recently, liquid exposed to plasma remained chemically active long after the initial plasma exposure [53], [54] i.e. 'plasma-activated media' (PAM). The next section explores this chemistry, and the generation mechanisms that are responsible.

2.2.2. Plasma-liquid Chemistry

Interaction between plasma and liquid can be generally categorised into three conditions: discharges ignited directly in the liquid phase, discharges ignited over a liquid, and discharges in multiphase environments i.e. gas-phase plasma and water vapour/droplets [8]. In the latter two conditions, gas-phase charged species (ions and electrons), radicals and neutrals bombard the liquid, resulting in diffusion into the liquid and the formation of secondary species at the interface. The interaction between plasma and liquid is of particular importance for biomedical applications due to the high liquid content of cells and of their surrounding environment [6]. Liquid surrounding the cell is

integral for maintaining osmotic balance and, therefore, viability. Discussed below is a select summary of chemistry initiated by the interaction between plasma and liquid, with particular attention focussed on determining the mechanistic origin of the species.

Within certain well-defined parameters, computational studies can estimate what species exist when plasma is in contact with a liquid surface. A comprehensive global model of an rf-driven He/H_2O diffuse plasma (i.e. multiphase environment) including 46 species and over 500 reactions was developed to try to determine the species generated [55]. The simulation calculated that the predominant ionisation mechanism in the plasma (n_e 10^{17} m^{-3}) was due to long-lived excited species i.e. metastable species. For low water concentrations (1 and 3 ppm), He ions were the predominant species e.g. He_2^+ ~ $6x10^{16}$ m^{-3} at 1 ppm. As water concentration increased, so too did the density of water molecule clusters. The largest calculated density was for the cluster $H_{11}O_5^+$ (n_{H11O5+}) ~ $3x10^{17}$ m^{-3} at 3000 ppm water concentration. For the same water concentration, the negative ion with the largest calculated density was $H_5O_3^-$ ~ $2x10^{17}$ m^{-3}. n_{OH} increased with water concentration by approx. 2 orders of magnitude (n_{OH} ~ $5x10^{14}$ m^{-3} at 1 ppm water and reached a maximum density of ~ $2x10^{16}$ m^{-3} at 3000 ppm). The effect was more pronounced for n_{H2O2}; $7x10^{15}$ at 1 ppm water up to ~ $6x10^{19}$ at 3000 ppm water [55]. Energetic collisions between clusters maintain the plasma when the ionisation energy of the molecule that collides with the cluster is lower than the clusters own energy, known as the Penning Effect [43]. Reactive molecular dynamics simulations between plasma-generated gas-phase O, $^{\bullet}OH$, HO_2 and H_2O_2 interacting with pure water found that species can penetrate deep into the liquid [56]. 500 H_2O molecules were assembled in a layer, with a thickness of approx. 3.25 nm (20 Å $\rightarrow$ 52.5 Å; 1 Å = 0.1 nm). O atoms interacted with H_2O molecules at the interface, forming two $^{\bullet}OH$ that subsequently reacted with other H_2O molecules to form secondary $^{\bullet}OH$ and water molecules. As a result, O atoms did not penetrate into the liquid layer. Gas-phase $^{\bullet}OH$ and H_2O_2 showed complete migration through the liquid layer; HO_2 travelled ~ 50 % of the thickness [56].

Gorbanev *et al* [57] experimentally distinguished between species generated in the gas phase and those generated in the liquid phase by using two distinct water types: H_2O and D_2O. One acted as the collector while the other was vapourised and added upstream to the parallel-field, kHz-driven plasma jet [57]. Species that were formed from the direct interaction between plasma and the vapourised water type were measured in the collection liquid composed of the other liquid type,

suggesting gas-phase generation of species followed by diffusion into liquid. Feed gas humidity affected the concentration of species produced both in the gas phase and in the liquid. When no water vapour was introduced to the plasma, only a small amount of H_2O_2 was measured in the liquid downstream from the plasma. The concentration of H_2O_2 increased with relative feed gas humidity, as measured by UV-vis spectroscopy, and was unaffected by the distance between the core plasma region and the liquid [57]. This suggests the measured H_2O_2 in the liquid located downstream from the plasma was generated in the gas-phase and diffused into the liquid, and not formed through the dissociation of water molecules triggered by plasma-generated species. A different plasma configuration and experimental design reported a similar relationship; H_2O_2 concentration was proportional to feed gas humidity [53]. H_2O_2 was generated in the gas-phase from a humid Ar plasma and transported into liquid that was placed downstream from the plasma. The authors proposed the mechanism for detection of the gas-phase species in liquid was due to diffusion as a consequence of the molecules solubility i.e. high Henry's constant. An rf-driven glow discharge ignited between two parallel plates was another configuration that showed a relationship between H_2O_2 detection in the liquid phase and water concentration in the gas phase [58]. In addition to water content, the power used to maintain the plasma influenced the amount of H_2O_2 that was generated, showing a near-linear relationship with the measured H_2O_2 concentration [58]. H_2O_2 production rates from the literature have been calculated and are shown in Chapter 4.

H_2O_2 is a stable reaction product that remains detectable in liquid long after the initial plasma exposure. Radical species are short-lived and more difficult to experimentally measure as they tend to react with other species or molecules before detection. Nevertheless, quantitative measurements of O atoms and $^{\bullet}$OH radicals in the afterglow of a micro-scaled atmospheric pressure plasma jet (μ-APPJ) operating in helium were recently reported [59]. A controlled admixture of water vapour acted as a precursor for the oxygen species detected from the interaction with the μ-APPJ (13 MHz) parallel-plate with $<10^4$ ppm H_2O (n_e ~10^{11} cm^{-3}). Spectroscopic measurement of plasma emission showed that both $^{\bullet}$OH density (n_{OH}) and oxygen atom density (n_O) increased as water content increased, until saturation at ~ 7000 ppm H_2O. When H_2O content was 6000 ppm, the maximum n_{OH} and n_O was ~2 x10^{14} cm^{-3} and ~3.2 x10^{13} cm^{-3}, respectively [59]. Plasma-generated $^{\bullet}$OH was also measured in liquid by molecular spin-trapping analysis, which uses a molecule that forms a stable adduct with OH that is detectable [57]. Different isotopes of water were used for species generation and collection to

determine which species were formed in the gas phase and those in the liquid phase. When He was used to form the plasma, the $^{\bullet}$OH-adduct concentration was sensitive to the relative feed gas humidity, with the maximum $^{\bullet}$OH-adduct concentration of ~23.5 µM at ~20% humidity and then tailing off. The addition of 0.5% O_2 caused a reduction in the concentration of $^{\bullet}$OH as the relative gas humidity increased. Isotope analysis of the liquid suggested that, as with H_2O_2, $^{\bullet}$OH was generated in the gas-phase and diffused into the liquid [57]. Absolute $^{\bullet}$OH densities in the gas phase were determined from UV absorption spectra of a diffuse He-H_2O rf-glow discharge [60]. n_{OH} was proportional to the power supplied to the plasma (n_{OHmax} ~ $1.1x10^{20}$ m^{-3} at 120 W). When the plasma power was 120 W, n_{OH} increased with water content but began to saturate at high water concentrations (n_{OHmax} ~ $3.5x10^{20}$ m^{-3} at 15000 ppm water). The same detection technique measured absolute $^{\bullet}$OH density from a DC glow discharge using water as an electrode (n_{OHmax} ~ $1x10^{23}$ m^{-3}, [61]. The next section will review the interaction between plasma and cells, and the possible species thought to be involved.

2.3. Cell Interactions with Plasma

Atmospheric-pressure plasmas are composed of electric fields and generate UV radiation, excited species, charged particles and neutral species [26], [62] all of which can damage cells when applied in significant concentrations alone. Electric fields can directly influence cell permeability by causing structural rearrangement and pore formation through which solutes can flow freely into the cell (see Chapter 2 section 2.1.4. Electroporation). The application of electric fields to a bacterial suspension resulted in a 2-log reduction in viable bacteria cells [63]. Significant synergistic effects were observed when the cells were exposed to plasma prior to electric field treatment, but minimal effects were observed when cells were exposed to electric fields before plasma [63]. UV-C was applied to suspensions of bacteria and viability was assessed after exposure by flow cytometry and agar plate counts [31]. The mechanisms of cellular damage differed according to UV exposure time and the cell type. *E. coli* (Gram-negative) experienced an initial rapid reduction in viability but the gram-positive *L. innocua* remained metabolically active after UV exposure but did not grow on agar plates [31]. It is experimentally possible to expose cells to plasma and eliminate the effects of the UV radiation. However conflicting reports exist of plasma-generated UV effects on bacteria viability being negligible [64]. This discrepancy will be discussed in more detail in Chapter 5.

2.3.1. Plasma-generated reactive species

The cell response to plasma-generated species exposure is likely to be the result of a synergistic interaction between two or more constituents since the charged species produced are highly reactive. The reactive species generated by plasma-liquid interactions can impact upon all cell types since they are also involved in inherent cell signalling pathways [7]. The cell type is an important factor when attempting to elucidate the plasma-induced biological response in vitro. Prokaryotic cells appear to be more sensitive to plasma treatment compared to eukaryotic cells [65]. Differences in sensitivity towards plasma treatment exists in mammalian cells; cancerous cells appear more sensitive to the ROS burst supplied by plasma than normal eukaryotic cells, possibly due to their increased rate of metabolism [66]. Similar to UV exposure, Gram-negative bacteria have less resistance to plasma treatment than Gram-positive bacteria [10], [67], [68], [69], [70]. The efficiency of plasma inactivation was shown to be inversely proportional to the initial cell density in the treated sample [71].

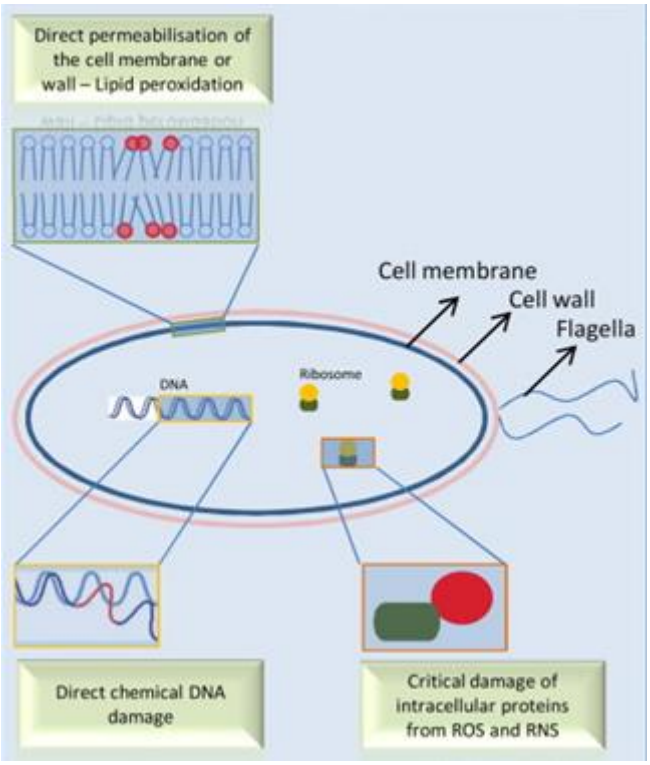

Figure 2.8 Schematic representation of a bacteria cell and the main mechanisms of interaction: (i) Cell Envelope Permeabilisation, (ii) DNA damage and, (iii) Damage to proteins critical for normal cell function [72]

Figure 2.8 is a general overview of the possible pathways plasma-generated reactive species are thought to influence biological systems through increased cell membrane permeability, chemical

modification of DNA and critical damage to proteins involved in normal cell function [72]. Strong evidence suggests that the RONS generated by plasma-liquid interaction are involved in cell-signalling pathways and directly influence the cells response. Genetically-modified *E. coli* were defective in their oxidative defence pathways and exposed to plasma-induced ROS [64]. Mutant *E. coli* lacked soxS, an activator of superoxide stress genes, showed the greatest sensitivity to plasma treatment; full inactivation was observed after 3 min plasma treatment (APGD; Q_{He} 5 slm). Another study used a DC-APPJ to treat suspensions of *E. coli* mutants and the major contributing factor to inactivation was attributed to ozone (O_3) [73]. The initial interaction site between plasma-generated species and the cell is on the outer surface structures. The specific molecular interactions, beginning with surface interactions and then onto intracellular biomolecule interactions, are outlined below.

2.3.1.1. Cell Envelope Damage

Short-lived radicals interact with the cell surface and $^{\bullet}OH$ has been proposed as the species responsible for the initiation of the lipid peroxidation cascade (see section 2.1.3.1.1. Lipid peroxidation). DNA was detected in an *E. coli* suspension after exposure to an rf-APPJ (kINPen 09 – Q_{Ar} = 4.9 slm) [74]. The DNA absorbs light at 260 nm, due to the aromatic ring structure of the nucleotide base. Using an incident light of wavelength 260 nm, the absorbance of the plasma-treated suspensions was measured and DNA concentration calculated using the Beer-Lambert Law. Detection of *E. coli*-specific DNA in the treated liquid was confirmed using a quantitative polymerase chain reaction (qPCR) assay) [74]. The detection of genetic material in the plasma-treated cell suspension suggests that some cells have lost membrane integrity but this does not infer that all cells have been inactivated. Bacteria suspended in the liquid may enter a viable but non-culturable (VNBC) state upon sub-lethal exposure to a harmful treatment [75], including exposure to plasma [74]. Loss of membrane integrity was also observed using propidium iodide, a membrane-impermeable dye under normal conditions, and the cells were imaged using fluorescence microscopy after plasma treatment [74]. The origin of species generation, either gas phase or liquid phase, was investigated and the density and temperature of plasma-produced $^{\bullet}OH$ was measured using laser-induced fluorescence (LIF). $^{\bullet}OH$ in the liquid phase was reported to be the main species responsible for cancer cell permeabilisation [76]. Terephlatic acid (TA) reacts with $^{\bullet}OH$ and, under UV light exposure, the reaction product can be visibly observed; the intensity of the signal is proportional to the concentration of the TA-OH adduct.

2.3.1.1.1. Lipopolysaccharide deactivation

The outer membrane of *E. coli* contains important endotoxins that are responsible the pathogenicity of certain strains'. Lipid A is the primary toxic region of lipopolysaccharide (LPS) and was the target for APPJ treatment operating using Ar with different admixtures of gases [77]. Biotinylated LPS was exposed to plasma and horse-radish peroxidase-conjugated streptavidin was added to the treated sample. The binding affinity between biotin and streptavidin was used as an indicator for LPS damage. Ar plasma with an admixture of 1 % O_2 resulted in a greater LPS deactivation rate for short treatment times, compared to when 1 % N_2 was used; there was little difference between admixtures for longer treatment times [77]. This suggests ROS production is largely responsible for LPS deactivation and is most rapid in the initial exposure phase before plateauing. Reactive molecular dynamics (MD) simulations studied the interaction of LPS with ROS, specifically $^{\bullet}OH$, HO_2^- and H_2O_2 [18]. All three ROS break chemical bonds which would lead to deactivation of LPS.

2.3.1.1.2. Lipid peroxidation

Detection of stable products of the lipid peroxidation cascade is a useful indicator for plasma-induced oxidative stress of treated *E. coli*. Thiobarbituric acid reactive substances (TBARS) assay is commonly used to detect a by-product of the reaction, malondialdehyde (MDA). The technique has been employed in a number studies involving *E. coli* and atmospheric-pressure plasma. Cells in suspension exposed to an rf-APPJ using Ar (kINPen) generated ~ 47 nM MDA [74]. The same author deposited cells onto a membrane and used a DBD to treat the cells and subsequently generated ~ 28 nM MDA [3]. MDA generation from plasma-treated *E. coli* in suspension showed a linear correlation with treatment time [78], [79]. DBD generated in air caused membrane lipid peroxidation that was dependent on the concentration of plasma-generated ROS and exposure time, such as singlet oxygen and hydrogen peroxide [78]. Addition of ROS scavengers greatly reduced the extent of the plasma-induced lipid peroxidation. An kHz-driven APPJ was used to treat suspensions of *E. coli* and the maximum MDA concentration was observed after 120 s exposure time (~ 31 µM) [79]. [MDA] production rates have been calculated from the literature and can be viewed in the discussion section in Chapter 6.

2.3.1.2. Intracellular Biomolecule Interactions

Recently, in situ formation of $^{\bullet}OH$ initiated by the interaction between plasma-generated species and intracellular iron was proposed as a possible mechanism for cell death upon plasma exposure [80, 81]. Iron-containing enzymes exist inside cells and generate $^{\bullet}OH$ by catalysing the degradation of O_2^- and H_2O_2 via Haber-Weiss Reaction.

2.3.1.2.1. DNA

Detection of DNA in plasma-treated cell suspensions has already been addressed (see section 2.1.3.1.2 Deoxyribonucleic acid (DNA) oxidation). The degree of structural damage can be assessed in a number of ways. Stained nucleic acids can show plasma-induced damage [81]. COMET assay was employed to investigate the DNA damage induced by APPJ treatment using Q_{He} 2slm + 0.3 % O_2 [82]. The DNA damage led to necrotic cell death of primary pancreatic epithelial cells. The proportion of plasmid DNA damaged by an rf-APPJ operating with He increased with treatment time, inducing both SSB and DSB when plasmid DNA was exposed [83]. In the presence of a radical scavenger, the proportion of both strand breaks was reduced implying an important role for plasma-produced reactive species in DNA damage induced by plasma treatment [83]. The change in the relative length of DNA induced by APPJ treatment was modelled and shown to decrease with increasing treatment duration [84].

Plasma-treated DNA that is subsequently subjected to PCR may not generate any product if the DNA molecule was too damaged to be replicated correctly, or that the molecule was absent. The intensity of the PCR product can be used as an indication of the amount of DNA that was available at the start of the reaction. DNA band intensity of the PCR product decreased after plasma exposure in a time-dependant manner [85], [86]. The effect of plasma treatment on plasmid DNA was assessed under two separate conditions: DNA on glass treated with plasma then transformed using *E. coli* [87], and extracted plasmid DNA degradation assessed after plasma treatment [88]. Two separate techniques assessed the structural [88] and functional [87] effect of plasma treatment on DNA. Plasmid DNA, originally isolated from *E. coli*, was suspended in PBS and exposed to APPJ and then subjected to gel electrophoresis [79]. Three distinct bands were observed on the gel, corresponding to supercoiled, linear and open circular plasmid conformations. Plasma treatment caused the supercoiled plasmid DNA to unravel and become linear conformation, which is indicative of DSB [79].

2.3.1.2.2. Protein

Proteins under dry conditions were degraded by low-temperature atmospheric pressure plasma exposure [89]. Direct exposure to the reactive plasma species causes bond breakage/degradation and a change in structure and loss of function. Individual amino acids in solution were also exposed to plasma [90]. The amino acid side chains are targets for the reactive species generated by plasmas and the oxidation reactions can be summarised into four reaction groups: hydroxylation, nitration, dehydrogenation and dimerization. Sulphur-containing carbon-chain amino acids would be the most sensitive to plasma-generated ROS and can be rapidly oxidised/sulphonated [90]. The five-membered ring amino acids can have the ring structure opened by reactive species more easily than the aromatic amino acids. The formation of unsaturated bonds after plasma treatment of carbon-chain amino acids led to a number of products being detected [90].

Ribonuclease (RNAse) activity was assayed after exposure to two different plasma sources [91]. Enzyme was exposed as a dry sample and in solution to two types of plasma: DBD and APPJ. Inactivity was observed after DBD treatment but not after APPJ exposure, and inactivation kinetics was more rapid when the RNAse was in solution compared to when a dry sample was exposed [91]. A solution containing Proteinase K was treated with an APPJ using He with 0.5 % O_2 admixture; enzyme inactivation was observed in a time-dependant manner [79].

2.3.2. Plasma-activated Media

A volume of liquid that interacts with plasma becomes chemically active. Ringer's solution with lactate exhibited anti-tumour effects, however it was hypothesised that only the lactate was 'activated' after the liquid was exposed to plasma [92]. Gas-phase plasma-generated species diffused into the liquid and induce molecular alterations of the compounds that composed the media. Therefore, the effect of plasma treatment on cells in suspension is facilitated through this liquid phase. Cells suspended in growth media were found to be less susceptible to cells treated in a buffered solution [9], which implies the more complex liquids used to suspend cells during plasma treatment will have a protective effect against plasma. The chemical activity of plasma-treated liquid was determined by liquid pre-treatment before the addition of cells to the solution and assessment of the biological response. There was no difference in the reduction in viability when cells were added after NaCl was plasma-treated compared to direct plasma treatment of the bacteria in NaCl [54].

Comparatively long-lived neutral species, like H_2O_2, are thought to be predominantly responsible for the prolonged chemical activity and has been measured months after initial plasma treatment. Previous studies showed that pre-treated liquid added to cancer cells could induce apoptosis without the cells ever coming into direct contact with the plasma [93], [92]. The liquid retained its cytotoxic and mutagenic potential towards cancer cells and could offer a new anti-tumour strategy. Liquids treated by plasma were found to contain species that were generated in the gas phase [57]. Recently, OH density was measured up to 6 mm into liquid that was treated with Ar APPJ [94].

2.4. Plasma-droplet interactions

Low volume liquid droplet interaction with a non-thermal plasma, where the droplet doesn't completely evaporate, may offer enhanced rates of mass transfer from the gas-phase to the small droplet due to the high surface area-to-volume ratio [95]. A high energy yield for H_2O_2 was reported from water spray interacting with a low power gliding-arc discharge operating in Ar [96]. The presence of a liquid droplet offered the more soluble plasma-generated H_2O_2 a protective medium to diffuse into and prevent degradation from other, more reactive species e.g. $^{\bullet}OH$ (Figure 2.9). Other studies have confirmed this sequestering of plasma-generated gas-phase H_2O_2 into liquid using humidified Ar with an additional O_2/N_2 shroud gas [53]. H_2O_2 concentration in the plasma-treated liquid increased with feed gas humidity until saturation at ~ 140 µM at 1300 (ppm) humidity.

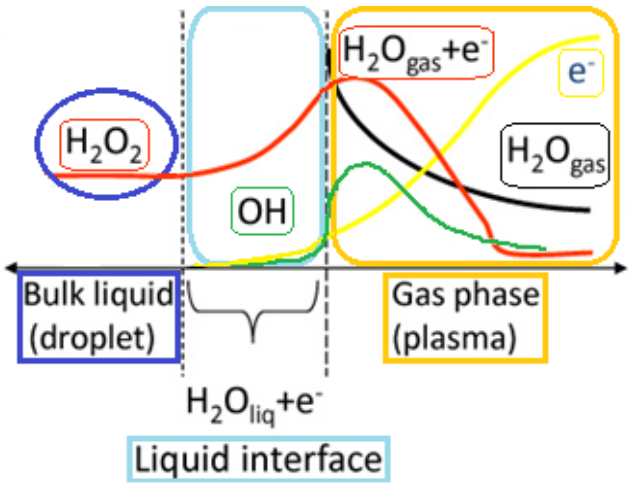

Figure 2.9 Schematic representation of the reactions occurring at the plasma-droplet interface (adapted from [95])

Current estimates of gas-phase $^{\bullet}OH$ lifetime generated in humid corona N_2/O_2 mixtures are between 10-100 µs [97]. Therefore, the possibility exists to transport short-lived, plasma-generated reactive species i.e. $^{\bullet}OH$ away from the plasma region and remotely induce a chemical effect, as long as the species reaches the target before its quenched.

2.4.1. Plasma treatment of airborne *E. coli* in-flight

Literature is limited on the atmospheric-pressure plasma inactivation of bacteria that are in-flight i.e. airborne. The primary application has been towards improvement in air decontamination systems that don't require any mechanical or physical filtration membrane. Non-pathogenic bacteria that aren't normally found in the airborne state, e.g. *E. coli*, are still a useful cell model in such studies since pathogenic bacteria require special containment laboratories. A Dielectric Barrier Grating Discharge (DBGD) device caused a 1.5 log reduction immediately after plasma treatment that increased to a 5-log reduction measured 2 minutes post-treatment [10]. DBGD consisted of a plane of electrodes in parallel with gaps of 1.5 mm between each electrode. A rapid treatment time is possible because of the high gas flow rate (25 slm), resulting in a high velocity bioaerosol particle in flight and a short plasma residence time (~ 0.73 ms). Plasma-treated cells were collected by impingement as this collection technique reduces the desiccation stress on the bacteria. The same group later investigated 'direct versus indirect' plasma exposure and the possible species that influenced inactivation, particularly ozone [13]. Cells exposed to ozone (28 ppm for 10 s) did not produce similar inactivation kinetics to those cells that were exposed to the same dose of (plasma-produced) ozone; the plasma-exposed cells showed a faster reduction in viability post-treatment. A different DBD electrode configuration allowed for nebulised *E. coli* to pass through 1.5 mm holes and through a discharge region [12]. Plasma-treated bacteria were collected onto agar plates and any colonies enumerated after sufficient incubation time. Different gas compositions were used in order to generate different concentrations of species responsible for inactivation. When N_2 was used, no ozone was detected and there was incomplete inactivation of *E. coli* (77 % maximum reduction). Inactivation was attributed to high electric field exposure, excited N ions, reactive species (e.g. $^{\bullet}OH$) and UV radiation. When air was used, complete inactivation was achieved. The discharge voltage also has a crucial role in bacteria cell inactivation; inactivation rate increased with the discharge voltage for both gases used. In both plasma devices [10], [12] there appears to be a synergistic action of the short-lived reactive species and ozone. Another DBD-type device was arranged as two coaxial cylindrical mesh coils

separated by a dielectric layer [11]. The aerosolised *E. coli* become entrained in the fan-assisted air flow and are transported over/around the discharge and collected onto agar. A positive correlation between reduction in viable cells and plasma treatment time occurred, although the precise reduction was < 1 log in total. Direct deposition onto silicon wafer for SEM analysis showed gross morphological damage after plasma treatment. FTIR spectroscopic analysis showed differences in the chemical bond composition of the *E. coli* cells that were plasma treated compared to those that were only aerosolised. The generation of free hydroxyl groups was evident from the FTIR spectra of the DBD-treated cells, as well as the detection of a new band that was absent in the cells only aerosolised. It is thought that the free $^{\bullet}$OH caused oxidation on the cell surface, which resulted in the surface damage observed from the SEM images and plays a key role in the underlying interaction between DBD treatment of aerosolised *E. coli* [11]. This study showed that extensive chemical modifications occur on the cell surface of plasma-treated bacteria but have a limited effect on viability. Cell surface interaction from another DBD treatment was also reported for aerosolised *E. coli* [14]. A specific intracellular pathway was influenced through the result of the misfolding and/or unfolding of outer membrane porin precursor proteins in response to heat stress. Heat-shock protein (hsp) activation was enhanced in plasma-treated cells and hsp mutants were found to be extremely susceptible to plasma-charged aerosols [14]. In addition to hsp mutants, strains that were deficient in defending against peroxidative stress were also susceptible to plasma treatment. Collecting the cells in presence of catalase did not prevent complete inactivation and the addition of thiourea, an $^{\bullet}$OH scavenger, protected the catalase-deficient cell type. This suggests that the accumulation of intracellular $^{\bullet}$OH in the catalase-deficient cells after exposure to plasma is effectively scavenged [14]. Protection against plasma-generated $^{\bullet}$OH prevented complete inactivation of *E. coli* in droplets, which could indicate an important role for the species in similar studies.

Research to date involving the generation of bacteria in droplets and subsequent exposure to plasma is primarily focussed towards proof-of-principle application for air decontamination. Less is understood about the droplet reactivity and the species generated from the plasma-droplet surface interaction. Low volume liquid droplet exposure to cold plasma and its survival post-treatment offers a unique opportunity to study the plasma-liquid interface on microscopic length scales under controlled conditions.

2.5. A New Approach: plasma-droplet system for isolated cell treatment

The biological effect that plasma-produced reactive species exert is not well understood and remains a fundamental challenge [98]. The complexity of the biological system is matched by the large number of possible species generated at the plasma-liquid interface and potentially all could influence cellular chemistry one way or another. Simplification of the plasma chemistry, such as excluding O_2 and N_2 from the feed gas, would prevent the formation of certain ROS. Limiting species formation by removal of precursor gases could result in a better understanding of the fundamental processes that govern species formation. Confining the discharge within a defined geometry prevents interaction with ambient air molecules and the reactive species are generated only from the bulk plasma region and limited species formation outside this area is thought to occur. The use of scavengers of specific radicals, and the comparison of the biological response with and without this intervention, allows for a preliminary estimation of a possible effect related to a particular species. However, plasma-cell studies often use bulk liquid systems and it is difficult to determine what concentration of species was required to induce the observed response due to the complex nature of species diffusion into bulk liquid and the dispersal of cells throughout the suspension. For clinical applications, it is especially important to know what species are responsible for the effect [99].

3. MATERIALS AND METHODOLOGY

3.1. Introduction

The next chapter informs the reader of the equipment and techniques used in the experimental investigations that follow. Where possible, the product code for purchased apparatus and consumables is given in the equipment list. All chemicals that were used are included and any calculations for concentration conversion between units are presented. Information is then given on the diagnostic techniques employed in each chapter, detailing how measurements were obtained. In some instances, the technique may be explained in more detail in the chapter that it was used.

3.1.1. Aims and Objectives

3.1.1.1. Aims

- Stabilise an atmospheric-pressure electrical discharge with droplet flow
- Design apparatus to assess plasma-generated reactive species and collect plasma-treated bacteria
- Construct and maintain a sterile experimental working environment
- Standardise plasma-droplet system operating protocol and bacteria/droplet analyses

3.1.1.2. Objectives

- Establish a suitable working range of plasma operating conditions i.e lowest input power required to maintain a stable plasma with droplet flow and increments thereafter
- Devise a suitable technique to recover plasma-exposed droplets/cells for analysis
- Engineer a workstation to ensure airtight electrical and liquid tubing connection to plasma-droplet system; decontaminate all apparatus prior to use
- Generate reproducible results from optimised techniques and analysis

3.2. Materials

A comprehensive list of all the equipment used in this study is detailed can be viewed in Appendix section 8.1.1.

3.2.1. Plasma-droplet System

Droplets can be easily generated in the laboratory by supplying a nebuliser with adequate gas and liquid flows. The liquid may contain living cells i.e. bacteria, offering the opportunity to study isolated cells under controlled conditions. A Burgener enhanced parallel path nebulizer enabled the liquid to interact with the central portion of the gas stream (see Appendix: Figure 8.1). Surface tension between the inner capillary wall and the liquid caused the delivery of the liquid into the central portion of the gas flow, and the force of the gas flow interacting with the liquid caused droplet formation. A hollow inner cavity within a custom-engineered Perspex block (i.e. Shroud) allowed for simultaneous gas flow containment to generate the plasma and for the production of small droplets entrained within the same gas flow. Liquid was delivered to the nebuliser using a syringe pump (flow rate (Q_{liquid}) = 10 µl min^{-1}). Gas flows of helium (Q_{He}) at 3.5 standard litres per minute (slm) and neon (Q_{Ne}) at 1.0 slm were used to generate and transport the droplets along a quartz tube that was fixed to the Shroud (Figure 3.1). Effective nebuliser operation and reliable atmospheric plasma production were needed for consistent plasma-droplet system operation. Heavy gases such as air, argon or neon are required to provide efficient nebulisation; at atmospheric pressure, high helium content plasmas are relatively easy to sustain. An in-house optimisation study showed that, while plasmas from Ar:He mixtures were difficult to ignite or sustain, Ne:He mixtures provided stable plasmas with droplet flow. The optimum Ne:He mix in our device was found to be approximately 1:3.5.

A copper ring electrode, coupled to an electrical power generator operating at 13.56 MHz, was placed around the quartz tube as it exited the Shroud separated by 2 mm from a second, grounded copper ring electrode. Net plasma power was measured using an impedance probe connected in-line to the powered electrode and the input power was varied, starting with the lowest power able to maintain a plasma with droplet flow and increasing in 20 W increments (i.e. 80 W, 100 W, 120 W and 140 W). The plasma region was contained within the internal diameter (I.D.) of the quartz tube (2.0 mm) and was 2.0 mm in length as determined by the electrode gap. The high voltage electrode was positioned ~176 mm from the nebuliser tip. The droplet flow was previously characterised as laminar at the exit of the quartz tube and the average transit time through the plasma for any given droplet was 120 µs [100].

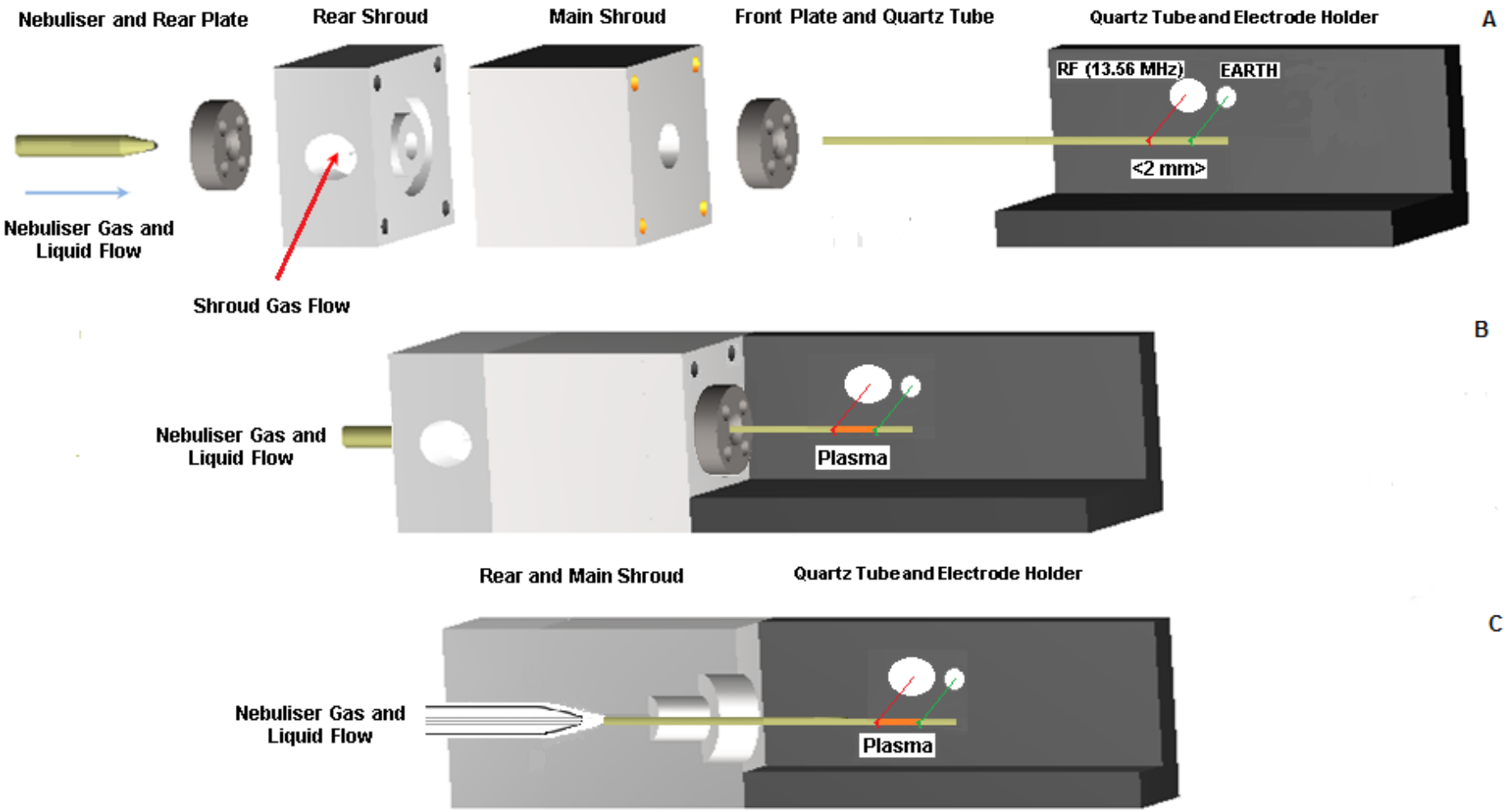

Figure 3.1 This assembly of components allowed for droplet generation and transport through a diffuse atmospheric-pressure plasma. (A) shows the individual components of the Shroud; (B) is a representation of the Shroud when assembled. (C) is a cross-section through the middle of the system

3.2.1.1. Evolution of Impingement Collection Apparatus

Impingement was the technique of choice employed to collect bacteria-loaded droplets exposed to plasma and study the biological effect of the interaction with reactive species over a short timescale (total droplet time of flight ~ 10 ms). Impingement protects the bacteria against desiccation that would otherwise be experienced when collected onto agar i.e. impaction [101]. Commercially-available impingement devices generally operate with a vacuum pump to draw the droplets into the chamber for collection. Unless extensive calibration was carried out to equilibrate the inward gas flow with the outward vacuum pump flow, available impingement devices would not be suitable to use with the plasma-droplet system. Therefore, it was necessary to design impingement apparatus suitable for coupling to the plasma source and simultaneous recovery of plasma-exposed droplets.

3.2.1.1.1. Horizontal plasma-droplet system: Gas-washing bottle

The first attempt at collecting plasma-exposed droplets employed 'gas washing' apparatus. Typically, this equipment is used to humidify gases for downstream applications. The plasma-droplet flow could be passed through the inlet and interact with a liquid reservoir, before exiting the outlet using a Dreschel-style bottle head arrangement (Figure 3.2). The smallest bottle size that could be attached to the lid was 100 ml and the lowest volume of liquid which submerged the transport tubing (15 cm Tygon ®) was 15 ml. One end of the tubing was attached to the end of the quartz tube and the other end was submerged in the liquid. The plasma source was raised using a scissor jack so that the quartz tube was parallel to the inlet opening of the collection bottle to facilitate laminar flow.

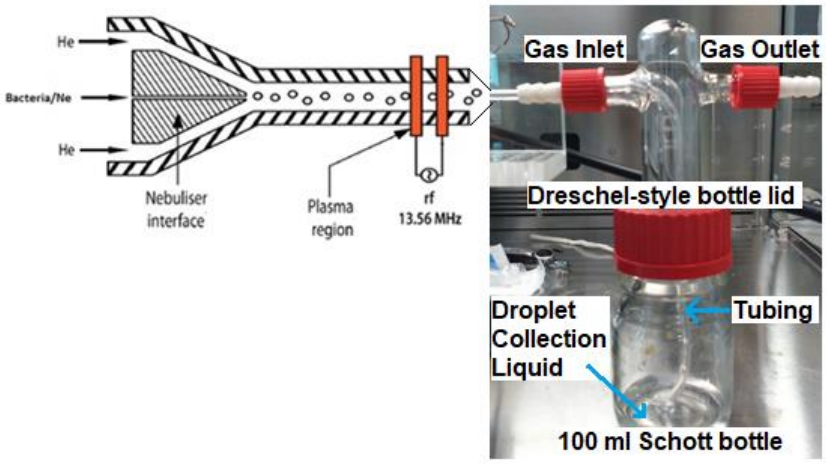

Figure 3.2 Cross-sectional schematic diagram of the nebuliser/shroud interface and droplet transport through the plasma (modified from [100]) and the gas washing bottle apparatus used to collect plasma-treated bacteria when the system was in the horizontal orientation

During operation in the horizontal orientation, liquid droplets were observed to accumulate within the shroud and not proceed through the plasma. In an attempt to improve droplet transport, the plasma source was rotated 90º so that the nebuliser, shroud, plasma path was vertical (Figure 3.3).

3.2.1.1.2. Vertical Plasma-droplet system: Custom-made micro-fluidics-based apparatus

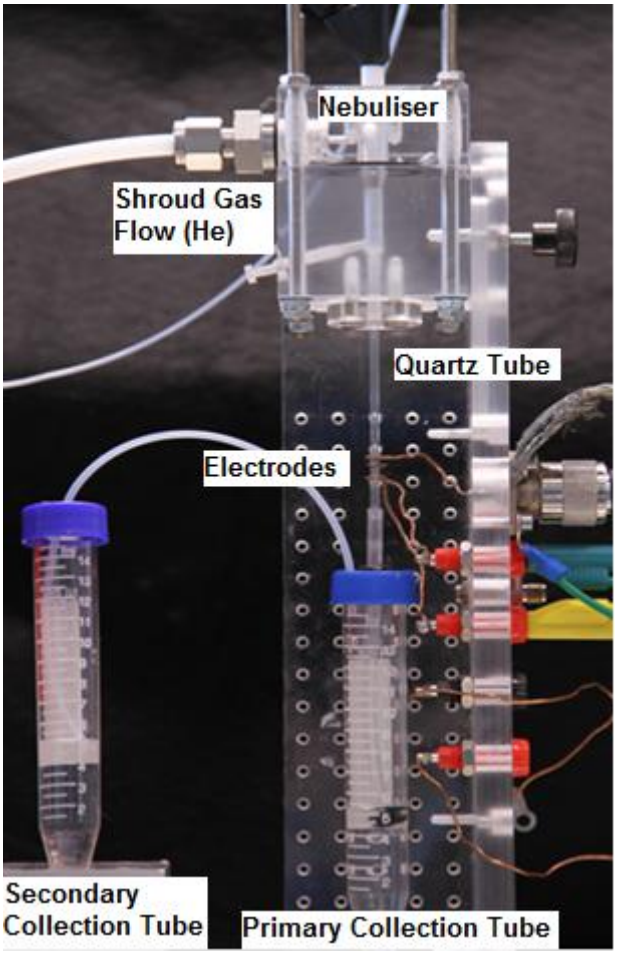

Figure 3.3 Collection apparatus for plasma-treated bacteria when the plasma-droplet system was aligned perpendicular to the workstation base

The vertically orientated system was used for the generation, treatment and collection of bacteria-loaded plasma-exposed droplets in the remainder of this study (Figure 3.3 and Figure 3.4). The idea evolved from micro-fluidics equipment and the liquid reservoir chamber used in that technique. The basic working principle is the delivery of liquid from a reservoir, using 'forward' pressure, which drives liquid out of the reservoir towards the desired location. It was thought the plasma-exposed droplet flow could enter the reservoir and be captured, with the pressure (i.e. gas flow) operating in the opposite direction to the micro-fluidics system. Most importantly, the alignment of the micro-fluidics apparatus allowed for easy coupling to the vertically-aligned quartz tube. An extended quartz tube was used to transport the droplets through the plasma region and was directly

submerged in the collection liquid. A sterile 15 ml conical tube was used to contain the collection liquid and the lid was modified with a grommet-lined hole to allow air-tight quartz tube entry into the collection tube, without the need for additional (Tygon ®) tubing. The reduction in collection vessel size allowed for the volume of collection liquid to also be reduced (from 15 ml to 5 ml), and it was hoped this would aid sample concentration to aid analysis.

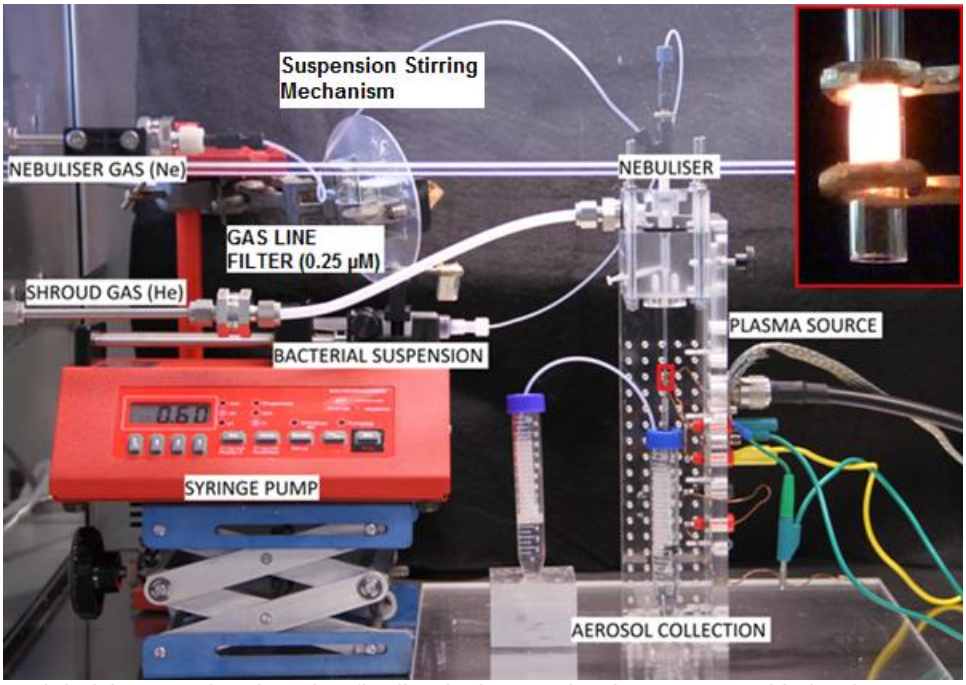

Figure 3.4 Digital image showing the finalised plasma-droplet system with impingement collection apparatus attached. Inset image is a typical He/Ne discharge, without additional tubing attached

3.2.1.2. Droplet Impaction/Collection

For these studies the droplet collection apparatus was removed to allow for the plasma-droplet effluent to interact with liquid and semi-solid surfaces. The distance between the quartz tube end and surface was varied and the plasma-produced species could be protected from interaction with ambient air by flow containment within Tygon ® tubing. Plasma-treated droplets generated from deionised water (dH_2O) interacted with bacteria on agar, as well as agar containing a chemical indicator for hydroxyl radical detection (see section 3.4.2). A cuvette with a redox-indicator solution was positioned under the plasma-droplet effluent and near real-time absorbance measurements of the liquid were taken (see section 3.4.1.2). Please refer to Chapter 4 (Figure 4.1) for schematic diagrams of the experimental apparatus employed for these analyses.

3.2.1.3. Sterility

The syringe pump, shroud, plasma source and droplet collection apparatus were all placed within a sealable workstation equipped with a UV-C (254 nm) lamp and stainless steel interior. All gas lines accessed the cabinet interior through airtight bulkhead unions with particulate filters. Electrical connections entered through the workstation wall using PVC grommets. This arrangement facilitated pre and post experimental decontamination of the workstation interior (15 min UV treatment). The shroud interior and quartz tube were flushed with a solution of 70% Ethanol, rinsed with dH_2O, and finally purged using the gas flows previously mentioned, to remove any residual liquid before and after each experimental run. The gas flows were established and allowed to stabilise for 5 minutes prior to each experiment. All equipment associated with the plasma-droplet system was decontaminated before use by placing in an ultrasound bath (Ultrawave) in deionised water for 20 min, and washing in 70 % ethanol before reassembling. All consumables (e.g. pipette tips, tubes etc.) were purchased sterile, autoclaved at 121 ºC for 15 min or washed with 70 % ethanol and allowed to dry prior to use.

3.2.1.4. Workstation Modifications

The entire plasma-droplet system had to be contained within a controlled environment (i.e. sterile). This workstation, normally used for DNA/PCR analysis, was chosen because it was relatively easy to decontaminate the surface and environment interior before and after experiments, as well as the relative ease at which it could be further modified to suit the projects specific requirements. In order to maintain a sterile (airtight) working environment throughout the experiments, all connections required for the plasma-droplet system had to enter through the workstation walls since the front access window had to be closed during operation. The maximum outer diameter (O.D.) of electrical cables (BNC, banana), gas lines (bulk-head adapters), and miscellaneous (USB cable for impedance probe and fibre-optic cable) were measured using Vernier calipers (Mitutoyo Absolute Digimatic). The tubing was threaded through the centre of an appropriately-sized grommet and then the grommet was positioned inside a pre-drilled hole in the workstation wall.

3.2.2. Bacteria Strain

Escherichia coli (E. coli), non-pathogenic strain 'K-12' (National Collection of Type Cultures (NCTC) 10538) were stored at -80^{o}C in Microbank Cryoprotect vials until required (see section 3.3.2 for cell growth information).

3.2.3. Chemicals

3.2.3.1. Catalase stock solution (Sigma-Aldrich Company Ltd, Dorset, UK: C30-100 MG, Lot# SLBG8704V, 45 mg ml^{-1})

Catalase is an inherent anti-oxidant enzyme present in every *E. coli* cell. It has a molecular arrangement, with a heme group in the active site, which specifically interacts with H_2O_2 to produce relatively inert H_2O and O_2. The addition of catalase to samples allows efficient quenching of the interaction between H_2O_2 and recovered bacterial cells. 100 µl of stock solution was added to 9.9 ml deionised water to achieve a working concentration of 450 µg ml^{-1}. Catalase (0.5 ml) was added to 4.5 ml Ringer's solution used to collect plasma-treated bacteria; final catalase concentration for plasma-treatment of bacteria was 45 µg ml^{-1}. 0.5 ml of catalase was added to 4.5 ml of bacteria suspension to stop the interaction between H_2O_2 for differing exposure times (short exposure study; same concentration as above).

3.2.3.2. Hydrogen peroxide (H_2O_2) – (Sigma-Aldrich Company Ltd, Dorset, UK: 30 % solution)

3.2.3.2.1. Calculation of Molarity

$$\text{Molarity} = \frac{\text{Percentage purity}}{100} \times \frac{\text{density (g L}^{-1})}{\text{molecular weight (g mol}^{-1})}$$

$$= \frac{30}{100} \times \frac{1110}{34.0147}$$

$$= 0.3 \times 32.637$$

$$= 9.79 \text{ M } (9.79 \text{ mol L}^{-1})$$

3.2.3.2.2. Production of 100 ml (V2) of 0.1M (C2) stock solution using 9.79 M H_2O_2 solution (C1)

$$C1 \times V1 = C2 \times V2$$

$$9.79 \times V1 = 0.1 \times 99$$

$$V1 = \frac{0.1 \times 99}{9.79}$$

$$V1 = 1.011 \text{ ml}$$

3.2.3.3. Titanium (IV) oxysulphate – sulphuric acid (Ti-S) (Sigma-Aldrich Company Ltd, Dorset, UK)

Use as supplied; no dilution required.

3.2.3.4. Methylene blue [15 g L^{-1}] (Sigma-Aldrich Company Ltd, Dorset, UK: 03978, Lot# BCBQ0951V)

A redox indicator, methylene blue (MB) was used to probe the chemical activity of the plasma-droplet effluent. This indicator forms a dark blue solution when exposed to an oxidising agent i.e. O_2 under normal laboratory conditions. Interaction with a reducing agent causes molecular re-arrangement and the solution becomes clear (leuco-MB). Further oxidation of the molecule can also result in discolouration. The rate/extent of this reaction can be monitored by measuring the change in absorbance of the solution during exposure (peak wavelength = 668 nm). A stock solution of MB was made by transferring 1 ml of the purchased solution to a 100 ml Scott bottle, covered in aluminium foil, and making a final volume of 100 ml using deionised water (second stock concentration: 150 mg L^{-1} = 4.7 mM). The final reaction concentration of MB was 1.5 mg L^{-1} = 4.7 µM for all experiments.

3.2.3.4.1. Molarity calculation of final reaction concentration

$$\text{Molarity (M)} = \frac{\text{concentration (g L}^{-1})}{\text{molecular weight (g mol}^{-1})}$$

$$= \frac{0.0015}{319.85}$$

$$= 0.00000468 \text{ M}$$

$$= 4.7 \text{ µM}$$

3.2.3.5. Iron (II) sulfate heptahydrate ($FeSO_4.7H_2O$, MW = 278.0146 g mol^{-1}, Sigma-Aldrich Company Ltd, Dorset, UK: 215422-250G Lot#MKBT1090V)

A 1 mM stock solution was made by adding 0.0278 g into 100 ml deionised water was and adjusted to pH 3 (H_2SO_4) using a calibrated pH meter. A working concentration of 0.5 mM was obtained by 1:1 dilution of the stock solution with dH_2O.

3.2.3.6. Agarose (Sigma-Aldrich Company Ltd, Dorset, UK: A-2929 25g, Lot# 053K1496)

One gram of agarose was added to 100 ml dH_2O and dissolution was aided by gentle heating and stirring on a magnetic hot-plate to make a 1% formulation. Ethidium bromide (EtBr) (Sigma) was added to solution and poured into casings for gel electrophoresis.

3.2.3.7. Potassium hydroxide (KOH, MW = 56.11 g mol^{-1})

A 10 mM solution was prepared by adding 1.4028 g to 250 ml dH_2O.

3.2.3.8. Terephthalic acid (TA) 98% (MW = 166.13 g mol^{-1}, Sigma-Aldrich Company Ltd, Dorset, UK: 185361-100g Lot#MKBX0976V)

0.1661 g was added to 100 ml of 10 mM (see above); final concentration of TA = 10 mM.

3.2.3.8.1. TA in agar (custom formulation)

A 1% agarose formulation was added to a solution containing a chemical indicator for detection of •OH and poured into petri dishes. The agar plates provided a semi-solid surface that could detect plasma-generated reactive species. 50 ml of the 10 mM TA/KOH was added to 50 ml of the 1% agar solution and poured into sterile petri dishes. Final volume in petri dish ~ 10 ml; final concentrations of solvents: agar = 1%, TA /KOH = 5 mM.

3.2.3.9. Tris-EDTA (TE) buffer solution (*pH 8.0, Fluka Biochemika*)

Use as purchased; no dilution required

3.3. General Methodology

3.3.1. Quality Control

Balances used to weigh media were performance-checked over the appropriate range using calibrated weights (Oertling). All pipettes were performance-checked before use by dispensing deionised water into a weighing vessel upon a performance-checked balance, and all pipettes used were within 2% of the volume dispensed (i.e. for a 1000 µl pipette, tolerance was ± 20 µl).

3.3.2. Bacteria cell culture

A single bead was removed from the purchased tube stored at -80 ºC and inoculated into 100 ml Nutrient Broth. The bottle was placed in an orbital incubator set at 100 rpm and 37ºC (24 h). 1 ml of the resultant culture was inoculated into 100 ml Nutrient broth and further incubation in the same orbital incubator for 4 hours to achieve a mid-exponential phase culture. 1 ml of cell suspension was transferred into a 1.5 ml sterile Eppendorf tube; the cells were recovered by centrifugation (8161.4 g for 10 min) and the pellet was re-suspended in 9 ml Ringer's solution (RS). The viable cell concentration of the suspension was determined by serial decimal dilutions and colony counting (adapted from [102]) using Nutrient agar. Inoculated agar plates were incubated (37 ºC for 24 h) and the resultant colonies were enumerated.

3.4. Diagnostic techniques: Chapter 4

The following section outlines the analyses used to investigate the plasma-droplet system, specifically the light emission from the plasma and chemical indicator use for plasma-generated reactive species detection and collection.

3.4.1. Optical Analyses

3.4.1.1. Plasma light emission

The end of a fibre-optic camera had a threaded attachment that allowed for easy coupling to a brass block which encased the quartz tube and electrodes. An opening in the brass block, containing the fibre-optic camera, was perpendicular to the quartz tube and the distance between the end of the fibre-optic camera and the nearside wall of the quartz tube was 10 mm. The fibre optic camera was connected to a spectrometer to measure the emission (199-299 nm, Ocean Optics) and the spectra

was analysed using Spectral-viewer. Ultra-violet (UV) light intensity (i.e. irradiance) was also measured using a fully-calibrated spectral radiometer that consisted of a monochromator, photomultiplier tube and integrating sphere. Each component is annually calibrated with a National Institute of Standards Technology (NIST)-traceable light source to accurately detect emission (W/m^2) within the resolution of one nanometre i.e. (W/m^2 nm^{-1}). Please refer to Figure 4.1 A for a schematic representation of the apparatus used.

3.4.1.2. Methylene blue absorbance

Near real-time monitoring of the change in methylene blue (MB) absorbance as a result of exposure to a reducing agent (i.e. plasma-droplet effluent/Fenton-generated $^{\bullet}OH$) was possible by measuring the reduction of the peak absorbance value at 668 nm. MB in a cuvette was placed in an Ocean Optics cuvette holder that allowed for fixed light source and fibre-optic camera connection. The other end of the sensor was connected to a spectrometer (Ocean Optics QE65000) to monitor the absorbance. Quartz cuvettes were pre-cleaned, using 70 % isopropyl alcohol, rinsed with deionised water, and allowed to air-dry before adding solutions. A Schott LED light source positioned directly opposite the other end of the fibre optic cable, allowing for stable absorbance measurement. 2 ml of MB ~ 4.7 µM was exposed to the plasma effluent, with and without aerosols. For comparison, MB degradation by the Fenton reaction (i.e. iron catalysis of H_2O_2, yielding $^{\bullet}OH$) was used. In order for Fe^{2+} to catalyse H_2O_2 and generate $^{\bullet}OH$ (measureable from MB degradation), a strict ratio between must be followed: 1 part Fe^{2+} to 20 parts H_2O_2. After some initial optimisation of the concentrations (data not shown), the initial working concentrations of the solutions were 0.5 mM Fe^{2+} and 10 mM [H_2O_2].

3.4.1.2.1. Methylene blue/Butanol solution exposed to plasma effluent

An $^{\bullet}OH$ scavenger, 1-Butanol, was used to make a stock solution of MB to be exposed to the effluent of the plasma-aerosol system. No change in absorbance was recorded for both plasma and plasma-droplet treatment.

3.4.2. Hydroxyl radical detection: Terephthalic acid

Detection of plasma-produced $^{\bullet}OH$ is possible by measuring the production of a hydroxylated compound generated in the presence of Terephthalic acid (TA), upon UV illumination (Figure 3.5).

The exposed agar plate was placed upon a gel electrophoresis imaging system: UV light source and metallic camera housing with Sony digital camera and UV filter attached to the lens.

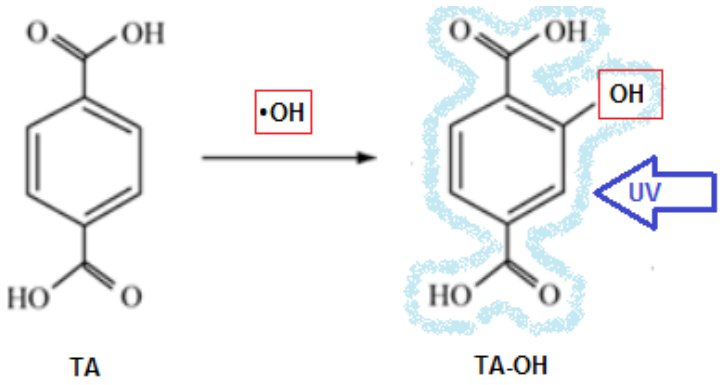

Figure 3.5 Molecular representation of TA interaction with ˙OH to generate TA-OH, which is detectable when irradiated with UV light (adapted from [103])

3.4.3. Hydrogen peroxide measurement in the collection liquid

The amount of H_2O_2 in the collection liquid was determined by its reaction with Titanium (IV) oxysulphate (Ti-S) in an acidic environment, and the reaction product was measured using UV-spectroscopy [104], [105]. The change in peak absorbance intensity (407 nm) is directly proportional to the amount of H_2O_2 present in the liquid. 100 µl of Ti-S was added to 900 µl of plasma-droplet collection liquid, harvested from the cell concentration step of the growth kinetics analysis (1 part Ti-S: 9 parts sample [104]. 200 µl was added to a well of a 96-well microplate (Nunc), with each sample measured in triplicate. Generation of a standard curve of known concentrations of H_2O_2 and the corresponding absorbance values allowed for estimation of H_2O_2 content in the plasma-droplet collection liquid

3.4.3.1. Catalase addition

The exposure of a uniformly dispersed population of bacteria to H_2O_2 over a short time period (10 s) is possible with the introduction of an adequate concentration of H_2O_2 scavenger: e.g. catalase. 0.5 ml catalase was added to 4.5 ml bacteria/H_2O_2 suspension after 10 s exposure to H_2O_2. 1 ml of the solution was centrifuged in order to concentrate the cells. 900 µl of the supernatant was transferred to a sterile Eppendorf tube and used for H_2O_2 measurement, as detailed above.

3.5. Diagnostic techniques: Chapter 5

The next section describes the methods used to assess the anti-bacterial effect of the plasma-droplet treatment system.

3.5.1. Exposure to plasma-generated UV and electric field

Since the plasma is confined within a quartz tube, it is possible to expose cells positioned outside the plasma region in order to eliminate the effect of direct plasma-produced reactive species/chemistry. Bacteria suspension was inoculated onto agar and placed 20 mm from the plasma region, contained within a brass casing with a 2.0 mm diameter hole which the agar was aligned with. Please refer to Figure 5.1 B for a schematic diagram of the positioning of the apparatus and agar plate.

3.5.2. Zone of Inhibition

The diameter of the region devoid of growth after exposure to the plasma and plasma-droplet effluent was measured (droplet liquid type = dH_2O). Incomplete zones of inhibition made determination of the precise region difficult. Contrast analysis across the inhibition zone was carried out to try to standardise the reporting of the plasma treatment of bacteria on agar.

3.5.3. Cell reduction within the treatment area

The initial cell density was varied to ascertain the efficacy of plasma treatment. A less homogeneous inhibition zone was achieved when the cell density was high compared to when the cell concentration was reduced.

3.5.4. Plasma-droplet flow visualisation

A solution of green food dye was delivered to the nebuliser to generate droplets under the same conditions as the plasma-droplet experiments. It must be noted that the plasma was not on for this analysis; plasma interaction with droplets may influence the turbulence of the droplet flow post-plasma exposure. By using a coloured dye to generate droplets, it was hoped that this would aid visualisation of the droplet flow and their expected region of influence on an agar surface. Droplets impacted onto semi-transparent agar and the diameter of the impact region was measured.

3.6. Diagnostic techniques: Chapter 6

The final analyses relate to investigating bacteria viability after exposure to plasma within a liquid droplet, and recovery in liquid.

3.6.1. Cell viability

The number of viable bacteria cells collected after plasma exposure was determined by serial decimal dilutions using RS and inoculating Nutrient agar plates to determine total viable aerobic counts and Chromocult agar to determine total coliform counts. 100 µl of collection liquid was inoculated directly onto agar plates for '0' dilution (i.e. limit of detection = <10 cfu/ml); and 100 µl of collection liquid was added to 900 µl sterile filtered RS and 100 µl inoculated onto agar (i.e. representing a '1 in 10' dilution), and so on.

3.6.2. Growth kinetics of plasma-treated cells

The sample that was used for growth kinetics was also used for H_2O_2 measurement. 1 ml of the collection liquid was centrifuged in order to concentrate the cells. 900 µl of the supernatant was transferred to a sterile Eppendorf tube and used for H_2O_2 measurement; the remaining 100 µl cell suspension was re-suspended in fresh Nutrient broth and used for growth kinetics analysis. 150 µl volumes from each test and control conditions were placed in rows of wells of a 96-well plate (Nunc). Measurements were taken every 15 minutes at 600 nm for 24 h, incubated at 37ºC, using a microwell plate spectrometer (FluoStar Omega). General Settings: Positioning delay = 0.5 sec, No. of kinetic windows = 1, No. of cycles = 49, Measurement start time = 0.0 sec, No. of flashes per well and cycle = 20, Cycle time = 1800 sec / Wavelength settings: discrete wavelengths = Yes, No. of wavelengths = 1, Wavelength = 600nm / Shaking options: double orbital = Yes, Shaking frequency = 500rpm, Additional shaking = after each cycle, Shaking time = 300 sec).

3.6.2.1. Short-exposure to hydrogen peroxide solution

Bacteria cells were exposed to different concentrations of a stock solution of H_2O_2 until the reaction was stopped with the addition of catalase. The growth kinetics analysis of the H_2O_2-exposed cells was processed in the same way as the plasma-treated cells. The absence of H_2O_2 after catalase addition was measured using the technique detailed previously (see section 3.4.3. H_2O_2 measurement in the collection liquid).

3.6.2.2. Fenton Reaction-generated hydroxyl radical exposure

Iron-catalysed degradation of H_2O_2 generates $^{\bullet}OH$. *E. coli* in suspension were subjected to Fenton-generated $^{\bullet}OH$ and the effect on viability and growth kinetics was assessed. The reaction was quenched with the addition of catalase, an efficient scavenger of H_2O_2. Detection of a biomarker for lipid peroxidation was also conducted, as well as H_2O_2 measurement post-treatment. This analysis was then used to compare with the plasma treatment, specifically plasma-generated $^{\bullet}OH$.

3.6.3. Lipid peroxidation: Thiobarbituric acid reactive substances assay

Lipid peroxidation due to the action of plasma-produced reactive species was assessed using the Thiobarbituric Acid Reactive Substances (TBARS) assay (Cayman Chemical Company, U.S.A.) and the protocol was followed as per the manufacturer guidelines. Malondialdehyde (MDA) is an inherent by-product of lipid peroxidation and can be used as an indicator of cellular oxidative stress. Under strict experimental conditions (i.e. at ~100ºC and low pH), Thiobarbituric acid (TBA) forms an adduct molecule with MDA, which can be detected using light spectroscopy.

3.6.4. Deoxyribonucleic acid amplification by polymerase chain reaction

The samples collected in Tris-EDTA recovery liquid were used as a template for PCR and DNA quantification. 1 ml was transferred into a 1.5 ml Eppendorf tube, which contained whole cells and any released DNA from damaged cells. A second 1 ml sample was filtered through a 0.22 µm syringe filter (Nalgene) in order to remove any intact cells and the filtrate collected into a 1.5 ml Eppendorf tube. Both samples, filtered and unfiltered, were placed in a heat-block (Eppendorf Thermostat Plus) for 8 minutes at 99ºC. The tubes were then centrifuged for 10 min at 15682 g and the supernatant was subjected to PCR analysis, using primer set UAL1939b & UAL2105b [106], targeting the highly-conserved *E. coli* uidA gene. SYBR Green (Quantitect Mastermix, Qiagen) was used as the nucleic acid-specific dye for DNA detection using a real-time thermal cycler (Rotor-Gene Q, Qiagen). The thermal cycling programme was performed according to the mastermix manufacturer's instructions, using a primer annealing temperature of 60ºC.

4. PLASMA-DROPLET SYSTEM CHARACTERISATION

4.1. Introduction

Atmospheric-pressure non-thermal plasmas in contact with liquid generate ultra-violet (UV) radiation and biologically-active species (e.g. hydroxyl radical, $^{\bullet}OH$ and hydrogen peroxide, H_2O_2) making it a viable technology that is suitable for sterilisation applications across a number of industries. A key challenge in plasma-liquid studies is plasma stability and control of the resultant chemistry [107]. Plasma-liquid investigations have largely focused on the interaction with bulk liquid, either via electrical discharge within a volume of water or liquid surface interaction in direct contact with the plasma in dielectric-barrier discharge (DBD) or atmospheric-pressure plasma jet (APPJ)-like configurations. Optical emission spectroscopy (OES) of the plasma offers the researcher an insight into gas-phase species density within the bulk discharge region, however the technique is by no means definitive [108]. Reactive species generated in the gas-phase have been detected in liquid exposed to the effluent of an APPJ and the species diffused into the liquid from the gas-phase and did not form as a result of secondary reactions in the liquid phase [57]. Bulk-liquid treatment by plasma generates a complex cascade of reactions which makes experimental measurement of the short-lived reactive species difficult and largely dependent on the resolution of the detection technique. The more stable, neutral species generated from plasma-liquid interaction (e.g. H_2O_2) are thought to be responsible for the extended cytotoxicity and mutagenic effect towards cells [9]. Water vapour can be added to the feed gas to reduce the amount of bulk liquid interaction with the plasma to try to control species generation, but too much liquid content in the gas-phase prevents plasma formation. Comparison of OES profiles with varying water content allows for estimation of the contribution towards species generation in the gas-phase. The density of gas-phase reactive species decreases as a function of increasing water content in the plasma, due to a reduction in the effective ionisation energy of the plasma-water mixture [107].

Investigations of non-thermal plasma interaction with a controlled droplet flow are limited to gliding-arc and transient-spark discharges [96], [109], [110]. In these systems, the plasma zone is not well defined and the degree of plasma exposure any given droplet receives differs greatly. Nevertheless, droplets exposed to transient spark discharge plasma generated the highest yield of H_2O_2 production measured from liquid positioned underneath the plasma-droplet effluent [96]. The

disadvantages of this technique are the high power required to sustain the discharge and the lack of control over the droplet characteristics that enter the plasma zone.

The generation of stable atmospheric-pressure plasmas within confined geometries, that remain ignited with gas-entrained droplet flow, would allow for a relatively uniform droplet exposure without complete droplet evaporation. It is postulated that the plasma-droplet system will be able to transport short-lived reactive species away from the discharge zone, potentially enhancing the species lifetime in liquid. Using chemical indicators that produce a measurable change upon interacting with radicals, plasma-generated short-lived reactive species ($^{\bullet}OH$) were detected and estimates of $^{\bullet}OH$ lifetime in liquid exposed to plasma-generated UV are ~4 μs (N_{OH} ~ 1 x 10^{16} cm^{-3}, [94]. Liquid exposure to plasma and the chemical species produced are of biomedical relevance but the fast reaction rates and short life-times in liquid make precise measurement difficult [7]. The chemistry induced by plasma treatment of liquid is complex and poses a significant experimental challenge to measure and monitor the generation of species and the effect on biological systems. Reactive species are scavengers of the solvated electron, and a secondary reactive species acts as a scavenger of the first, and so on. The physical processes that occur at the interface are not well understood and quantifying the short-lived reactive species generated by plasma-liquid interactions remains a key experimental challenge [8]. It was hoped that by exposing low volume liquid droplets to the plasma in a controlled environment, the chemistry could be controlled and allow for better understanding of the plasma-liquid interface.

4.1.1. Aims and Objectives

4.1.1.1. Aims

- Detect short-lived $^{\bullet}OH$ generated by plasma-droplet system
- Investigate the relationship between plasma power and long-lived species generation and their stability/lifetime: Focus on H_2O_2

4.1.1.2. Objectives

- Monitor the interaction between plasma-produced species and a chemical indicator; compare with equivalence studies where possible
- Collect plasma-treated droplets and measure the content immediately after generation as a function of plasma power and at numerous time points thereafter

4.2. Methodology

The atmospheric-pressure plasma system used in the current study allows for the exposure of droplets in flight through a diffuse discharge. A schematic diagram of the plasma-droplet system (Figure 4.1) shows the electrical probe and optical equipment used to analyse the plasma emission and a redox chemical indicator. The apparatus in Figure A was used to measure the light emission from the plasma, namely OES and UV radiometry (FO = fibre-optic camera, S = spectrometer). In Figure B, an •OH-specific indicator (TA) was added to agar and exposed to the plasma-droplet effluent. Figure C displays how the change in methylene blue (MB) absorbance was monitored upon exposure to the effluent (LS = light source) and plasma-treated droplets were collected in a liquid reservoir for subsequent quantification by using the apparatus in Figure D. For more details, please refer to Chapter 3: Materials and Methods. Briefly, liquid contained within a syringe was delivered (Q_{liq} = 10 µl min^{-1}) to a nebuliser using Ne to generate droplets (Q_{Ne} = 1.0 slm). A second gas flow (Q_{He} = 3.5 slm) aided the Ne-droplet flow along a quartz tube towards the plasma. Droplets were entrained within the gas flow and had a parabolic flow profile [100]. After being exposed to the plasma for ~ 120 µs, the droplets passed through ambient air before collection in a liquid surface or interaction with a semi-solid agar surface. In another configuration, the path to the surface or collecting liquid was shielded from ambient air via an extended tube.

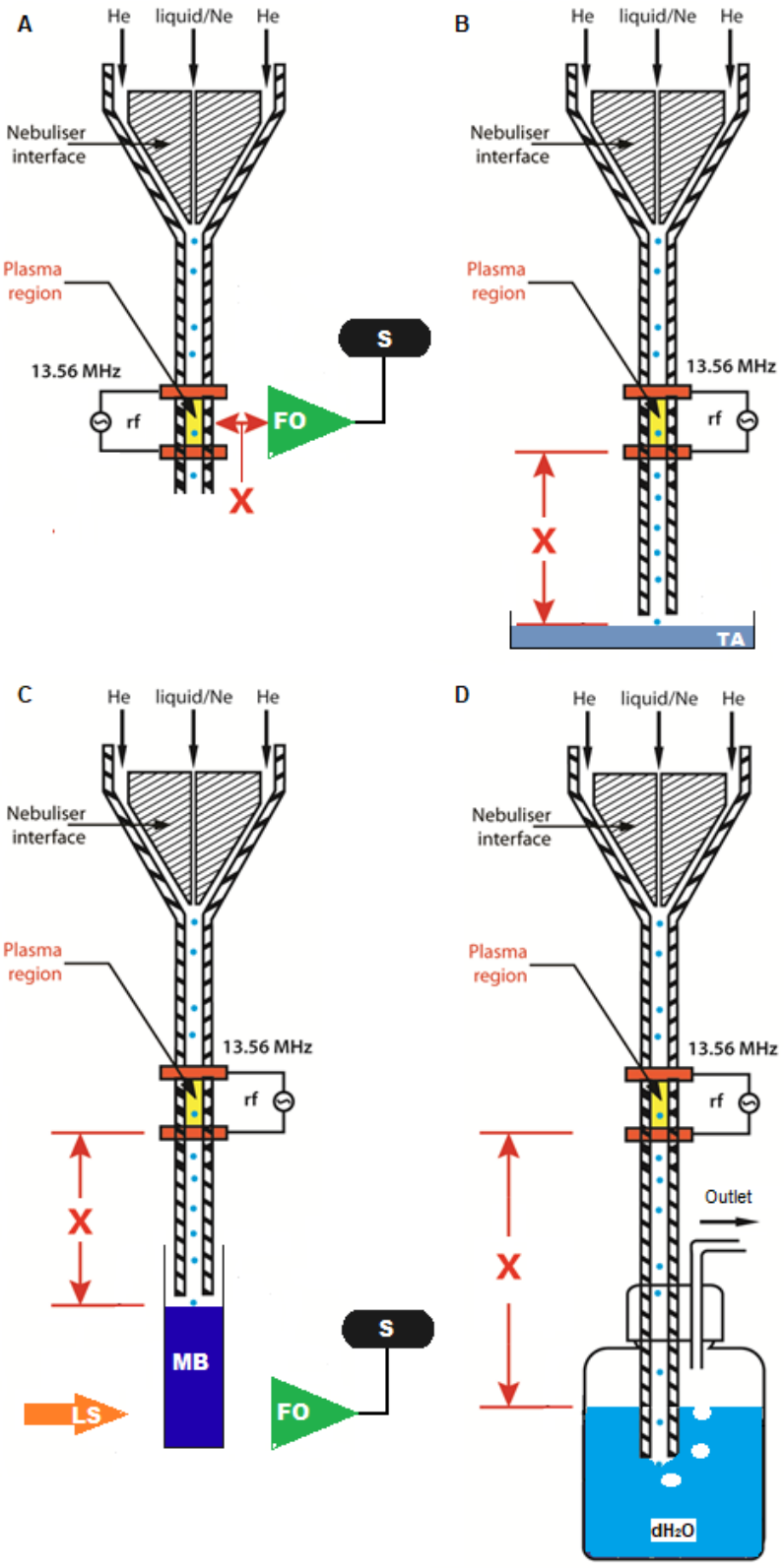

Figure 4.1 Schematic diagrams showing the different apparatus employed to investigate the plasma-droplet system: Figure A = OES and UV radiometry (FO = fibre-optic camera, S = spectrometer), Figure B, an $^{\bullet}$OH-specific indicator (TA) exposed to the plasma-droplet effluent, Figure C methylene blue (MB) change in absorbance upon exposure to the effluent (LS = light source) and plasma-treated droplets were collected in a liquid reservoir for subsequent quantification by using the apparatus in Figure D

4.3. Results

4.3.1. Electrical characterisation: Plasma Power and Electron Density

The electrical properties of the plasma were obtained using a radio-frequency (rf) current-voltage probe (Octiv VI, Impedans) connected in-line with the high voltage electrode. Power (13.56 MHz) was delivered to the electrode via an impedance matching network and nominal (set) input power values were varied from 80 W to 120 W. The net plasma power (P_{NET}) was calculated by first subtracting the measured rf reflected power from the forward power when the plasma was ignited ($P_{ONforward} - P_{ONreflected}$), and then from this deducting the power value when the plasma was off (P_{OFF}):

$$P_{NET} = (P_{ONforward} - P_{ONreflected}) - P_{OFF} \qquad \textbf{(4.1)}$$

There was a good correlation between the input power and the calculated net power of the plasma (Figure 4.2). In a similar plasma system, an estimate of the time-averaged electron density (N_e) was determined from the plasma resistance, and varied from 3 x 10^{12} cm^{-3} (without aerosol) to 7 x 10^{12} cm^{-3} (with aerosol) for set power values between 40W and 70W [100]. The gas parameters were He:Ne 3.5 slm:0 slm (without aerosol) and 3.5 slm: 1 slm (with droplets) The estimated N_e was observed to increase with plasma power. An additional probe was used to measure the current in the plasma afterglow and the electron temperature (T_e) was estimated to be 5 ± 2 eV. In a similar plasma configuration, substituting He with Ar, (100W set power, 0.2 slm), values of gas temperature (490K), electron density (1.8 x 10^{14} cm^{-3}) and temperature (1.1 eV) were determined [111].

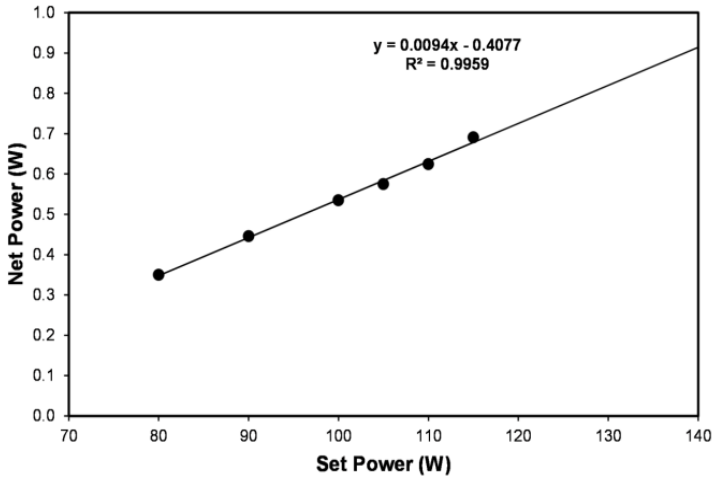

Figure 4.2 Graph showing the calculated net plasma power when the set (i.e. input) power was varied

There was little difference in the measured electrical data obtained when droplets were flowing through the plasma, compared to the gas-only (dry) plasma conditions. This suggests the electrical characteristics of the plasma are not greatly influenced by the presence of droplets. The following section investigates the relationship between the plasma electrical properties and the chemical species generated, with and without droplets, via detecting the light emission of the plasma.

4.3.2. Optical Emission Spectroscopy

Photons released from the reactive species generated by plasma can be detected by measuring the emission using a high-resolution fibre-optic cable connected to a spectrometer i.e. optical emission spectroscopy (OES). The end of the cable was fixed to a brass casing which enclosed the plasma, orientated at 90º to the quartz tube (Figure 4.1 A). Emission from the plasma-droplet system was obtained between 300 and 400 nm and analysed using Spectral-viewer software (Figure 4.3).

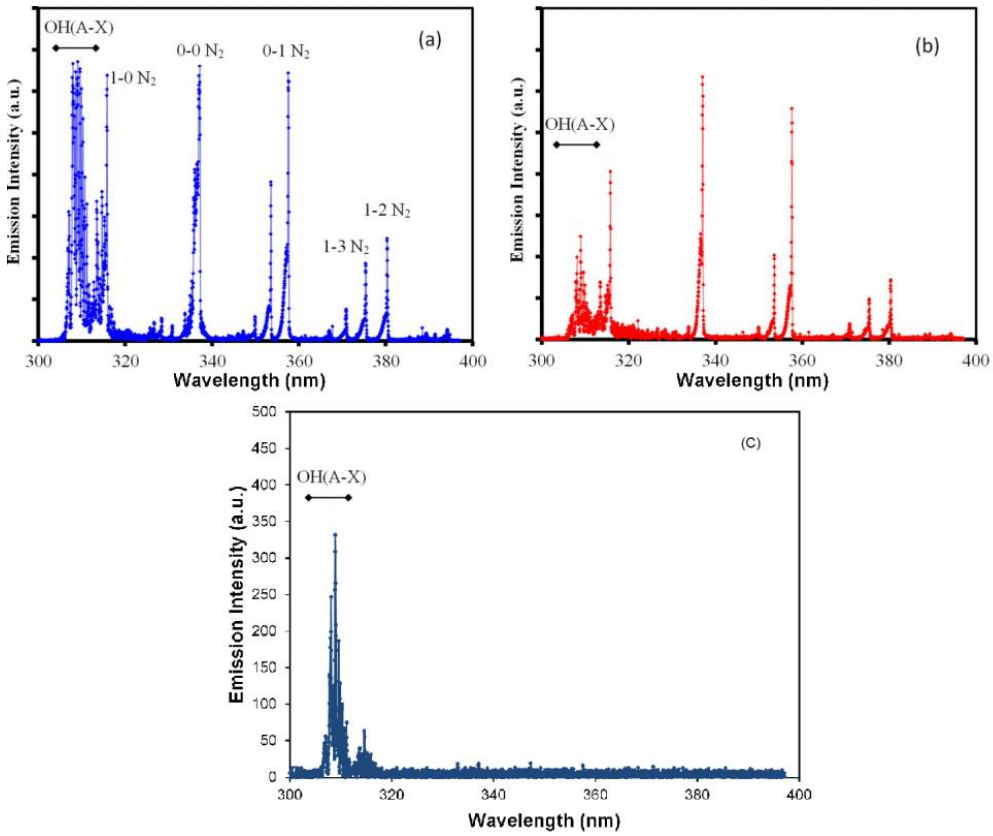

Figure 4.3 Emission spectra from He/Ne plasma with additional 0.1 % N_2 without droplets (a) and with droplet flow (b). When no N_2 was added to the feed gas (c), only $^{\bullet}$OH(A-X) emission was observed. Graphs (a) and (b) are from [100]

A specific property of plasmas generated in contact with liquid is the generation of $^{\bullet}$OH [112]. The emission intensity of the $^{\bullet}$OH lines reduced when the droplet flow was on, relative to the 'dry' plasma condition when only gas was used i.e. without droplets (Figure 4.3). Hydroxyl radicals were produced without droplets possibly due to impurities in the compressed gas bottles or from imperfect seals between the components that compose the plasma-droplet system. The level of impurities, including water vapour, in the supplied He & Ne gas has a negligible effect in the plasma compared to the expected impurity levels derived from other sources within the experimental setup. The effect of the latter is negligible when compared to the water vapour produced by an evaporating droplet. In the absence of droplets, some $^{\bullet}$OH will be produced from water vapour from these other sources. From literature, under similar experimental setups with a nominal zero input water vapour content, the $^{\bullet}$OH concentration was found to be 1 – 2 orders of magnitude lower than that obtained from plasmas with <500ppm added H_2O vapour. Other studies have reported similar results from 'gas-only' plasmas [59]. Gas temperature estimated from the spectra were ~ 335 K for flow rates > 2 slm that increased up to ~600 K for low flow rates (0.15 slm; [100]. Removal of N_2 from the feed gas caused the

disappearance of the spectral lines associated with N-containing species and only $^{\bullet}$OH emission remained in the measured range (199 – 299 nm) (Figure 4.3 (c)).

4.3.2.1. Radiometry of ultra-violet light emissions (250-400 nm)

The biological importance of UV radiation was discussed in Chapter 2, causing dimerization of nucleotide bases in the DNA molecule that impairs normal cell function. Measurement of the UV emission from the plasma was conducted using a fully-calibrated spectral radiometer, which consisted of a monochromator, photomultiplier tube and integrating sphere. Each component is annually calibrated with a National Institute of Standards Technology (NIST)-traceable light source to accurately detect emission (W/m^2) within the resolution of one nanometre i.e. (W/m^2 nm^{-1}). Plasma emissions in the ultra-violet (UV) wavelength range are due to molecular bands of NO, $^{\bullet}$OH and N_2 [113]. Transitions between the ground and first excited states of $^{\bullet}$OH release energy in the form of photons that have a wavelength of ~ 310 nm [108]. The intensity of UV (i.e. irradiance) emission was measured by positioning a fibre-optic cable connected to the spectral radiometer at different distances along the horizontal plane from the plasma (Figure 4.1 A).

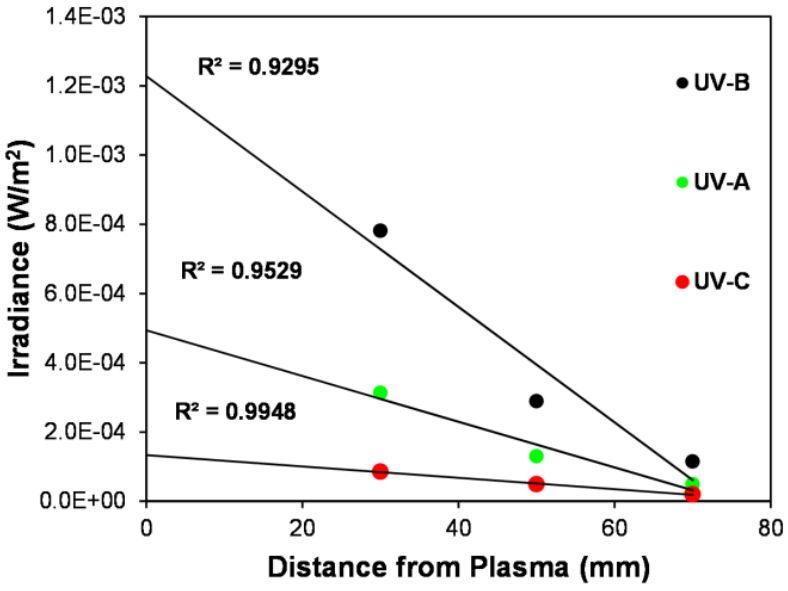

Figure 4.4 Irradiance of ultra-violet light measured at fixed distances from the plasma. Wavelength ranges: UV-A = 320-400 nm, UV-B = 280-320 nm, UV-C = <280 nm.

Mean irradiance measurements within wavelength ranges: UV-A = 320-400 nm, UV-B = 280-320 nm, UV-C = <280 nm are presented in Figure 4.4. Plasma-generated UV irradiance decayed as a

function of measurement distance at atmospheric-pressure. The majority of the irradiance was composed of UV-B light, a trend that existed for all 3 distances from the plasma. UV-A was the next most prevalent followed by UV-C. For details on how the irradiance measurements may affect biological material, please refer to Chapter 5, section 5.3.1.

4.3.3. Chemical Indicators for Species Detection

4.3.3.1. Plasma-generated hydroxyl radical detection: Terephthalic acid

Terephthalic acid (TA) has been used to detect plasma-generated $^{\bullet}$OH in liquid after direct exposure to the plasma [103] or through plasma-initiated UV photolysis of liquid [94]. $^{\bullet}$OH reacts with TA to form 2-hydroxyterephathalic acid (TA-OH) that is detectable upon UV irradiation of the liquid. TA was incorporated into agar positioned at different distances from the plasma and exposed to the plasma effluent, with and without droplets (Figure 4.1 B). The customised agar formulation that incorporated an $^{\bullet}$OH-specific chemical indicator (TA) successfully detected plasma-generated $^{\bullet}$OH due to the observation of a visible region on the exposed surface. The distance between the agar surface and the end of the tube was 0.5 cm. Numbers on the images denote centimetres from the end of the quartz tube; the plasma was an additional 1.5 cm inwards along the quartz tube. After exposure to the treatment, the agar plate was transferred onto a UV light source with a camera attached to metallic housing for imaging.

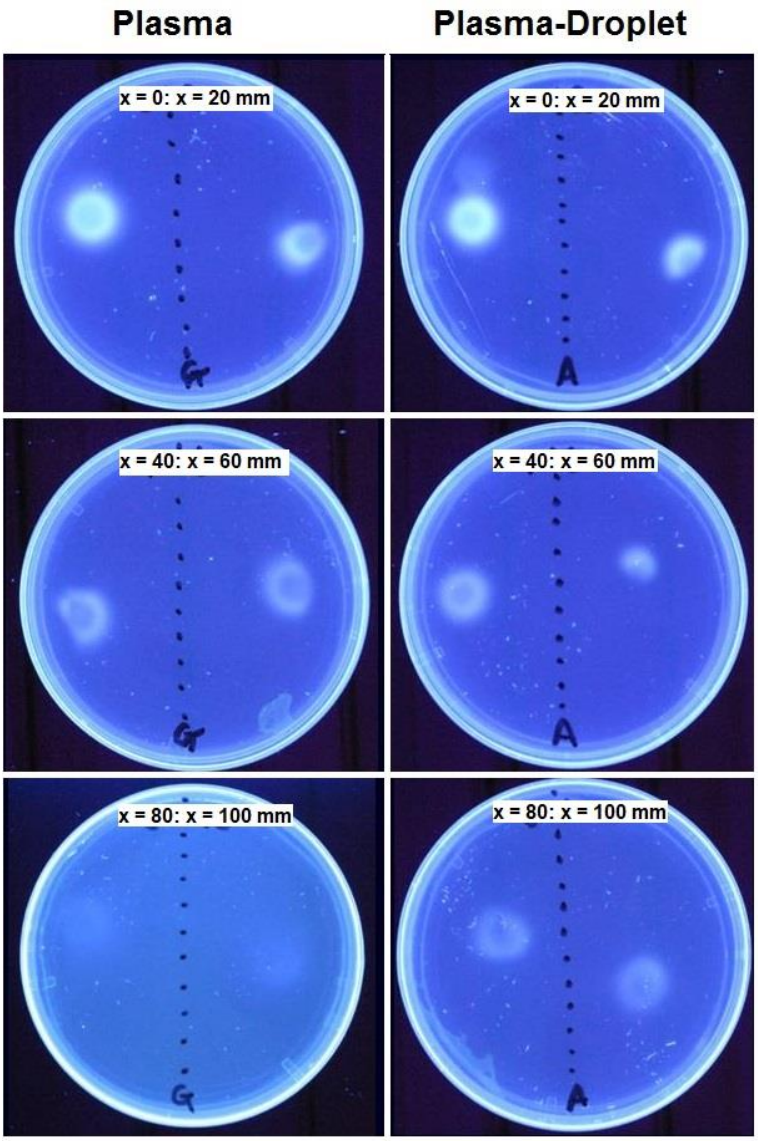

Figure 4.5 Images show agar plates containing ˙OH-specific indicator (TA) exposed to the plasma effluent with and without droplets placed upon a UV transilluminator (254 nm)

Figure 4.5 shows images of regions on the agar surface, where plasma-generated ˙OH had interacted with TA, and were visible up to 100 mm from the quartz tube end (115 mm from the plasma). The plasma effluent was completely enclosed within tubing which protected ˙OH from interacting with ambient air molecules and the distance between the agar surface and the end of the tubing that delivered the plasma-generated ˙OH was 5 mm. The amount of plasma generated ˙OH reaching the agar decreased as the TA agar to plasma distance increased. At the furthest distance, TA-OH was visually more evident from agar treated with plasma-droplet effluent compared to agar exposed to the plasma effluent without droplets. The impact area appears to have a ‘doughnut-like’

shape: stronger signal around the edge of zone compared to centre, possibly due to turbulent interaction between the plasma-droplet effluent and the solid surface.

4.3.3.2. **Reaction kinetics of plasma-generated hydroxyl radical**

Certain chemical compounds can be used as redox indicators due to their measurable, colourimetric response to oxidising/reducing agent exposure. One such chemical is tetramethylthionine chloride, more commonly known as 'methylene blue' (MB). MB forms a dark blue solution in ambient laboratory conditions i.e. exposed to an oxidiser (O_2). Further exposure to a highly reactive species such as $^{\bullet}OH$ causes the solution to lose colour (Figure 4.6). Measurement of the change in solution absorbance can be used to monitor the interaction with the reactive species and estimate the reaction kinetics. Atmospheric-pressure plasma treatment of MB causes the solution to turn colourless, thought to be a result of exposure to reactive species [114]. H_2O_2 was formed during plasmas interaction with MB and the reduction was enhanced with the addition of Fe^{2+}. H_2O_2 on its own did not affect MB solution absorbance and the direct interactions with plasma-generated $^{\bullet}OH$ as well as additional formation via Fenton-like reactions were thought to play a major role in MB degradation [115].

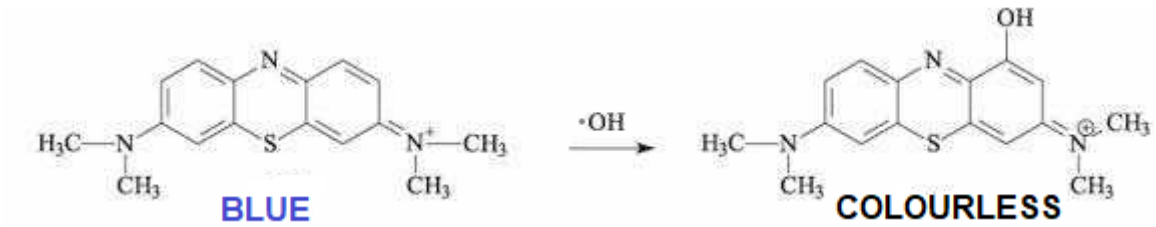

Figure 4.6 Molecular representation of the conversion MB undergoes in response to exposure to an oxidising agent e.g. hydroxyl radical (modified from [116])

Purchased MB solution was diluted with deionised water to create a range of concentrations and the absorbance of the solutions was measured at 668 nm to generate a calibration curve (Figure 4.7). There was a good correlation between MB concentration and the measured absorbance at 668 nm (R^2 = 0.9986). A custom optical system was used to monitor real-time absorbance changes during plasma treatment. This consisted of a cuvette holder (Ocean Optics) equipped with stable connections for a light source and the fibre optic cable positioned directly opposite. A cuvette containing MB was inserted beneath the plasma-droplet effluent for different treatment times and distances from the plasma (Figure 4.1 C). The calibration data also validated the custom optical

system, as well as the relationship between MB concentration and the solution absorbance measurement at 668 nm. The initial concentration of MB was 1.5 mg L^{-1} for all experiments (~4-5 x 10^{-6} M).

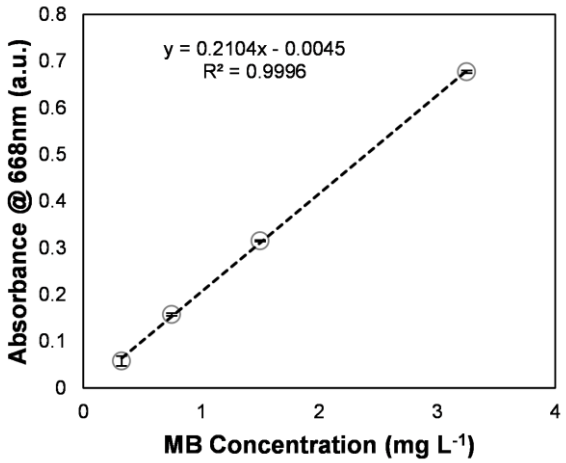

Figure 4.7 Calibration graph using custom-designed apparatus (Figure 4.1 C) showing a good correlation between different concentrations of MB and the absorbance of the solution measured at 668 nm

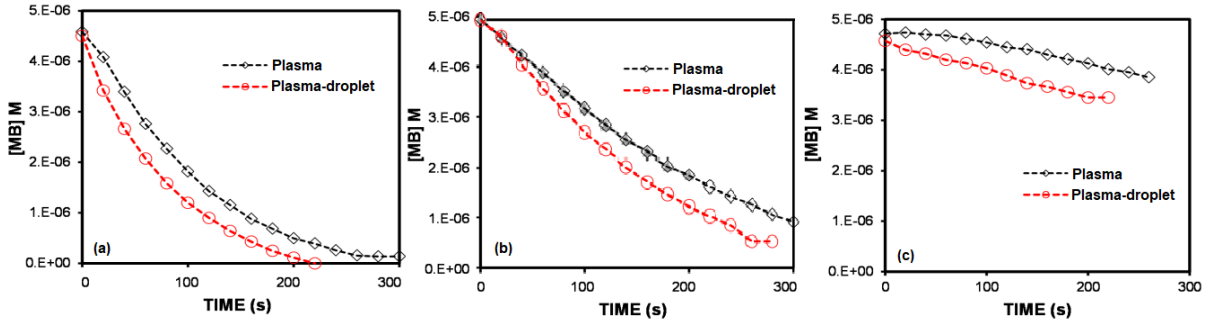

Figure 4.8 Images show the reduction on MB concentration as a function of time measured at three separate distances from the plasma: (a) = 50 mm, (b) = 95 mm, (c) = 150 mm.

MB concentration reduced upon exposure to the plasma effluent, and the reduction was more rapid when the solution was closest to the plasma (Figure 4.8). For all distances, MB reduced more rapidly when exposed to plasma-treated droplets, compared to when only a 'dry' plasma effluent interacted with the solution. MB absorbance was unchanged when droplets not exposed to plasma were used, thus eliminating any dilution effect from droplet addition. This suggests that the droplets became chemically-active after plasma exposure and can enhance reduction of MB, up to 150 mm from the plasma source. The rate of MB degradation during plasma treatment was shown to be

greatly dependant on the distance from the plasma (Figure 4.8). MB degradation rate was more rapid when the solution was closest to the plasma (50 mm). 150 mm was the furthest distance from the plasma that could be measured due to the vertical orientation of the shroud and limited space available underneath the system. It isn't known if larger distances from the plasma would show a greater distance between the two treatments.

4.3.3.2.1. Equivalence Study: Fenton Reaction

Fenton Reaction is known to generate $^{\bullet}OH$ radicals from Fe^{2+}-catalysed dissociation of H_2O_2 via at least 7 cyclic reactions involving Fe^{2+} and Fe^{3+} [117]. The initial $^{\bullet}OH$ generation, provided the concentration of H_2O_2 is much higher than Fe^{2+}, is 1:1 stoichiometric with $[Fe^{2+}]$ and the dominant reaction is

$$Fe^{2+} + H_2O_2 \xrightarrow{k_1} OH^- + {}^{\bullet}OH \qquad \textbf{(4.2)}$$

The initial $^{\bullet}OH$ generation rate is therefore given by [118]

$$\frac{d[{}^{\bullet}OH]}{dt} = k_1[Fe^{2+}]_0[H_2O_2]_0 \qquad \textbf{(4.3)}$$

The initial rate of MB degradation follows the kinetic reaction equation

$$R_{MB} = k_{MB}[MB]_0^{\,m}[Fe^{3+}]_0^{\,n}[H_2O_2]_0^{\,p} \qquad \textbf{(4.4)}$$

which was found to be almost first order in each reactant [117]. No change in MB absorbance was observed when in solution with H_2O_2 alone; only with the addition of Fe^{2+} did the reaction proceed. A ratio of 1 part Fe^{2+} to 20 parts H_2O_2 for the two Fenton reactants was chosen from the literature [119]. MB absorbance data was converted into MB concentration using the same calibration curve from the analysis of the plasma treatment (Figure 4.7).

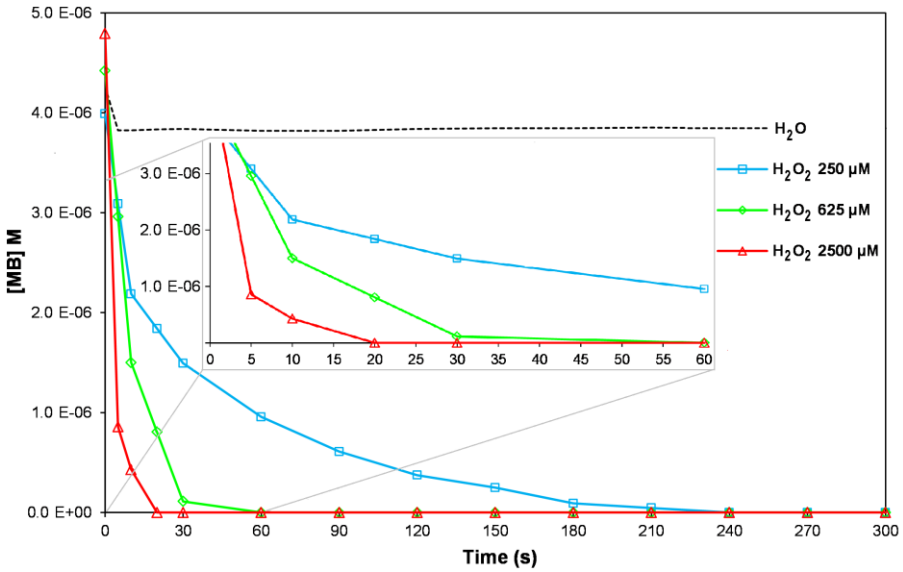

Figure 4.9 MB exposed to the Fenton reaction showed a reduction in concentration as a function of exposure time and Fe^{2+} concentration. It must be noted that H_2O_2 was also increased in a 1:20 proportion with Fe^{2+} in the reaction mix. 90 % degradation of MB was achieved after 10 seconds and there was complete degradation after 20 seconds exposure to the most concentrated Fenton reaction

Similar MB degradation profiles were produced for plasma-treated droplets at 50 mm from the plasma (Figure 4.8) and Fenton-type exposure using Fe^{2+} concentration of 250 µM. MB absorbance degraded 50 % after ~ 80 s for plasma exposure, after 55s of plasma-droplet exposure while with Fenton-like exposure, ~ 20 s was required. In the Fenton case, the $^{\bullet}OH$ is generated directly in the MB solution whereas the plasma-generated $^{\bullet}OH$ must diffuse from the MB surface before it can cause an effect.

4.3.4. Detection of plasma-generated hydrogen peroxide

In addition to impaction onto a liquid surface (i.e. MB), plasma-treated droplets were also collected via impingement (Figure 4.1 D). Plasma-liquid studies have reported H_2O_2 detection in the treated liquid [95] and the best yield was obtained using droplets sprayed through a low power Ar plasma [96]. In this study, the plasma-treated droplets were contained within the quartz tube and transported directly into the collection liquid. This prevented any losses through interaction with ambient air or any other external species that may impede droplet transport or H_2O_2 generation. A simple and effective technique for determining H_2O_2 concentration in solution is through its reaction with titanium sulphate (Ti-S) [104]. One part Ti-S is mixed with 9 parts H_2O_2 and the reaction product, perititanic acid (H_2TiO_4), is yellow with an absorbance peak around 407 nm:

$$Ti^{4+} + H_2O_2 + 2H_2O \rightarrow H_2TiO_4 + 4H^+ \quad \textbf{(4.5)}$$

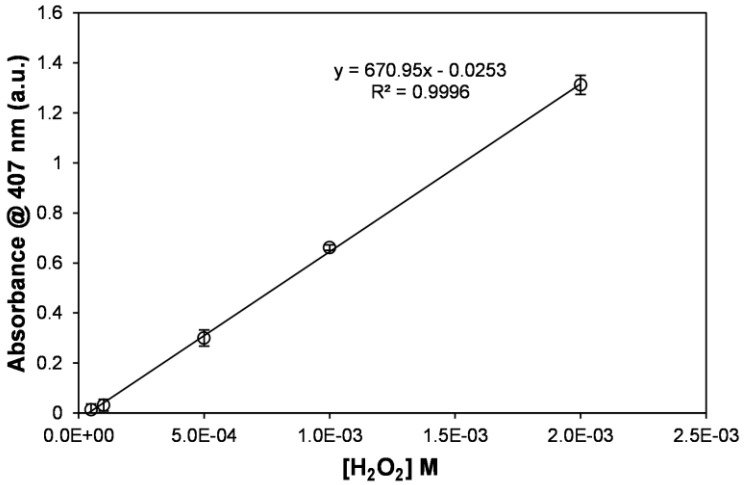

Figure 4.10 Calibration graph showing the absorbance measured at 407 nm due to the reaction of different concentrations of H_2O_2 with Ti-S. Assay limit of detection (LoD) = 10 µM.

There is a good linear relationship between the mean absorbance measurements at 407 nm from seven separate experiments for different concentrations of H_2O_2 after addition of Ti-S and (R^2 = 0.9996) (Figure 4.10). These data were then used to estimate H_2O_2 concentration in liquids that collected the plasma-treated droplets. Figure 4.11 shows the concentration of H_2O_2 in the droplet as a function of plasma power for two different liquid types, non-buffered deionised water (dH_2O) and buffered Ringer's solution (RS). Estimates of droplet concentration were made by measuring the amount in the collection liquid, and multiplying by a dilution factor of 13 which was determined from the amount of liquid used to generate the H_2O_2 divided by the final volume of collection liquid i.e. 300 µl/4000µl.

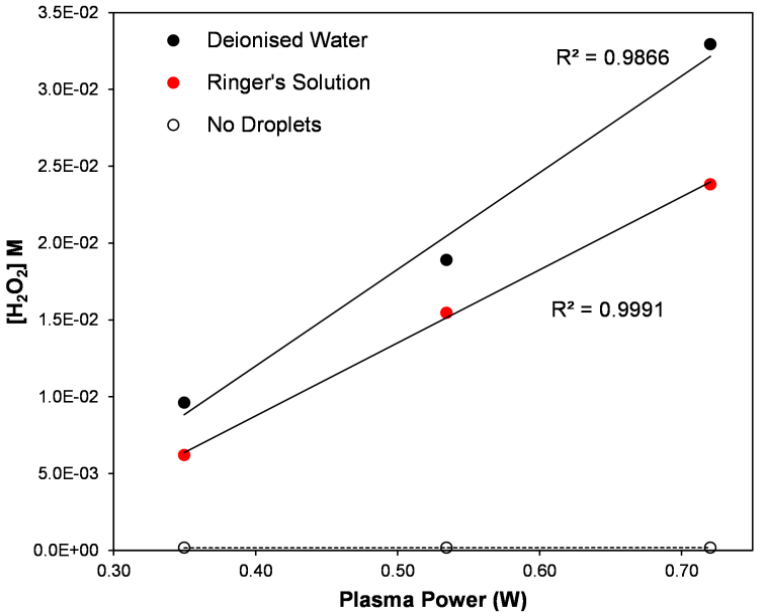

Figure 4.11 Graph showing the relationship between plasma power and H_2O_2 concentration when buffered and non-buffered solutions were used to generate droplets. When no droplets were plasma-treated, the concentration of H_2O_2 did not increase with plasma power (~170 µM across all powers).

For all plasma powers, the plasma-treated dH_2O droplets generated more H_2O_2 than when RS was used, reaching a maximum concentration of ~30 mM in the droplet after exposure to the highest plasma power.

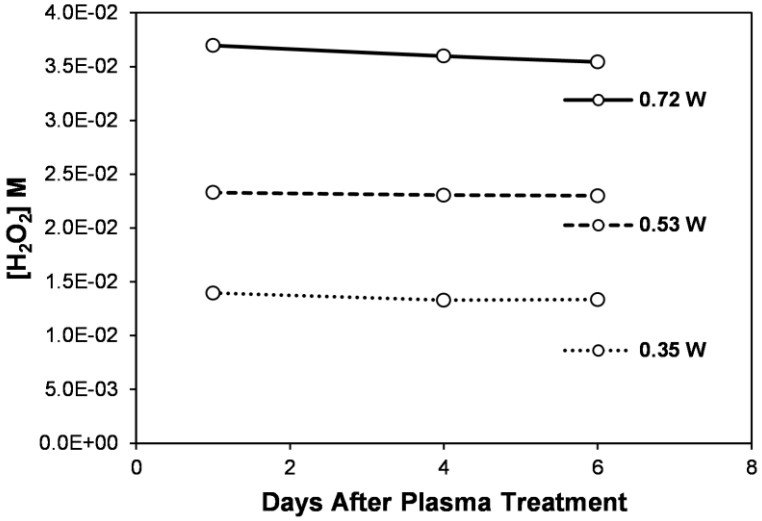

Figure 4.12 Graph of the calculated concentration of H_2O_2 from plasma-treated dH_2O droplets collected into deionised water. Samples were analysed 1, 4, and 6 days after plasma processing in order to assess the stability of the plasma-produced H_2O_2.

Figure 4.12 is a graph that displays the stability of H_2O_2 generated from dH_2O droplet exposure to plasma. There is little reduction in the H_2O_2 concentration up to 6 days after generation and similar stability was observed when RS droplets were plasma treated. All collection liquids showed excellent stability and the H_2O_2 can remain at a constant level for months after generation.

4.3.5. Droplet flow profile analysis

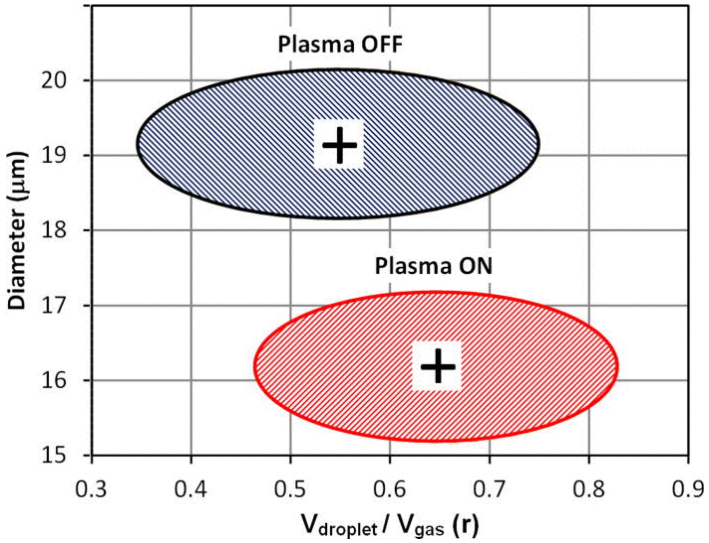

Figure 4.13 Droplet diameter and velocity normalised to the radial gas velocity, showing arithmetic mean values with and without plasma. The shaded areas represent 1 standard deviation for both parameters [100]

The diameter of droplets was estimated by hi-speed imaging upon exiting the quartz tube [100]. It was shown that the diameter of the plasma-treated droplets reduced, compared to droplets without plasma exposure. The droplet velocity relative to the surrounding gas flow was faster for the plasma-treated droplets, possibly due to the smaller droplet diameter allowing for less surface area to interact with ambient air molecules which would slow the droplet down. Figure 4.13 shows a reduction in droplet diameter was observed after plasma treatment, relative to the untreated droplets. It is thought that the reduction in diameter could be due to evaporation-related effects but droplets do remain intact after transit through the electrical discharge. Water vapour, as a result of droplet evaporation, might exist in the discharge zone and play a role in the species generation using this plasma-droplet treatment system.

4.4. Discussion

In this chapter the plasma induced chemical reactions within the droplet are investigated. The long-life H_2O_2 species can be directly measured in the collection liquid while short-lived hydroxyl radicals were investigated by exposing a Methylene Blue probe to the plasma effluent at different distances from the plasma source.

4.4.1. Hydrogen peroxide generation in droplets

H_2O_2 was detected in the liquid used for collecting plasma-treated droplets via impingement. There was a linear relationship between plasma power and H_2O_2 generation; H_2O_2 was not generated without plasma. The established protocol was to collect droplets in a liquid filled cuvette for 30 min collection time in order to achieve a reasonable signal after dilution in the cuvette. Acidification of the liquid after plasma treatment has been reported in the literature, however no change in pH was observed using the plasma-droplet system. The buffering capability of the liquid used for droplet generation and collection had some effect on plasma-generated H_2O_2; deionised water generated slightly more H_2O_2 than when Ringer's solution was used. Regardless of liquid type, the H_2O_2 generated is stable for weeks after plasma-treatment.

Vasko *et al* [58] modelled the chemistry in an rf plasma jet with He and H_2O gases and derived the main H_2O_2 production and loss mechanisms. The plasma density was simulated for ~10^{17} m^{-3}. The experimental values of H_2O_2 and $^{\bullet}OH$ used were ~10^{20} m^{-3}. The dominant H_2O_2 generation mechanism (>99%) was found to be by gas phase $^{\bullet}OH$ recombination involving a third body (M)

$$^{\bullet}OH + {}^{\bullet}OH + M \rightarrow H_2O_2 + M \ (>99\%) \qquad \textbf{(4.6)}$$

and the dominant loss mechanisms due to gas phase reactions are

$$\begin{aligned} &(a)\ {}^{\bullet}OH + H_2O_2 \rightarrow H_2O + HO_2 \\ &(b)\ e + H_2O_2 \rightarrow {}^{\bullet}OH + {}^{\bullet}OH + e \end{aligned} \qquad \textbf{(4.7)}$$

For $^{\bullet}$OH, the dominant gas phase generation mechanisms are

$$\begin{aligned}
&\text{(a) } e + H_2O \rightarrow H + {}^{\bullet}OH + e \\
&\text{(b) } H + HO_2 \rightarrow {}^{\bullet}OH + {}^{\bullet}OH \\
&\text{(c) } H_2O^+ + H_2O \rightarrow H_3O^+ + {}^{\bullet}OH \\
&\text{(d) } e + H_2O \rightarrow {}^{\bullet}OH + H^- \\
&\text{(e) } O(^1D) + H_2O \rightarrow {}^{\bullet}OH + {}^{\bullet}OH \\
&\text{(f) } OH(A) + H_2O \rightarrow H_2O + {}^{\bullet}OH \\
&\text{(g) } e + H_2O_2 \rightarrow {}^{\bullet}OH + {}^{\bullet}OH + e
\end{aligned} \qquad \textbf{(4.8)}$$

and dominant gas phase loss mechanisms are

$$\begin{aligned}
&\text{(a) } {}^{\bullet}OH + {}^{\bullet}OH + M \rightarrow H_2O_2 + M \\
&\text{(b) } He + H + {}^{\bullet}OH \rightarrow He + H_2O \\
&\text{(c) } {}^{\bullet}OH + {}^{\bullet}OH \rightarrow H_2O + O \\
&\text{(d) } O + {}^{\bullet}OH \rightarrow H + O_2 \\
&\text{(e) } {}^{\bullet}OH + H_2O_2 \rightarrow H_2O + HO_2 \\
&\text{(f) } {}^{\bullet}OH + HO_2 \rightarrow O_2 + H_2O
\end{aligned} \qquad \textbf{(4.9)}$$

The main generation reaction for H_2O_2 i.e. (4.6), and loss mechanism for $^{\bullet}$OH i.e. 4.9 (a) requires a third body. The presence of liquid droplets may act as such a body. Generation and loss of species may happen not only in the gas phase but due to plasma interactions with bulk liquid or droplets. For example electron bombardment can ionise $^{\bullet}$OH leading to OH^- and can dissociate H_2O_2 into $^{\bullet}$OH + OH^-. Schneider *et al.* [120] developed a global liquid reaction model to investigate electron and $^{\bullet}$OH effects in the radiolysis of water based on 79 reactions. However it has been found in plasma-liquid studies that H_2O_2 is mainly formed in the gas phase and then dissolves in the liquid [53], [57], [95], [121]. With droplets, the liquid surface is totally surrounded by plasma and there may be less mixing and dilution compared to bulk liquid. Therefore it may not be reliable to assume that the plasma – induced chemistry mechanism are the same in droplet and bulk liquids.

Locke and Shih [95] reviewed the plasma production of H_2O_2 and surveyed the variation in generation rate with different systems and configurations. They report a wide range from ~10^{-10} mol s^{-1} to a maximum of ~4 x 10^{-4} mol s^{-1} for a microwave plasma with steam. A similar generation rate was reported for plasma interaction with bubbles in an O_2 gas but for plasmas with droplets the rate is ~10^-

^{6} mol s^{-1} which is similar to that of rf glow discharge and corona interactions with bulk liquid. However in this work, the generation rate varied with power from ~0.7 mol s^{-1} to ~4.1 mol s^{-1}. This is almost 4 orders of magnitude greater than previously reported, for any configuration, and 6 – 7 orders of magnitude greater than reported for plasma – droplet generation rates. In Table 1, the measured generation rate (in M s^{-1}) is compared to a range of literature reports. Again the observed rate for our plasma – droplet configuration is greater by at least four orders of magnitude compared to other plasma configurations. This significant enhancement is similar to that observed in Au nanoparticle synthesis using the same plasma-droplet system employed in the current study [122]. A gold precursor $HAuCl_4$ (1mM) was loaded into the liquid and nanoparticles were formed by reduction of the Au ions to metal. Here we observed nanoparticle synthesis rates that we many orders of magnitude faster than from standard chemical or radiolysis methods. Other plasma studies that have used droplets have reported production rates ranging from 80 nM s^{-1} [123] to 2 µM s^{-1} [109]. The gliding-arc/transient spark discharges used in these studies are not diffuse, the plasma region is not well-defined and the H_2O_2 generation pathways are unclear. Zhao *et al* [124] obtained a yield of ~80 g kWh^{-1} for a H_2/O_2 DBD plasma over flowing methanol. A similar value was obtained by Burlica *et al* [125] using a spray nozzle in a pulsed gliding arc plasma with a high water flow rate of 30 – 120 mL h^{-1}. This is reported as the highest yield so far obtained from a plasma system, yet the H_2O_2 generation rate is low, 10^{-7} mol s^{-1} [95]. For the plasma – droplet system, with a 6 mL h^{-1} flow rate, the maximum energy yield is ~0.5 g kWh^{-1}. This value is similar to that obtained from RF and corona discharges over liquid [95].

Author	Plasma Type	Liquid (vol)	H_2O_2 synthesis rate (M s^{-1})	H_2O_2 Assay
Rutherford (this work)	rf (diffuse)	dH_2O (0.3 ml - droplets)	1.2 – 4.1	Ti-S
Rutherford (this work)	rf (diffuse)	RS (0.3 ml - droplets)	0.7 - 3	Ti-S
Shih [126]	in liquid	H_2O (bulk)	8.00E-04	Ti-S
Gorbanev [57]	Jet (parallel field kHz)	H_2O & D_2O (vapour)	5.00E-04	$K_2[TiO(C_2O_4)_2]•2H_2O$
Wende [127]	Jet (rf)	PBS (bulk - 0.1 ml)	1.33E-05	AR & Ti-S
Girard [128]	Jet (ns-pulsed)	DMEM (bulk 2.5 ml)	5.00E-06	Ti-S
Wende [127]	Jet (rf-kINPen)	RPMI/PBS	3.17E-06	AR & Ti-S
Machala [109]	Transient Spark	H_2O (spray)	2.67E-06	Ti-S
Machala [109]	Transient Spark	PB (spray)	1.33E-06	Ti-S
Porter [129]	GAD	H_2O (bulk 500 ml)	8.33E-07	Ti-S
Laurita [130]	DBD	PB (bulk - 15 ml)	8.33E-07	Ti-S
Kirkpatrick[131]	in liquid	H_2O (1000 ml)	6.25E-07	Ti-S
Laurita [130]	DBD	H_2O (bulk - 15 ml)	5.00E-07	Ti-S
Laurita [130]	DBD	ES (bulk - 15 ml)	5.00E-07	Ti-S
Burlica [123]	GAD	H_2O (spray)	7.95E-08	Ti-S
Hsieh [132]	DC (diffuse)	H_2O (bulk)	6.00E-08	Ti-S
Doležalová [74]	Jet (rf-kINPen)	NaCl (6 ml)	2.67E-08	Ti-S
Reddy [115]	DBD	MB (bulk)	1.18E-09	Ti-S
Mann [133]	Jet (rf-kINPen)	NaCl (2 ml)	6.17E-10	Ti-S
Doležalová [3]	DBD	H_2O (bulk)	2.80E-10	Ti-S
Hansch [54]	DBD	NaCl (5 ml)	1.25E-10	Ti-S

Table 1 Calculated H_2O_2 production rates rate (M s^{-1}) from plasma-liquid studies from the measured H_2O_2 and the plasma treatment time. Plasma type notations: rf = radio-frequency (13.56 MHz), GAD = gliding-arc discharge, DBD = dielectric-barrier discharge. n.b. H_2O_2 synthesis rate = gas flow x treatment time

A droplet passing through a plasma is possibly a more simplified system compared to standard plasma-liquid studies and it may be possible to estimate the expected H_2O_2 after a time in the plasma. Knowing the density of OH^{gas} or $H_2O_2{}^{gas}$ would allow calculation of the flux density and ignoring losses in the droplet, this would indicate the upper limit of $[H_2O_2]^{droplet}$. The flux density, Γ, ($m^{-2}\,s^{-1}$) of a gas species is given by

$$\Gamma = \frac{N\bar{v}}{4} \qquad \textbf{(4.10)}$$

where N is the species density and v the average velocity given by

$$\bar{v} = \sqrt{\frac{8k_B T_{gas}}{\pi m}} \qquad \textbf{(4.11)}$$

The dominant production mechanism for H_2O_2 is given in equation (4.6). It is accepted that this reaction occurs in the gas phase to form H_2O_2 which then dissolves in the liquid. Therefore knowledge of $H_2O_2{}^{gas}$ would be required. However with the droplet, OH from the gas phase may also recombine on the droplet surface to form H_2O_2. Reported OH densities in plasmas vary from 10^{19} m^{-3} to 10^{21} m^{-3} and are discussed in more detail below. For H_2O_2, Vasko *et al.* [58] report experimental values of ~10^{20} m^{-3} for an RF jet. Ding *et al.* [134] simulated a rf He/H_2O (1000ppm) plasma and obtained $H_2O_2{}^{gas}$ densities of 10^{19} – 10^{21} m^{-3} depending on model and conditions and 10^{20} m^{-3} for OH^{gas}. Liu *et al* [55] from simulation, obtained $H_2O_2{}^{gas}$ densities of 10^{16} m^{-3} for 1 ppm H_2O up to 10^{19} m^{-3} for 1000 ppm in a He/H_2O plasma. Winter *et al.* [121] observed $H_2O_2{}^{gas}$ fractions linearly dependent on humidity in the afterglow of a 1 MHz rf jet with Ar/H_2O gas. At 1000 ppm, they obtained a value of 4 ppm (~10^{20} m^{-3}) for $H_2O_2{}^{gas}$. They also estimated the generation rate at 8 x 10^{15} s^{-1} for $H_2O_2{}^{gas}$ molecules. This is much lower than what was achieved using the plasma – droplet system, as detailed above.

Assuming a $H_2O_2{}^{gas}$ density of 10^{20} m^{-3}, and a gas temperature of 350 K, the calculated flux density from (4.10) is 1.2 x 10^{22} $m^{-2}\,s^{-1}$. Using a mean droplet radius (at the plasma exit) of 6.8 μm and a residence time in the plasma of 120 μs, the total number of $H_2O_2{}^{gas}$ molecule impacts on the droplet is 8 x 10^8 (i.e. 10^{-15} moles) which leads to an average droplet concentration of 1 mM which is of

similar magnitude to that observed. This assumes that all the impacting molecules are dissolved in the liquid. Plasma-liquid studies that focussed on gas-phase H_2O_2 sequestering into a liquid phase have referenced Henry's Law as an important mechanism to consider [53]. Henry's constant (H^{CP}) relates to the proportionality between the concentration of gas in a liquid and its partial pressure in the gas phase and is dependent on temperature. This mechanism can also be applied to plasma-generated species in the gas phase and how they diffuse into a liquid. The maximum concentration of gas-phase H_2O_2 that can diffuse into a liquid can be estimated from

$$[H_2O_2]^{liquid} = H^{CP}_{H_2O_2}(T)\left(\frac{N_{H_2O_2}}{N_{los}}\right)P_{atm} \qquad \textbf{(4.12)}$$

where Henry's constant for H_2O_2 ($H^{CP}_{H_2O_2}$) at 298 K is ~ 1 M Pa^{-1}, ~ 0.21 M Pa^{-1} at 320 K and 0.03 M Pa^{-1} at 350 K. P_{atm} is atmospheric-pressure (~1 x 10^5 Pa) and the Loschmidt constant (N_{los}), the particle number density in an ideal gas, is 2.686 x 10^{25} m^{-3} at standard temperature and pressure (STP). Therefore, the maximum $[H_2O_2]$ in liquid is 0.1 M (at a liquid temperature of 320 K) and 0.016 M (at a liquid temperature of 350 K). These values are the maximum allowed at the surface of the droplet and the ability of droplet to absorb H_2O_2 depends on how quickly it diffuses away from the surface. The gas temperature is ~350K but the temperature of the droplet, due to evaporation, is given by the wet bulb temperature which cannot be calculated analytically. A numerical estimated value of 320K was used, based on a gas temperature of 350 K (private communication), and therefore the maximum allowed surface concentration is 0.1 M. If the H_2O_2 is located in a surface shell of penetration depth l_p, then for the maximum shell concentration (0.1 M) to match the average measured $[H_2O_2]$, l_p can be estimated from

$$l_p = \frac{\overline{[H_2O_2]}.Vol_{drop}}{[H_2O_2]_{\max} A_{drop}} \qquad \textbf{(4.13)}$$

For a maximum shell concentration of 0.1 M, l_p must be at least 40 nm. The diffusion constant for H_2O_2 ($D_{H_2O_2}$) in H_2O is ~1.4 x 10^{-9} m^{-2} s^{-1}, and over the droplet residence time in the

plasma the H_2O_2 diffusion length (L_{diff}) can be estimated from

$$L_{diff} = \sqrt{D_{H_2O_2} t} \qquad \textbf{(4.14)}$$

When t ~120 µs, H_2O_2 travel is ~ 400 nm, which is almost ten times the minimum allowed shell thickness and suggests that H_2O_2 is likely to diffuse fast enough so that the surface concentration limit is not reached and Henry's constant can be ignored. Therefore the assumption of a $H_2O_2^{gas}$ density of 10^{20} m^{-3} is reasonable. Also this analysis suggests that sufficient formation of H_2O_2 is possible due to $^{\bullet}OH$ recombination in the gas phase rather than on the liquid surface. The Henry's constant (H^{CP}) for $^{\bullet}OH$ is ~10^{-4} M Pa^{-1} and therefore much less $^{\bullet}OH$ can be absorbed by the droplet compared to H_2O_2 ($H^{CP}_{H_2O_2}$ (293 K) ~1 M Pa^{-1}). Equation (4.12) estimates that maximum possible [H_2O_2] according to Henry's Law is not reached and the molecule diffuses away from the surface before the opportunity to react with other gas-phase reactive species. These processes all occur during the total droplet time of flight (~ 10 ms) and it is unlikely that equilibrium will have been reached during this time period.

4.4.2. Hydroxyl radical delivery from plasma treated droplets

The results from the previous section indicate the droplet becomes chemically active after plasma exposure. $^{\bullet}OH$ was detected 115 mm from the plasma and the intensity was greater with droplet flow than without. The molecular structure of MB is altered upon exposure to the plasma effluent and in response to Fe^{2+}-catalysed degradation of H_2O_2, converting to leuco-MB and the solution becomes colourless. Both plasma and Fenton treatment techniques generated $^{\bullet}OH$, causing a change in absorbance therefore monitoring the absorbance change can also act as a diagnostic for plasma or Fenton-generated $^{\bullet}OH$. The plasma-exposed droplets caused a reduction in MB concentration and the rate was faster with droplets than without. When the distance between MB and the plasma was furthest, it took longer for the absorbance to change compared to when the distance was reduced. It was important to quantify the UV from the plasma since it can generate reactive species, and compare it to a known biocidal dose. Radiometry of the plasma-UV emission suggests the majority of the signal is within the UV-B wavelength range (280 – 320 nm), which corresponds well with the energy level diagram for $^{\bullet}OH$ (A-X) and the wavelength of the photon released. The

estimated maximum UV exposure of a droplet to UV is 10^{-3} W m^{-2} while travelling through the plasma for 120 μs, thereafter decreasing rapidly with distance for the remainder of flight. Exposure of MB to a PCR workstation UV source positioned at 50 mm (8 W/m^2, 254 nm) did not alter MB absorbance nor generate any measurable H_2O_2, OES data from the plasma without droplets detected $^{\bullet}OH$ radicals (peak absorbance at ~310 nm) which reduced in intensity when droplets were introduced. Since the majority of H_2O_2 is generated in the high density plasma region, an H_2O_2 generation rate of 0.08 mol s^{-1} was calculated by multiplying the measured concentration in the collection liquid by the droplet time of flight in plasma (i.e. 120 μs) and was shown to be much higher than currently reported in the literature. This will be discussed more fully after the following section, which attempts to gain a deeper insight into reactive species generation from liquid droplet exposure to plasma.

The change in MB concentration upon exposure to the plasma effluent, with and without droplets, allowed for determination of the reaction rate kinetics. For plasma with and without droplets, the concentration of MB with time at 3 distances (50 mm, 95 mm, 150 mm) from the plasma was obtained from the pre-determined calibration curve of absorbance (668 nm) vs MB concentration, Figure 4.7. A typical characteristic is shown for 50 mm Figure 4.14:

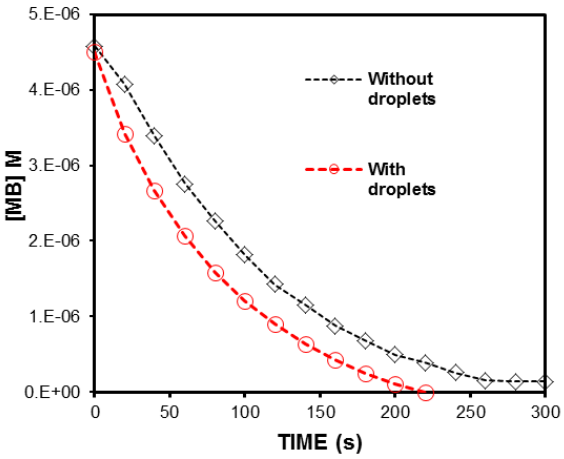

Figure 4.14 The change in MB concentration as a function of treatment time, with and without droplets (d = 50 mm)

The [MB](x,t) characteristic, for the plasma without droplets, can be obtained assuming a pseudo-1st order rate equation i.e.

$$[MB] = [MB]_0 e^{-k_{obsMB}t} \qquad \textbf{(4.15)}$$

and a $\log_e$-plot ($ln[MB]=ln[MB]_0 - k_{obsMB}t$) shows a high quality fit at all 3 distances, Figure 4.15:

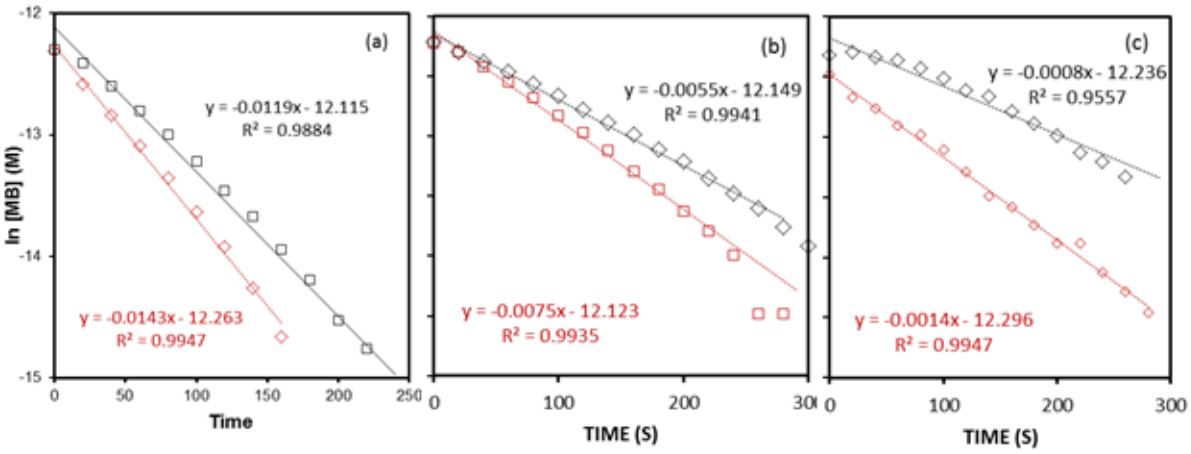

Figure 4.15 Logarithm of the concentration of MB as a function of exposure time (a) 50mm, (b) 95mm, (c) 150mm distance from plasma without (black) and with (red) droplets

From the y-intercept values in Figure 4.15 (a) to (c), the effective concentration at the plasma (t = 0) i.e. [MB](0,0) of 6 µM is obtained by extrapolation (Figure 4.16).

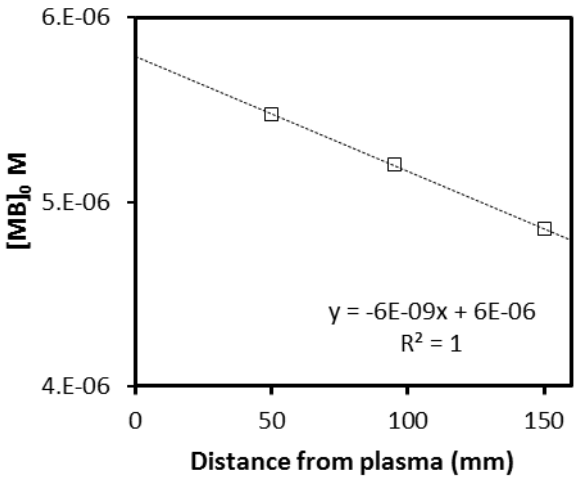

Figure 4.16 Plot of the y-intercept from Figure 4.15 for each distance to give a value for the initial concentration of MB when t=0

Following the approach by Liang *et al.* [135], a kinetic model for ˙OH oxidation of MB can be developed based on the main reactions:

$$\begin{aligned} MB + {}^{\cdot}OH &\xrightarrow{k_a} {}^{\cdot}MB - {}^{\cdot}OH \\ {}^{\cdot}MB - {}^{\cdot}OH + {}^{\cdot}OH &\xrightarrow{k_b} {}^{\cdot}MB - (OH)_2 \\ {}^{\cdot}OH + {}^{\cdot}OH &\xrightarrow{k_c} H_2O_2 \end{aligned} \qquad \textbf{(4.16)}$$

where ˙MB-(OH)$_n$ is a degradation intermediate. The MB degradation rate is given by:

$$\frac{-d[MB]}{dt} = k_a[{}^{\cdot}OH][MB] \qquad \textbf{(4.17)}$$

and assuming [˙OH] is constant, then from the pseudo-first order relationship in:

$$k_{obsMB} = k_a[{}^{\cdot}OH] \qquad \textbf{(4.18)}$$

This may be a reasonable assumption, given fit quality to the linear relationship in Figure 4.15. From the reactions in (4.19), the rate expression for ˙OH is

$$\frac{d[{}^{\cdot}OH]}{dt} = -k_a[{}^{\cdot}OH][MB] - k_b[{}^{\cdot}OH][{}^{\cdot}MB - {}^{\cdot}OH] - k_c[{}^{\cdot}OH]^2[H_2O_2] + G \qquad \textbf{(4.20)}$$

where G is the OH radical generation rate. If [˙OH] is constant, i.e. steady-state conditions, and $k_a \approx k_b$ [136] then

$$G = k_a[{}^{\cdot}OH][MB] + k_a[{}^{\cdot}OH][{}^{\cdot}MB - {}^{\cdot}OH] + k_c[{}^{\cdot}OH]^2[H_2O_2] \qquad \textbf{(4.21)}$$

Also, from (4.17) it can be stated approximately that

$$[MB] = [MB]_0 - [{}^{\cdot}MB - {}^{\cdot}OH] \qquad \textbf{(4.22)}$$

and using the ratio k_c/k_a ~0.5,

$$G = k_a[{}^{\cdot}OH]\left([MB]_0 + \frac{1}{2}[{}^{\cdot}OH][H_2O_2]\right) \qquad \textbf{(4.23)}$$

Inserting from (4.19) gives

$$G = k_{obsMB}\left([MB]_0 + \frac{1}{2}[\cdot OH][H_2O_2]\right) \qquad \textbf{(4.24)}$$

and if the $[^{\bullet}OH][H_2O_2]$ product is assumed to be negligible compared to the initial $[MB]_0$ (~6 μM) then the $^{\bullet}OH$ radical generation rate can be estimated from

$$G = k_{obsMB}[MB]_0 \qquad \textbf{(4.25)}$$

with $[MB]_0$ obtained experimentally from the y-intercept (Figure 4.16). Alternatively, for each distance the product $k_{obsMB}(x)[MB](x,0)$ can be obtained from the slope and intercept of each graph in Figure 4.15 as shown in Figure 4.17.

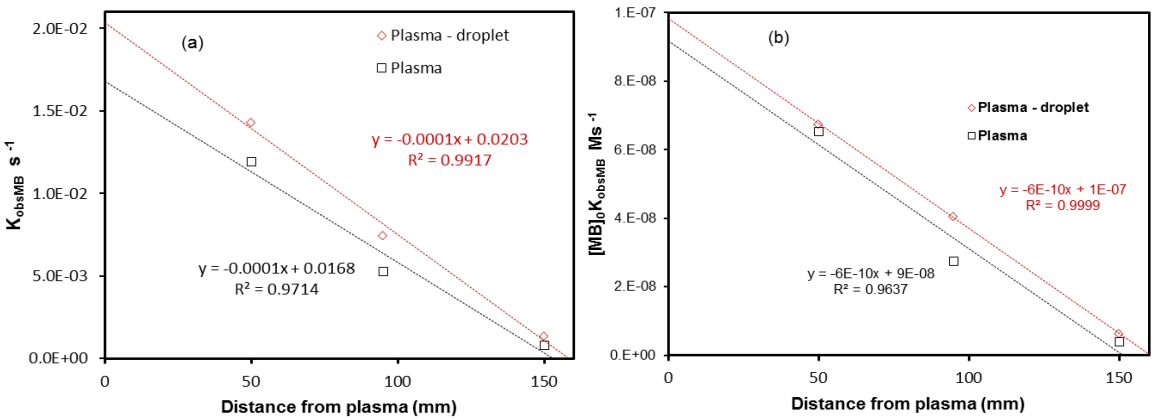

Figure 4.17 (a) Plot of the observed reaction rate constants (K_{obsMB}), derived from the slope in Figure 4.15 with (red) and without (black) droplets and (b) plot of product $[MB](x,0)k_{obsMB}(x)$ vs distance where [MB](x,0) is obtained from the y-intercept.

From the plot of molar flux (without droplets), Γ_{molar}, in Figure 4.17 (b), an estimate of the OH^{gas} density which acts as the generation source G, can be obtained at any distance from the plasma by obtaining the $^{\bullet}OH$ radical flux density, Γ,

$$\Gamma_{\bullet OH} = N_a \frac{\Gamma_{molar}}{A_{plasma}} \qquad \textbf{(4.26)}$$

and from this the OH^{gas} density

$$N_{\bullet OH} = \frac{4\Gamma_{\bullet OH}}{v_{\bullet OH}}$$
$$where \qquad \textbf{(4.27)}$$
$$v_{\bullet OH} = \sqrt{\frac{8k_B T_{gas}}{\pi m_{\bullet OH}}}$$

For a measured gas temperature (T_{gas}) of 350K, the $^{\bullet}OH$ gas density profile is given in Figure 4.18.

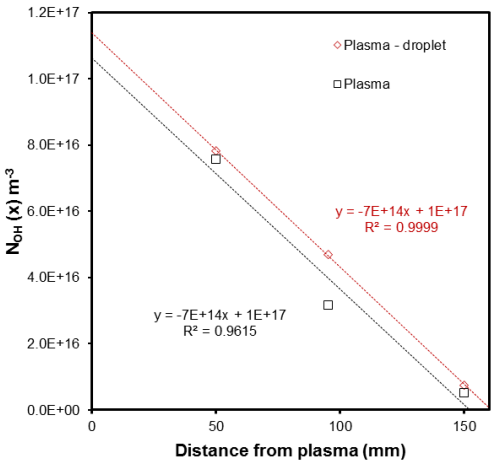

Figure 4.18 Estimated $^{\bullet}OH$ gas density (N_{OH}) with distance from the plasma (black). The estimate of equivalent $^{\bullet}OH$ gas density to produce the same effect as plasma treated droplets is shown in red

Plasma exposure of MB, without droplets, implies a nominally low water content as the path to the surface is enclosed, with a high He gas flow, except at the final 5 mm of travel. It is therefore to be expected that ingress of water vapour due to surface evaporation and laboratory humidity would occur only along the final millimetres (>5mm) of travel. Benedikt *et al.* [59] determined the minimum $^{\bullet}OH$ density in a He RF plasma of 2 x 10^{19} m^{-3}, attributed to H_2O trace impurities in Pure He (estimated at 10 – 100 ppm). Schröter *et al.* [137] indicate a similar value, while Verreycken *et al.* et al [138] observe a slightly higher value of ~10^{20} m^{-3}. In these cases the impact of background air has been minimised.

Srivastava *et al.* [139] (microwave jet into air, Ar) measured maximum $^{\bullet}OH$ densities at the tip of the jet of 3 x 10^{21} m^{-3} for 0% added H_2O. Using a 8 kHz He plasma jet into air, Yonemori *et al* [140]

measured spatial variation in $^{\bullet}OH$ density and the air ingress into the jet. They observed a peak $^{\bullet}OH$ density of 2 x 10^{18} m^{-3} where air ingress was ~0 along the central axis i.e. $^{\bullet}OH$ density reduces when the He is mixed with air. Li *et al* [141] measured the $^{\bullet}OH$ spatial profile in an RF jet (Ar/H_2O) and observed that radical generation was confined mainly to the visible (plume) region and that density and location are functions of H_2O content. They suggest that $^{\bullet}OH$ generating reactions occur in the mixing region where feed gas meets laboratory air and the H_2O concentration is highest. These involve OH^+ ion-neutral and Ar^m metastable-neutral reactions with H_2O. At the lowest added H_2O content (0.1%), $^{\bullet}OH$ density was spatially uniform at ~10^{19} m^{-3} up to 13 mm from plasma. Kim *et al* [142] (using a 35 kHz jet, Ar) measured the $^{\bullet}OH$ density >2 x 10^{21} m^{-3} in the headspace above a liquid. In their case, the distance between liquid and electrode was 3 mm and the visible plasma was in contact with the liquid. In the system used here, the visible plasma extended beyond the ring electrode by less than 1 mm.

In a number of cases the decay in $^{\bullet}OH$ density with distance from the plasma was measured. However it is not always clear if the plume/visible region ends and an effluent region is also considered. Benedikt *et al.* [59] observed, for relatively high added H_2O (7000ppm) complete decay in $^{\bullet}OH$ by 20 mm beyond the plasma nozzle. Their chemistry model neglects reactions with air impurities (O_2, N_2) and considers losses are mainly due to (1) $^{\bullet}OH + O \rightarrow O_2 + H$, (2) $^{\bullet}OH + {}^{\bullet}OH \rightarrow H_2O + O$ and (3) $^{\bullet}OH + {}^{\bullet}OH + He \rightarrow H_2O_2 + He$. They suggest $^{\bullet}OH$ generation is due to the dissociation of water, hence increases with H_2O content but O generation is due mainly to secondary production i.e. reaction (2). $^{\bullet}OH$ density decay is determined by $^{\bullet}OH$ recombination in reactions (2) and (3). Verreycken *et al* [138] also observed an $^{\bullet}OH$ density decay to <1% of peak after 9 mm travel from the plasma nozzle. Srivastava *et al* [139] and Yonemori *et al* [140] also noted a rapid decay in $^{\bullet}OH$ density with distance (~ 10 mm and ~ 20 mm) respectively for jets in contact with air.

Although there are different plasma systems and gas mixtures described above, a number of points can be made. For nominally 0% H_2O, the water impurities would lead to a minimum $^{\bullet}OH$ density of ~10^{18} m^{-3} [140] to ~10^{19} m^{-3} [59]. However recombination losses are significant over the first 10 mm – 20 mm beyond the plasma nozzle. Therefore, at the distances used for the plasma – MB study, we must assume that the majority of the $^{\bullet}OH$ radicals have recombined. Typical lifetimes of gas phase $^{\bullet}OH$ radicals at low concentrations are likely longer, possibly allowing the molecules to travel the full distance, over ~10 ms. In normal atmosphere the $^{\bullet}OH$ lifetime is <1s [143].

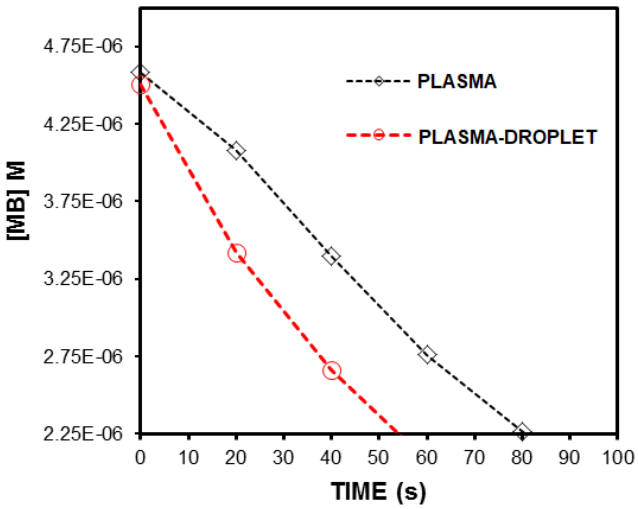

Figure 4.19 Exposure time for 50% reduction in initial MB concentration with and without droplets

For all plasma – MB distances, the degradation of MB occurred much faster with the inclusion of droplets in the plasma. The [MB] falls to 50% of the initial value in 55s with droplets compared to 80s without (Figure 4.19). However the lifetime of $^{\bullet}$OH in liquid is <10 µs, which implies that the concentration in the droplet, due to exposure in the plasma, would be negligible after ~200 µm travel beyond the plasma region. The droplet may absorb OH from the gas along the full length of its travel. However since the gas density of $^{\bullet}$OH is decreasing with distance and the absorbed OH recombines in the liquid as it travels, only the final stages of travel, where the OH^{gas} density is minimal ($<10^{17}$ m^{-3}) would be expected to contribute to the final droplet $^{\bullet}$OH concentration. In Figure 4.19, at 50 mm, the estimated $^{\bullet}$OH density is 7 x 10^{16} m^{-3} without droplets compared to an equivalent value with droplets of 8 x 10^{16} m^{-3}. The increase in flux with droplets is ~14%, and overall the number of impacts ($^{\bullet}$OH equivalent flux x time) required to reach the 50% $[MB]_0$ level is about 80% that of the plasma without droplets. A similar ratio is obtained for the 150 mm distance in order to reach the 85% $[MB]_0$ level.

This difference of 20% suggests either liquid related factors e.g. higher $^{\bullet}$OH density in liquid or additional liquid chemistry related to secondary radicals from OH decay or possibly the enhanced $^{\bullet}$OH generation in the upstream plasma due to the presence of droplets which may translate into a higher background level in the effluent. The droplets supply H_2O molecules to the gas phase by evaporation

and the evaporation rate was determined [100]. Using this value and the average number of droplets counted in the plasma at any one time (< 5), the average contribution was < 1000ppm, taking the volume of the whole plasma. However it may be that the H_2O molecules diffuse slowly away from the droplet and therefore enhance the local vapour concentration around the droplet. Since $^{\bullet}OH$ density rises rapidly with H_2O content (up to ~7000ppm) [59] this may result in enhanced $^{\bullet}OH$ absorption in the droplet while it is in the plasma. In the effluent, the droplet may be surrounded by water clusters and any enhanced $^{\bullet}OH$ may also diffuse into the inter-droplet regions, which would be low density. In atmospheric chemistry, the presence of water clusters can significantly influence the reactivity of gas-phase radical species due to their ability to create hydrogen bonds with gas-phase reactive species [144]. The mechanism of water cluster interaction with plasma-generated species is not well understood and the presence of droplets may mean an entirely different scenario from normal H_2O based plasmas because of possible non-uniformity in the vapour density and therefore much higher H_2O concentrations.

Transition metal (i.e. Fe^{2+})-catalysed production of $^{\bullet}OH$ by the degradation of H_2O_2 is more commonly known as the Fenton Reaction. MB was degraded when subjected to the Fenton Reaction and was used as a comparison with plasma-induced degradation. The ratio of Fe^{2+} to H_2O_2 is critical in the generation of $^{\bullet}OH$ and variations in this composition lead to a wide range of Fenton-induced $^{\bullet}OH$ concentrations reported in the literature. A 1:2 ratio of Fe^{2+}:H_2O_2 caused an initial reaction rate of 1.2×10^{-6} M s^{-1} and led to an $^{\bullet}OH$ concentration of ~3.5×10^{-6} M after 200 s [145]. It was also shown that the H_2O_2 concentration decreased linearly with time during the first 60 s of the reaction. When $[H_2O_2] >> [Fe^{2+}]$ then 1:1 stoichiometry is found between Fe^{2+} and $^{\bullet}OH$ produced via the reaction $Fe^{2+} + H_2O_2$, with a rate constant of 50 – 200 $M^{-1}s^{-1}$ [118]. A ratio of 1:1000 (~7 µM:~6 mM) generated a maximum $^{\bullet}OH$ concentration of ~2.8×10^{-4} mM after 40 min [146]. The results indicated a biphasic pattern of $^{\bullet}OH$ concentration, whereby there was an initial sharp rise followed by a tailing off. The first phase can be explained by $^{\bullet}OH$ generation from Fenton was greater than the $^{\bullet}OH$ consumed in the process of dye degradation. The rate of $^{\bullet}OH$ generation then decreases with decreasing H_2O_2, which is the second phase [146].

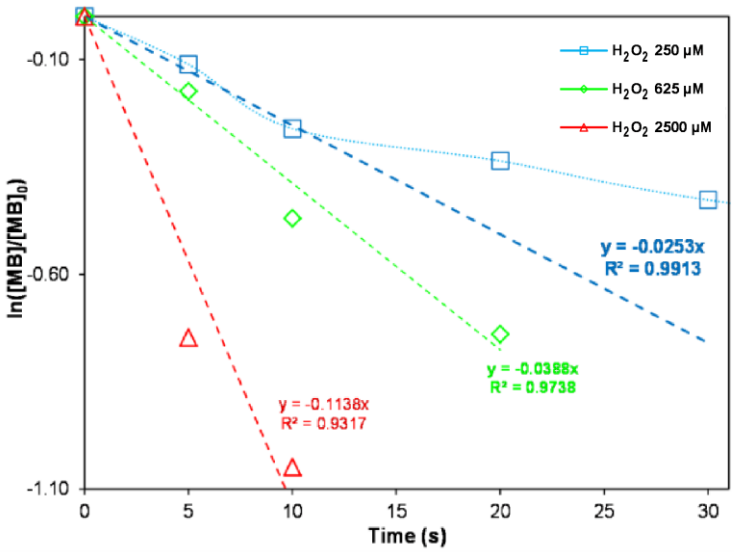

Figure 4.20 Plot of ln([MB]/[MB]$_0$) against time during the initial phase of the Fenton reaction as a function of different initial concentrations of H_2O_2

The current study used 1 part Fe^{2+} to 20 parts H_2O_2, as used in Satoh et al [119] however no value was given for $^{\bullet}OH$ generation. Given the complex reactions it was not possible to find a Fenton process that produced a degradation rate the same as the plasma-droplets. The Fenton characteristic most similar was for Fe^{2+}:H_2O_2 concentrations of 250 µM and 5 mM respectively. From the ln(MB/MB$_0$) plot, Figure 4.20, the initial reaction rate coefficient is observed to be constant over the first 10s. Using equation (4.28) which is based on the initial 1:1 stoichiometric Fe^{2+}:OH reaction (4.2) and for rate constant of $k_1 = 55\ M^{-1}\ s^{-1}$, the $^{\bullet}OH$ generation rate in the initial stages is of the order of 70 µM s^{-1}, similar to that found by [145]. Over the initial 10 s, ~0.7 mM of $^{\bullet}OH$ is generated while 25% of MB (~1 µM) is converted, a ratio ($^{\bullet}OH$/MB) of 770. For the plasma droplet case, for 10 s exposure of MB (50 mm), a 13% degradation is observed. Calculating the $^{\bullet}OH$ flux density at 50mm, (4.26) using an $^{\bullet}OH^{gas}$ density of 8 x 10^{16} m^{-3}, Figure 4.18, gives the $^{\bullet}OH$ flux at the exit of the 2mm diameter tube of 4 x 10^{13} $^{\bullet}OH$ molecules s^{-1} which is collected in 5 mL of liquid. Hence the molar ratio $(^{\bullet}OH/MB)_{plasma}$ is 0.2 i.e. 600 nM of MB is converted with 130 nM of $^{\bullet}OH$. This may indicate an underestimation of the $^{\bullet}OH$ flux but it may also show a much more efficient conversion that in the Fenton process.

For an estimated $^{\bullet}OH^{gas}$ density in the plasma region of 10^{20} m^{-3}, similar to $H_2O_2^{gas}$, and a Henry constant value at 320 K of 1.13 x 10^{-4}, the maximum possible surface $^{\bullet}OH^{liquid}$ concentration is

164 μM. Ignoring the Henry limit and any losses in the droplet the $[^{\bullet}OH]^{liquid}$ would reach 4 mM, much greater than the maximum allowed. However losses due to the recombination of $^{\bullet}OH$ with $^{\bullet}OH$ or OH^{-} are very fast reactions which would limit the average $^{\bullet}OH$ concentration. In the effluent for an estimated $^{\bullet}OH^{gas}$ density of 10^{17} m^{-3}, the maximum allowed $^{\bullet}OH^{liquid}$ concentration is 1.3 μM.

4.5. Conclusion

The plasma-droplet reactor system used for this work has shown some initial promise with regards to plasma-induced chemistry, specifically $^{\bullet}OH$ and H_2O_2 production. The H_2O_2 generation rate was found to be much higher that with other plasma – liquid configurations and analysis indicates that the droplet can sequester sufficient H_2O_2 from the gas phase. Delivery of the hydroxyl radical was demonstrated over relatively long distances (>100 mm) from the plasma and more so when the droplets were present. The next stage is to investigate the antibacterial properties of the plasma-activated droplets when bacteria are exposed to the plasma effluent on an agar surface.

5. PLASMA-DROPLET EFFLUENT TREATMENT OF BACTERIA ON AGAR

5.1. Introduction

The design of the atmospheric-pressure plasma system used in this study allows for single-pass droplet interaction and subsequent transport away from the discharge region. The droplet, entrained within the gas flow used to generate the plasma, receives a relatively uniform plasma exposure. Gas-phase reactive species are sequestered into the liquid droplet and the results from Chapter 4 indicate that the droplet may acquire some chemical activity as a result of this short exposure to the plasma. This chapter attempted to investigate the antimicrobial effect of a pure He/Ne atmospheric-pressure plasma, with and without liquid droplets. Recent studies have assessed the antibacterial efficacy of plasma by measuring the inactivation kinetics of cells exposed to plasma (i.e. reduction in cell number as a function of exposure time [64] and the diameter of the region on the exposed agar surface that lacked growth after incubation i.e. the 'zone of inhibition' [147]. The zone of inhibition can sometimes be incomplete; a cell might survive the treatment and form a colony within the treatment zone, although the numbers of surviving cells are rarely sufficient to prevent identification of the zone of inhibition. Image processing software, e.g. Image J, offers the opportunity to analyse a particular parameter e.g. contrast variation across a selected region, and compare between images taken using the same camera system after different treatments conditions.

5.1.1. Aims and Objectives

5.1.1.1. Aims

- Determine the antibacterial effect of droplets exposed to plasma with bacteria on agar
- Establish the expected droplet flow area of impaction on agar

5.1.1.2. Objectives

- Measure zone of growth inhibition while varying the distance from the plasma, with and without droplets
- Relate the area on agar that showed dye impaction to the area devoid of bacteria

5.2. Methodology

An rf-driven plasma (13.56 MHz) was ignited using pure He & Ne gas flows within the internal geometry of a quartz tube and confines of two ring electrodes positioned concentrically around the outside of the tube (Figure 5.1). The mean transit time for any given droplet through the plasma, as determined by the gas and liquid flows was ~ 120 µs [100]. All distances are measured from the end of the quartz tube; the additional distance from the plasma to the end of the quartz tube was 15 mm (ground electrode)/17 mm (powered electrode). Droplets of deionised water (dH_2O) generated at the nebuliser tip became entrained in the gas flow and were transported through the plasma region. A petri dish (55 mm diameter) containing pre-poured microbial growth agar was exposed to the effluent flow, with and without droplets. In a control experiment, bacteria (*E. coli* K-12) were added to the agar directly after the plasma treatment. Bacteria growth on such a treated surface was normal, i.e. no growth inhibition was observed. The time between plasma exposure and cell inoculation was one hour. This suggests that H_2O_2 generated from the plasma is unlikely to be sufficient to prevent subsequent *E. coli* growth. In all subsequent plasma – agar tests, the bacteria were inoculated onto the agar prior to treatment. 100 µl of *E. coli* at a concentration of 10^5 cfu/ml in Ringer's solution (RS) was added to a pre-poured agar plate and allowed to dry at room temperature for 30-45 min. Bacteria inoculated onto agar and not exposed to the plasma effluent were used for the positive control; the negative experimental control was agar without any bacteria exposed to the same gas/droplet flow (plasma off).

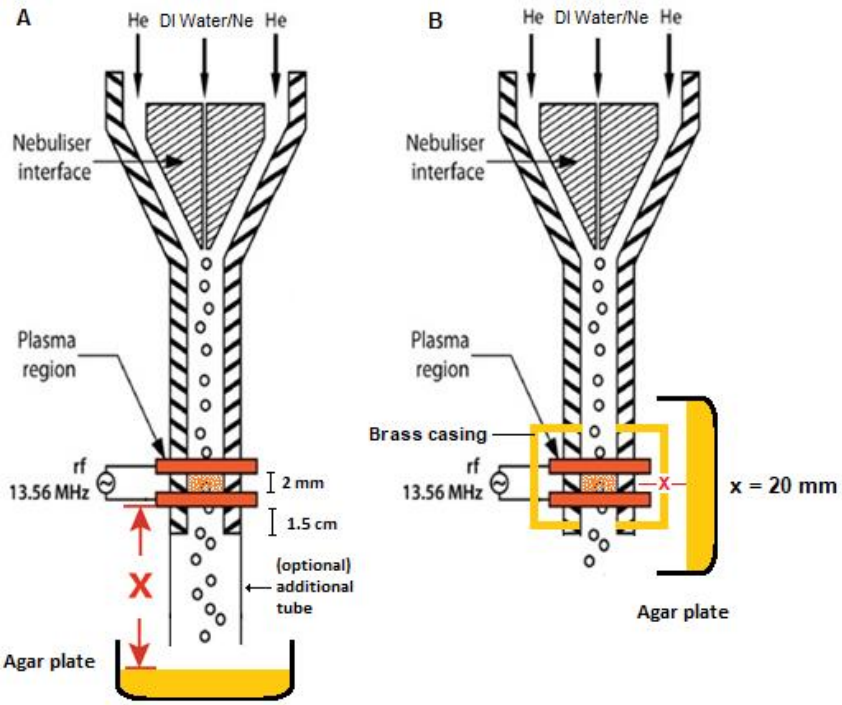

Figure 5.1 Schematic cross-section diagram of the plasma-droplet system used for treatment of microbial growth agar. Figure A shows the plasma-droplet effluent treatment of bacteria on agar, where the distance between the quartz tube end and the agar surface was varied. Additional tubing could be attached to the quartz tube which aided transport of the plasma-exposed droplets. Figure B shows the positioning of the agar plate to expose the bacteria to only the electric field and UV components of the plasma

Plasma-treated agar plates were incubated for 24 h at 37ºC to encourage bacterial growth. Treatments were performed in duplicate and the images were taken using a digital camera. The diameter of the zone of inhibition was measured, as well as analysing the contrast variance across the treated area. Colonies that grew within the treated area were analysed in relation to their diameter and prevalence. Food dye was aerosolised and allowed to impact onto the agar in an attempt to visualise the flow of droplets and penetration into the agar.

5.2.1. Experimental conditions

G: gas flow through quartz tube; no plasma

BGP: bacteria treated with gas plasma ($80W_F/1W_R$)

GA: gas + aerosolised sterile water (10 µl min^{-1})

BGAP: bacteria treated with gas & aerosolised water plasma.

UV irradiance from the plasma-droplet system was previously measured in Chapter 4, so it would be appropriate to assess its antimicrobial effect here. An agar plate with bacteria was placed at

the side of the system, parallel to the quartz tube, opposite an open channel to expose the bacteria only to the plasma-generated UV (Figure 5.1 B). The open channel in the brass casing was previously used to house the fibre-optic camera used to measure plasma OES from Chapter 4 (I.D. = 2.0 mm). The distance from the top of the agar surface to the quartz tube wall was 20 mm. The lid of the brass casing was removed to expose bacteria on agar to the plasma-generated UV in addition to the electric field.

5.3. Results

5.3.1. Plasma-generated ultra-violet radiation and radio-frequency signal exposure

Bacteria were inoculated onto agar and exposed to the plasma-generated UV, measured in Chapter 4, at a distance of 20 mm (the closest distance experimentally possible). The rf signal from the powered electrode was shielded from the inoculated agar plate by a brass casing which surrounded the plasma, apart from an open channel (2.0 mm I.D.) to allow bacteria treatment by the plasma-generated UV (Figure 5.1 B). For exposure times up to 30 min, there was no inhibition of growth detected on the inoculated agar surface. When the brass casing lid was removed, thus exposing the agar surface to the plasma-generated UV in addition to the rf signal, there was no effect on growth. Lackmann *et al.* [87] investigated UV and plasma species separately in the same system. While synergistic effects were observed, the presence of oxygen was required in the gas phase. Also the UV photons only weakly penetrate liquid and bacteria are more easily UV inactivated on dry surfaces. In Chapter 4 section 4.3.2.1, UV irradiance from the plasma was measured at 30 mm to be ~1.2E-03 Wm^{-2}, decreasing by approx. one order of magnitude at 70 mm from the plasma (~ 1.8 2E-04 Wm^{-2}). These are well below the International Commission on Non-Ionizing Radiation Protection (ICNIRP) Guidelines on exposure limits to UV radiation [148]. They state that for light with a wavelength of 310 nm, the exposure limit for one second duration is ~2.0E3 Wm^{-2}, nearly 6 orders of magnitude greater than what was measured from the plasma. It must be concluded that bacteria growth is not affected by the UV or the rf electric field produced by the plasma-droplet system used in this study. The potential effect of bacterial DNA exposure to plasma will be investigated in the next chapter.

5.3.2. Plasma effluent exposure: unshielded

No growth was observed on the negative control agar plates subjected to the same treatment as the experimental samples. This indicates that the system was sterile prior to experiments and that no pre-existing bacteria within the system contributed to the analysed growth on agar. There was a slight indentation on the agar surface as a result of the gas flow, however, this did not have any effect on bacterial growth within the exposed area (see Appendix Figure 8.2.3).

5.3.2.1. Variable: Distance from plasma (fixed exposure time)

Inoculated agar plates were placed upon a scissor jack, which allowed for the distance* between the plasma and the surface to be varied (*distance from plasma to quartz tube end = 15 mm in addition to the reported distance: from quartz tube end to agar surface). The bacteria were exposed to the plasma effluent for three minutes and this prevented growth on the treated agar surface after incubation, with an enhanced effect observed when droplets were added upstream from the plasma (Figure 5.2).

5.3.2.1.1. Zone of Inhibition

After plasma treatment and incubation, inoculated agar plates showed central clear zones (i.e. no bacteria growth), surrounded by opaque zones of partial bacteria growth (Figure 5.3). This extended outwards until there was no growth inhibition, similar to that of the positive control i.e. untreated cells. The presence of growth within the treated zone could indicate that some bacteria survived the plasma treatment. It was observed that larger colonies were formed within the zone of inhibition compared to those at the edge. This may be due to less microbial competition facilitating the development of larger colonies (see Appendix 8.2.1). As before, there was no growth inhibition when droplets not exposed to plasma impacted on the agar surface with bacteria.

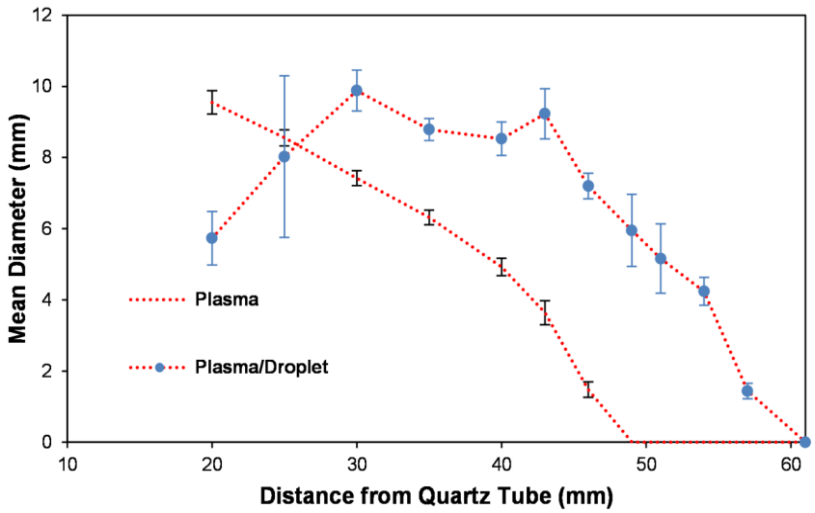

Figure 5.2 Graph showing the diameter of the growth inhibition zone after 3 min exposure to the plasma (droplet) effluent, measured at different distances from the end of quartz tube. Plasma-droplet treatment produced a larger zone of inhibition for distances greater than 25 mm from the plasma

The diameter of the zone of inhibition was measured between two points where there was 'lawn' growth i.e. no inhibition (Figure 5.3). For the plasma treatment without droplets, the largest

diameter of growth inhibition was observed when the agar was closest to the quartz tube. The zone diameter decreased as the agar surface was moved away from the tube end. No growth inhibition was observed beyond approx. 49 mm. Droplet additions to the gas flow upstream from the plasma caused an increase in the distance where growth inhibition was observed (61 mm). No inhibition of growth was measured for the plasma-droplet effluent treatment at distances greater than 61 mm.

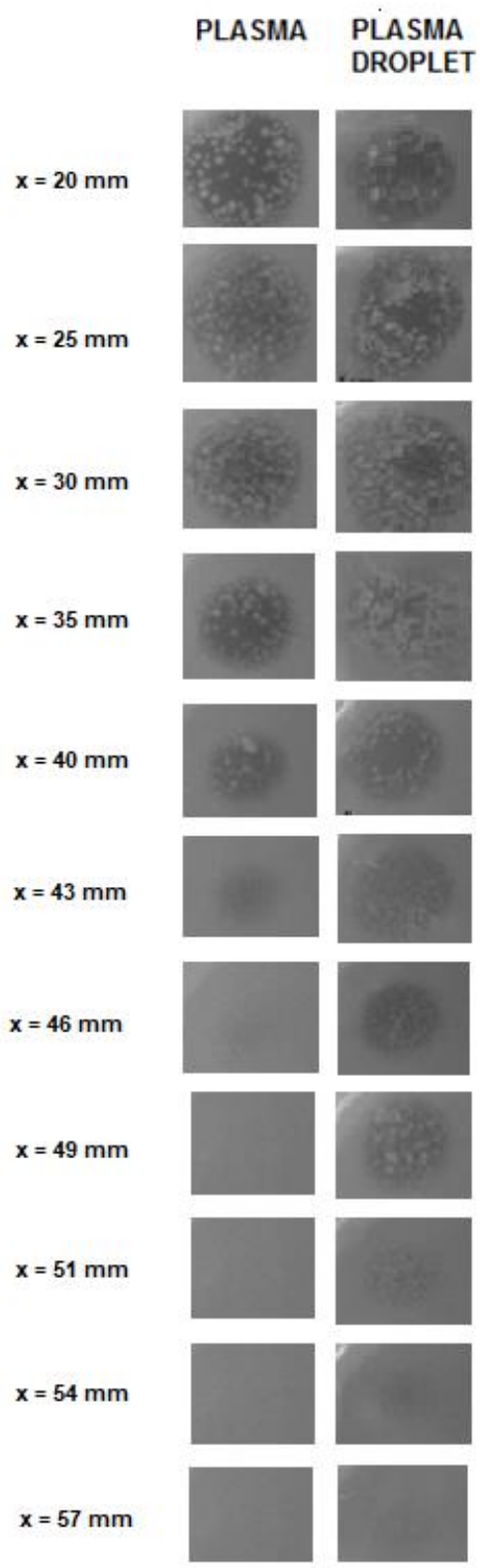

Figure 5.3 Images of the treated areas of agar at various distances from the quartz tube end after exposure to the plasma effluent and plasma-droplet effluent. The inhibition efficacy reduced as the distance from the plasma increased.

The incomplete zone of inhibition makes it difficult to accurately ascertain where the plasma effect ceases. Agar exposure to the plasma effluent at the shortest distance did not produce a well-defined zone of inhibition. The initial cell concentration was 10^5 cfu/ml and the positive control (2 µl

ethanol solution) was capable of generating a clear inhibition zone. In an attempt to gain a more comprehensive insight into the zone of inhibition, contrast analysis of the photos was performed using an image software programme (Image J). The change in contrast from a point with complete growth, across the zone of inhibition, to another point with complete growth was represented as an arbitrary unit of depth, where the maximum depth value corresponded to the greatest difference in contrast between the 2 points of complete growth i.e. a clearer zone of inhibition (Figure 5.4).

5.3.2.1.1.1. Contrast Analysis

Figure 5.4 shows the contrast profiles across the zone of inhibition after plasma treatment. The treatment without droplets produced profiles that became less deep as the distance from the quartz tube end increased. The closest distance from the quartz tube end to the agar (2 cm – red) had the widest and deepest profile. At 4.3 cm (yellow), the depth of the profile is much less than that at 2 cm. As the distance increased between the agar and quartz tube end, the profile becomes narrower.

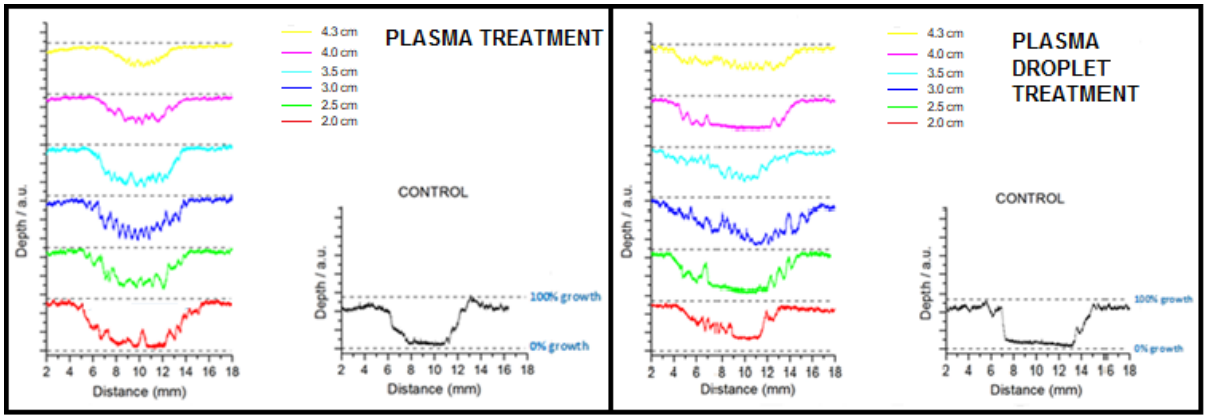

Figure 5.4 Contrast analysis profiles of the zone of inhibition after exposure to plasma effluent and plasma-droplet effluent as a function of distance. The control profile is obtained by the addition of ethanol and analysing the contrast change across the inhibition zone, as per the experimental conditions

For the plasma treatment with droplets, the profiles for all distances follow a different pattern (Figure 5.4). The deepest and widest profile was at the second closest distance (2.5 cm – green line). The width of the profile appeared fairly uniform for all distances. The above differences in the contrast profiles suggest different antibacterial mechanisms operate after plasma treatment and plasma-droplet treatments.

5.3.2.1.1.2. Reduction in cells within plasma treatment area (cfu/cm^2)

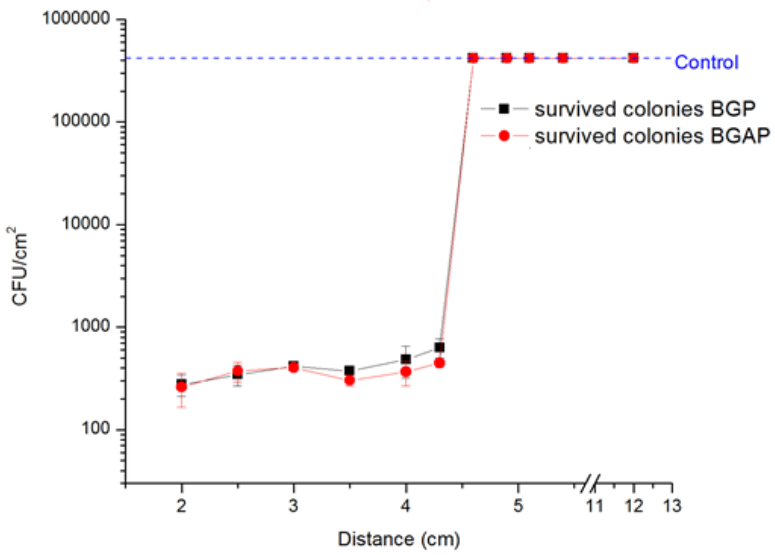

Figure 5.5 The graph shows the number of viable cells that were recovered from within the area exposed to the plasma/plasma-droplet effluent. The number of cells within the treatment area increased as a function of the distance from the plasma

The reduction in viable cell numbers in the treatment area was greatest for the closest distance to the plasma for both experimental conditions (Figure 5.5). There was a rapid increase in survivors in the treatment zone between distances 4 – 5 cm, after which there was no difference between the plasma-treated agar plates and the positive control growth area (~3 log). There was a slightly greater reduction in the numbers of viable cells after plasma treatment with droplets flow than without at distances 3.5 – 4.3 cm.

5.3.2.1.1.3. Cell density effect on plasmas anti-bacterial efficacy

The observation of survivors within the treatment zone (initial cell concentration = 10^8 cfu/ml) could be due to a cell-shielding effect and the inability of reactive species in the plasma effluent from penetrating through the cell population. The initial cell concentration was varied and exposed to the same plasma treatment and assess any differences in inactivation (Figure 5.6).

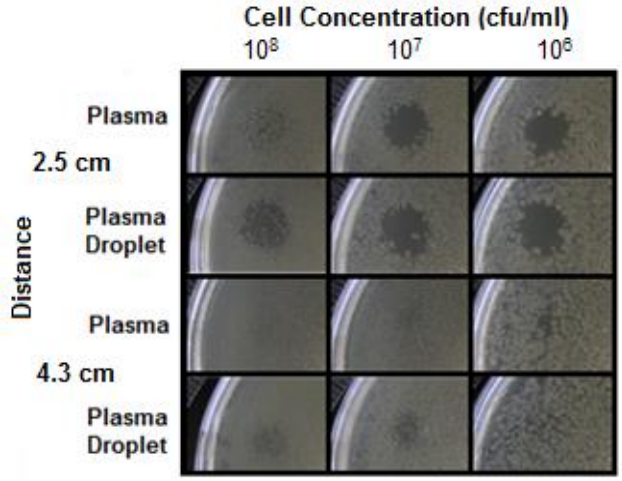

Figure 5.6 Images of treated agar that were inoculated with varying concentrations of bacteria prior to exposure to the plasma effluent and plasma-droplet effluent. Treatment time was 3 minutes

The images in Figure 5.6 appear to show that initial cell concentration does have an effect on the size of colonies that are produced after plasma treatment. The zone of inhibition is clearer for lower cell concentrations, for a given plasma exposure. Plasma-droplet treatment appears to have greater efficacy than exposure to plasma effluent alone.

5.3.2.1.2. Visualisation of droplet flow using food dye: zone of impact v distance from the tube

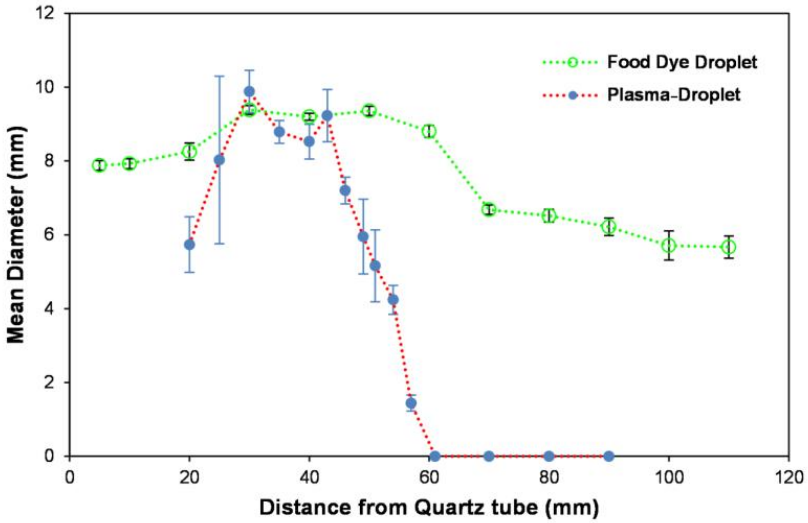

Figure 5.7 Graph showing the diameter of the growth inhibition zone after plasma treatment with droplet flow (red line, blue circle marker) at different distances from the quartz tube end, along with the diameter of the coloured aerosol impact region on agar (green line)

The droplets generated from the green food dye impacted onto the agar surface in order to visualise the area that the plasma-droplet effluent flow would be expected to cover. Growth inhibition

was observed up to approx. 61 mm, however the diameter of the zone of inhibition rapidly reduced as the distance from the quartz tube end increased (Figure 5.7). The dye droplet flow was detected up to the maximum distance possible due to the operational limit of the vertically-aligned system within the workstation (110 mm). The density of the food dye was only slightly higher than that of water (<1%), so density could not be the reason why the dye aerosol travelled further in the gas stream than the droplets in the plasma effluent. A droplet flow interacting with plasma may cause more turbulence compared to a droplet flow without plasma. Food dye droplets were not plasma treated for this analysis which could explain the difference between the two conditions. Another possible explanation could be that the plasma-activated droplets can travel the same distance as the dye but cannot inhibit growth due to bacteria cell shielding. This would result in incomplete growth inhibition and a non-uniform zone of growth inhibition. Also, there is a minimum of amount of aerosol droplets required to cause any effect and the greater the treatment time, the more uniform the growth inhibition (see Appendix 8.2.2).

5.3.2.2. Variable: Exposure time (fixed distance)

A distance of 43 mm was chosen for plasma effluent exposure of bacteria for varying durations, since it was the distance that showed the largest variance in zone diameter (Figure 5.2). Exposure times ranged from 1 to 15 minutes.

5.3.2.2.1. Zone of Inhibition

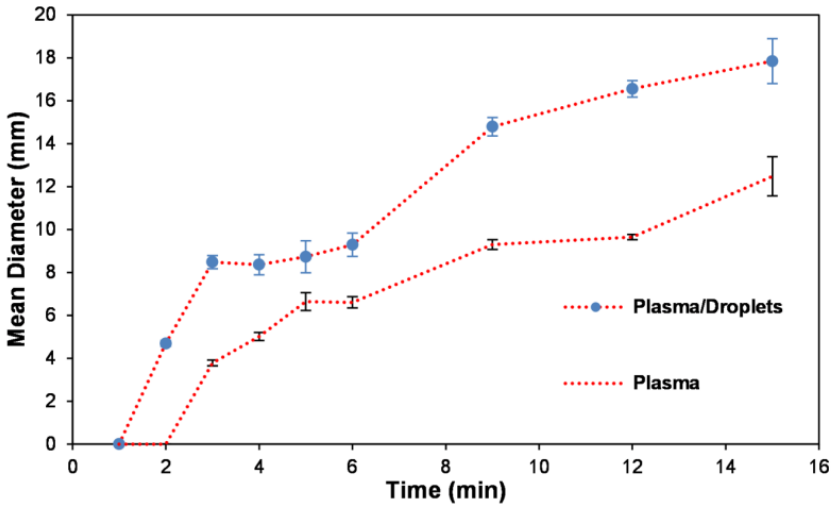

Figure 5.8 Diameter of the zone of growth inhibition after plasma treatment for different exposure times, with and without droplet flow

When the exposure time was 1 min, there was no growth inhibition for either plasma treatment (Figure 5.8). However, growth inhibition was observed for the plasma-droplet effluent treatment after 2 minutes. The plasma effluent without droplet flow inhibited growth after 3 minutes exposure time. The diameter of the zone of inhibition increased as a function of exposure time for both conditions. For a given exposure time, the plasma-droplet effluent treatment resulted in a larger inhibition zone diameter compared to a ‘dry’ plasma effluent. Figure 5.9 shows images of inoculated agar plates after exposure to the plasma-droplet effluent for various treatment times.

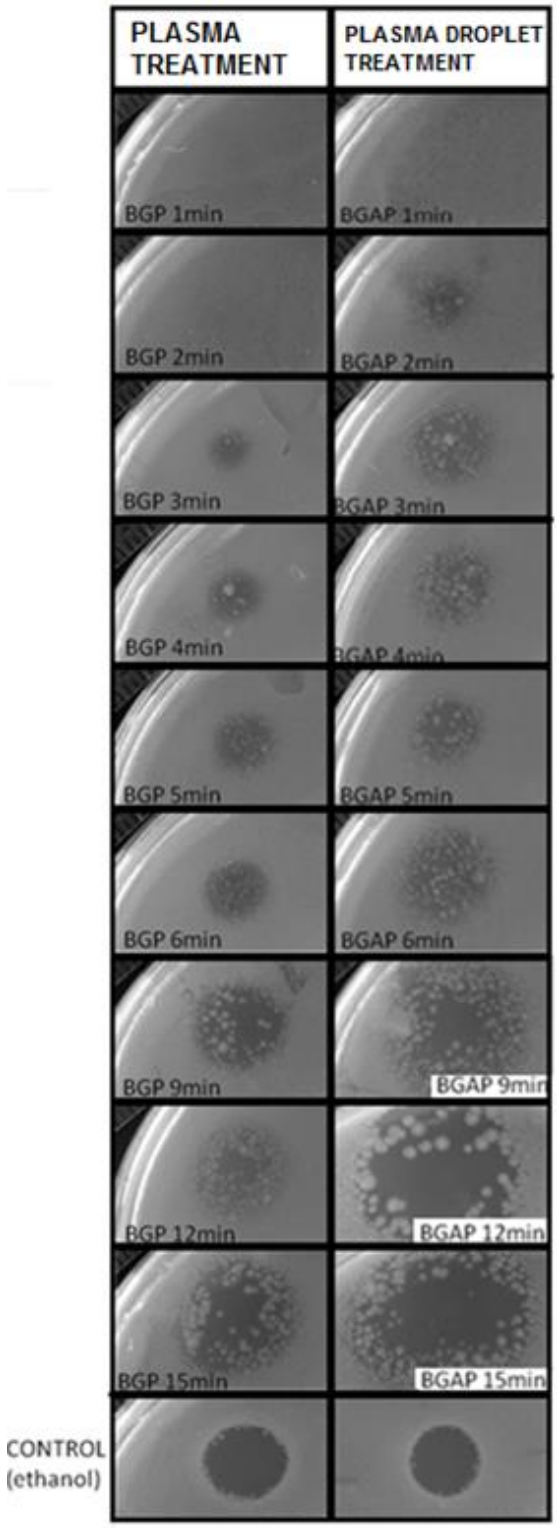

Figure 5.9 Images of the treated areas of agar exposed to the plasma effluent and plasma-droplet effluent for different durations. Incomplete inhibition of growth was observed for the longest treatment time (15 min). A larger zone of inhibition was observed after plasma-droplet effluent treatment for a given exposure time, compared to plasma treatment (without droplet flow). For a reference of complete growth inhibition, 2 ul of 70% ethanol was applied to the agar (see 'CONTROL')

5.3.2.2.1.1. Contrast Analysis

Contrast analysis of the images above was performed to study in greater detail the area of growth inhibition (Figure 5.10).

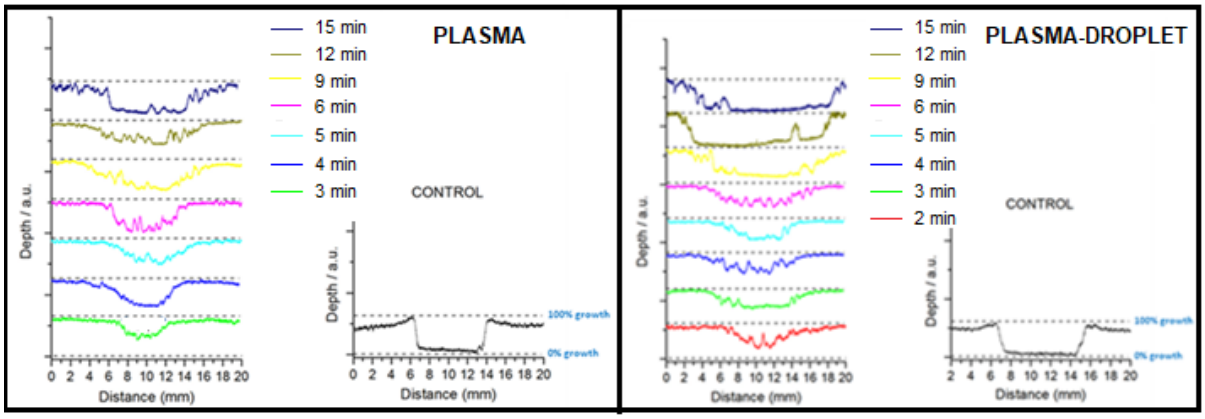

Figure 5.10 Contrast analysis profiles of the zone of inhibition after exposure to plasma effluent and plasma-droplet effluent as a function of treatment duration

The profiles of the zones of inhibition increase in depth and width with increased treatment time for both experimental conditions. For the longest plasma treatment time (15 min – dark blue line), the contrast profile of the zone of inhibition after exposure to the plasma-droplet effluent was much deeper and wider than for the 'dry' plasma effluent treatment. There does appear to be a correlation between treatment time and width of the profile, for both plasma treatments but this effect was more pronounced for the plasma-droplet treatment.

5.3.2.2.1.2. Reduction in cells within plasma treatment area (cfu/cm^2)

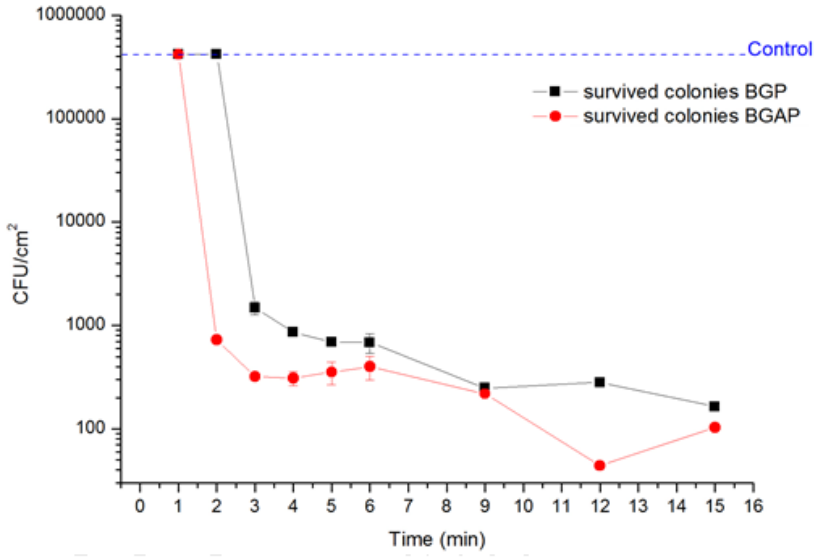

Figure 5.11 Graph showing the reduction in viable cells after various treatment durations, calculated by counting the number of surviving colonies in the treatment zone and deducting this from the starting concentration i.e. control

The reduction in viable cell numbers in the treatment area was greatest after the longest treatment time for both experimental conditions (Figure 5.11). There was a rapid reduction in survivors in the treatment zone when the exposure time was increased from 1 to 2 minutes for the plasma-droplet effluent treatment, and from 2 to 3 minutes for the plasma only treatment (~2 log reduction from control concentration). The rates of decline in bacterial numbers decreased after these initial periods of exposure (1 log reduction between 2 min and 15 min). There was a slightly greater reduction in the numbers of viable cells after plasma treatment with droplets flow than without.

5.3.3. Plasma effluent exposure: shielded

5.3.3.1. Variable: Distance from plasma (fixed exposure time)

The studies carried out in section 5.3.2 were repeated with one modification i.e. the addition of a piece of tubing connected to the end of the quartz tube and protected the plasma effluent from interacting with ambient air. Figure 5.12 showed that the plasma treatment became less effective, as the distance between the quartz tube and the agar surface increased. The plasma effluent interacted with ambient air before reaching the agar surface and it was hoped that the addition of tubing may enhance the antibacterial effect over longer distances. The distance between the end of the piece of tubing and the agar surface was fixed at 5 mm.

5.3.3.1.1. Zone of Inhibition

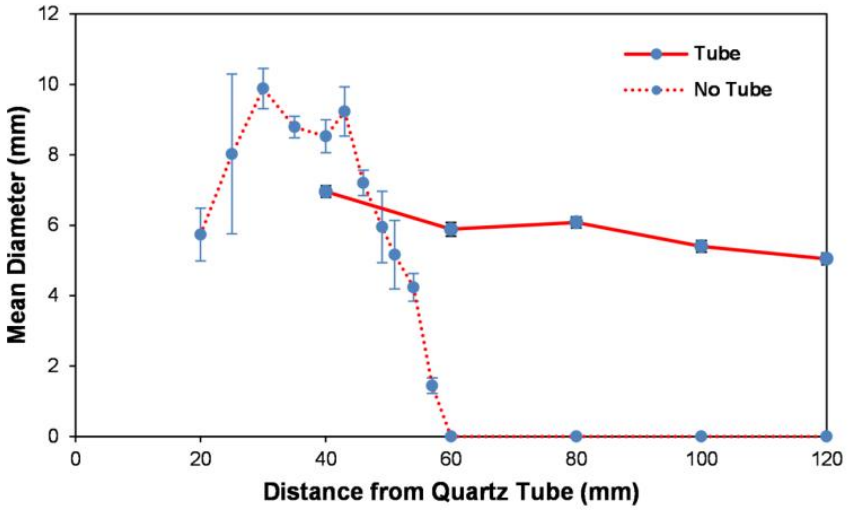

Figure 5.12 Graph showing the diameter of the inhibition zone as a result of exposure to plasma effluent and plasma-droplet effluent for 3 minutes with additional tubing

The diameter of the inhibition zone was slightly lower when the distance was 40 mm between the quartz tube end and the agar surface with the additional tube, compared to without (Figure 5.12). However, at 60 mm there was no growth inhibition when the tube was not present. The addition of the tube maintained a fairly constant diameter of growth inhibition, regardless of distance from the quartz tube end. Growth inhibition was observed up to 120 mm, which was the maximum distance possible to be investigated using the plasma-droplet system. The discrepancy observed between the diameters of the inhibition zones could be attributed to droplet interaction with ambient air molecules before reaching the agar surface without the tube. The addition of the tube eliminates this interference and can transport the plasma-generated species away from the core discharge region.

5.4. Discussion

Atmospheric-pressure plasma treatment of bacteria on agar or in liquid has shown to be an effective mechanism for inactivation. This has led to clinical trials which studied the inactivation of bacteria on surfaces using a well-characterised plasma jet device: kINPen MED (Neoplas, Germany). This provides a useful benchmark for comparison. The device has a central pin electrode within a quartz tube and a plume was visible outside the device up to 12 mm [133]. The gas temperature was measured along the axial plasma plume and decreased with distance from the device. At the tip of the device the gas temperature was ~ 48 ºC, which would be too hot to safely use on human tissue, therefore the authors proposed a recommended working distance of between 9 – 11 mm [133], which corresponds to a gas temperature between 34-38 ºC making the plasma treatment biologically tolerant. Its predecessor, the kINPen 09 (neoplas, Germany) are identical in many respects, except for how the power is delivered [149]. The continuous mode in the kINPen 09 resulted in a longer plume and a higher gas temperature measured at 8 mm from the device tip compared to the pulsed mode used in the kINPen MED; 45°C for the kINPen 09 compared to 37°C for the kINPen MED [149]. The kINPen MED was specifically designed to be used also in the clinical environment through the incorporation of its own mass flow controller to aid portability as well as optimised housing that suitable for application of treatment. Winter *et al* [53] have observed with KinPEN 09 that for humid feed gas (Ar), a low vapour content (<1000ppm) has a much larger effect on OH (and cell viability) and ambient humidity can be ignored. However control of the feed gas humidity is significantly compromised with the use of polymeric supply tubes and if dry gas is used, then the ambient humidity becomes an important factor. This is an example of practical multi-parameter constraints facing implementation of a reliable plasma medicine technology. It would be worthwhile to investigate whether the use of plasma treated droplets could allow treatment (i) improved efficacy (ii) at sufficient distances to avoid gas temperature effects (iii) control of plasma activated chemistry with less susceptibility to surrounding air.

The plasma-droplet system has shown have an effect over distances up to 150 mm, and the effect was enhanced when droplets were plasma treated prior to surface interaction. Areas of inoculated agar that were exposed to the plasma-droplet effluent had no bacteria growth after

incubation i.e. a zone of inhibition was created, and the diameter of the zone was related to the distance from the plasma. Contrast analysis across the zone of inhibition allowed for more quantitative assessment of the anti-bacterial effect, however due to the requirement of lawn growth obtaining a calibration curve of contrast (i.e. optical density) as a function of cell concentration was not possible. Agar is molten at temperatures above 40 ºC, but there was no indication that the plasma or plasma-droplet effluent caused any heating effects and the agar remained solid throughout all experiments. This would suggest that at the distances used in the current study, the effect of the gas temperature in negligible.

Inoculated agar exposure to plasma-droplet effluent for 3 minutes resulted in a 3-log reduction in the number of viable cells when the distance between the plasma and agar was 40 mm. The diameter of the zone of inhibition was larger than the inner diameter of the quartz tube from which the plasma effluent exited. For the same treatment duration, Ikawa *et al* reported a 7-log reduction in viable *E. coli* with He as the feed gas using an APPJ-like configuration [150]. The cell suspension was placed 20 mm from the plasma, which is approximately half the maximum distance used in the current study. Laroussi *et al* achieved the same reduction in *E. coli* after only 30 s plasma treatment using a similar plasma type operating in He with 0.75 % admixture of O_2 [151]. The distance between the tip of the plasma device to the sample was 30 mm. A different plasma configuration, DBD, was used to treat *E. coli* suspensions and caused complete inactivation after 5 minutes when the cells were suspended in dH_2O but complete inactivation was not achieved when the cells were in buffered solution [152]. The distance between the plasma and bacteria suspension was fixed at 5 mm. *E. coli* cells deficient in DNA repair pathways were particularly susceptible to plasma treatment when the sample was placed at an extended distance [153]. A 5-log reduction was observed when the cells were 440 mm from a humid Ar plasma, and a 6-log reduction when placed at 20 mm. The authors reported that the particular strain was chosen to cause a high mortality, however comparison to 'normal' *E. coli* is not available.

Figure 5.2 shows the diameter of the zone of inhibition as a function of distance and the maximum difference between plasma treatment and plasma-droplet treatment was at ~ 43 mm. The gas temperature in the plasma is ~ 80ºC but the agar surface does not show any effects of adverse

heating, therefore we assume the gas temperature at the agar surface is < 40 ºC. As droplets exit the plasma, they interact with ambient air and it is not known what proportion do not reach the surface. The interaction between plasma and the background gas is known to affect the impact on bacterial sterilisation [150], [151], [152], and generally the expected distance between plasma and surface is < 20 mm. Considering, the plasma only (Figure 5.2), the apparent roll off in efficacy after 20mm would imply that a practical device would be best operated at <20mm to avoid the sensitivity with distance. With the plasma treated droplets, this point is not reached until 45 mm, which is a useful extension. The cause of the roll-off in the plasma only case is likely to be similar to that reported in other studies and involve quenching of short-lived active species and possibly dispersion/dilution as the feed gas mixes with the lab air. The plasma treated droplet may also suffer similar effects but to a lesser extent. The light droplets may be lost due to turbulence outside of plasma. However the studies with food dye indicate droplets can travel up to 120 mm, Figure 5.7, although it should be noted that complicated rare gas structuration has been observed in plasma jet experiments [154] so the plasma treated droplets may not follow the same trajectory. In order to clarify this, the plasma container tube was extended, Figure 5.12, and the zone of inhibition remained almost constant up to a distance of 120mm. This is the longest testable distance in our system and in this configuration the effect of turbulence would be negligible. In Chapter 4, the droplet chemistry was evaluated and the impact of MB degradation with distance was determined. A simple model was developed that indicated a background $^{\bullet}OH$ concentration in the plasma effluent which decreased with distance. With the inclusion of droplets, the enhanced MB degradation is possibly due to scavenging of the gas phase of $^{\bullet}OH$, within an $^{\bullet}OH$ lifetime equivalent distance from the MB surface. In the case of MB, the presence of H_2O_2 in the droplets or gas has a negligible effect and the focus was on $^{\bullet}OH$ radicals. In the agar study, the effect of H_2O_2 can be mostly discounted because in the agar control experiment where *E. coli* was dispersed onto the agar after plasma treatment, a similar concentration of H_2O_2 should still be present as that delivered during the normal experiments. The fact that *E. coli* growth was normal in the control case is a strong indication of the limited impact of plasma/droplet delivered H_2O_2 on bacterial growth.

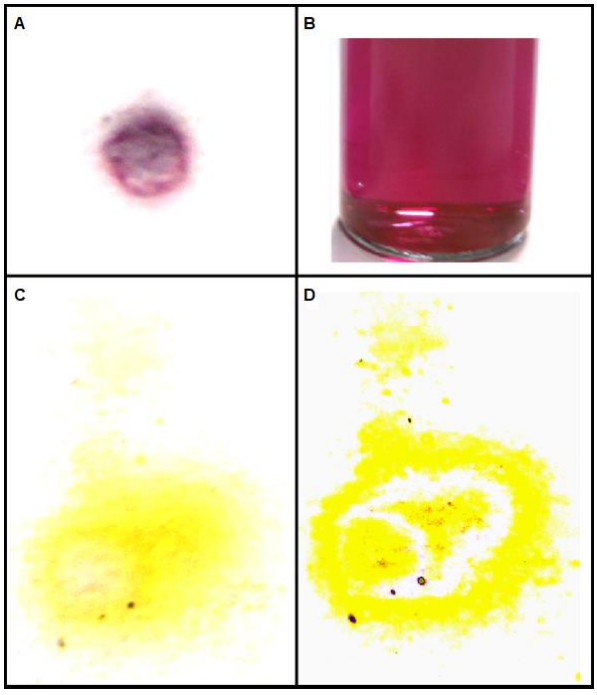

Figure 5.13 Low resolution images showing the colourimetric change of aerosolised solutions exposed to plasma. Figure A is from a plasma-treated silver nanoparticle solution and allowed to impact onto white filter paper; B is the solution collected in a quartz cuvette. Figures C and D is when Ti-S (H_2O_2 indicator) was used

From the $^{\bullet}OH$ model in Chapter 4, the estimated equivalent $^{\bullet}OH$ radical flux density from the plasma with droplets was 1.2 x 10^{19} $m^{-2}s^{-1}$. It is not clear whether the pattern of the inhibition zone (and food dye) indicates where droplets arrive or whether the droplets land on the agar over a 2 mm central zone – equivalent to the diameter of the delivery tube and then spread out. It has been difficult to image this effect but careful observation of fluid formation on microscope slides tends to suggest a deposition diameter close to 2 mm. In Figure 5.13 A, the impact pattern of an Ag nanoparticle loaded droplet stream shows a purple ring diameter of ~2 mm. The colour change is similar to that of the Ag nanoparticle colloid (Figure 5.13 B) when the droplet stream is collected in liquid. In Figure 5.13 C and D, Ti-S loaded into the droplet passes through the plasma and reacts with the droplet H_2O_2; C is the original image and D is digitally enhanced to show the outline at ~2 mm more clearly. These images were taken at a distance of ~10 mm from the quartz tube outlet. The further use of Ti-S in-flight was not continued due to its corrosive properties. In Figure 4.5 the images of TA-OH on agar show interaction zones with a central region of ~2 mm (petri dish diameter = 55 mm) and an extended region beyond, with diameter which depends on distance. It is reasonable therefore to assume the droplets land within the ~2 mm zone which matches the plasma tube outlet.

Using this diameter value, the estimated equivalent $^{\bullet}OH$ radical flux at 50 mm, due to droplets, is ~3.8 x 10^{13} s^{-1} and ~3.3 x 10^{13} s^{-1} for plasma only. This small difference is insufficient to explain the relative improvement of the droplets over plasma, Figure 5.2, and it is likely therefore that the active species in the droplet is protected for longer from the ambient air than the same species in the gas effluent. The initial reduction rate in cell count, Figure 5.11, in the droplet case was negligible after the first 2 minutes, then reduced ~4 log after a further 10 minutes. From estimated flux, this is equivalent to a kill effectiveness of ~ 4 x 10^{-10} cells per $^{\bullet}OH$ radical (or 2 x 10^{9} radicals per cell). Cho *et al* [155], using $^{\bullet}OH$ radicals generated from UV/TiO_2, measured the time for 2 log inactivation against $^{\bullet}OH$ radical concentration in the sub-pM range for a starting bacteria concentration of 10^{5} – 10^{6} cfu/mL. Although the inactivation is concentration and cell count dependent, the maximum number of $^{\bullet}OH$ radicals required per *E. coli* cell inactivated was of the order of 10^{5}. In this case the UV interaction with the TiO_2 particle slurry created a number of active species close to the bacterial cells, of which $^{\bullet}OH$ was found to be the most effective. At a distance of 120 mm, with the extended tube, the kill rate is not greatly reduced, although the equivalent flux is reduced by a factor of ~10 (Figure 5.12). A more detailed time-based study also involving active species scavengers is required to fully investigate the droplet induced inactivation mechanism further.

Another consideration is cell density; the zone of inhibition was more clearly defined for lower cell concentrations after exposure to the plasma-droplet system and the efficiency of the plasma treatment appeared greater, even though the treatment conditions are exactly the same i.e. distance and exposure time. When the agar surface is completely covered with bacterial growth, a layered growth structure is created due to the confinement within the petri dish. The cells that are on the upper layer are directly exposed to the plasma-generated reactive species whilst consequently protecting those cells that are located underneath. This phenomenon, termed ‘cell shielding’ is a common problem in topical bacterial treatments where an infection persists due to inefficient anti-bacterial penetration through the layers of cells. It is likely a problem in plasma – bacteria studies and makes it difficult to compare between studies. Fernandez *et al* [71] observed the inactivation rate of bacteria on agar exposed to N_2 plasma effluent was inversely proportional to the cell density of the treated sample.

5.5. Conclusion

The plasma system used in the current study has the unique capability of exposing low volume droplets to a uniform treatment with respect to transit time through the plasma. The droplets acquired chemical activity and were shown to be effect towards inactivating bacteria on agar up to 120 mm from the plasma, when the additional tubing was attached. The direct impact of $^{\bullet}OH$ on living cells has been investigated in this chapter although the effects of other active species cannot be excluded. Reactive nitrogen species (RNS), such as nitric oxide ($^{\bullet}NO$) and nitrate radical ($^{\bullet}NO_3$), are involved in intracellular signalling pathways. Because the plasma-droplet system is located within a closed environment devoid of ambient air e.g. nitrogen, it was assumed that the concentration of reactive nitrogen species generated by plasma-droplet interaction was negligible. OES spectra from Figure 4.3(c) indicate that under normal operating conditions i.e. He/Ne plasma, spectral lines attributed to N were absent. Reactive oxygen species other than $^{\bullet}OH$ may be generated from the plasma-droplet interaction, for example superoxide radical ($^{\bullet}O_2^-$) and hydroperoxyl radical ($^{\bullet}HO_2$), and affect intracellular chemistry however the main experimental focus was towards the highly reactive hydroxyl radical ($^{\bullet}OH$).

There is a slight contradiction with the $^{\bullet}OH$ analysis which would require further exploration; $^{\bullet}OH$ flux estimates from MB investigation (Chapter 4) and relationship with distance do not correlate with the inactivation efficiency from the plasma-droplet treatment reported in this Chapter, regardless of distance. $^{\bullet}OH$ radical damage is known to be extremely important in biology but direct generation of the $^{\bullet}OH$ radical is only truly possible using a plasma source. It would therefore be interesting to develop the plasma-droplet approach to investigate $^{\bullet}OH$ radical impact on microbial cells further. In the next chapter, individual cells are loaded into the droplet and passed through the plasma.

6. BACTERIA-LOADED DROPLET EXPOSURE TO PLASMA

6.1. Introduction

The plasma droplet system has demonstrated high efficiency production of H_2O_2 over the short exposure time, compared to other plasma configurations (Chapter 4). Direct measurement of $^{\bullet}OH$ radical concentrations in the droplet is not possible due to their short lifetime. However downstream measurements of Methylene Blue conversion provide a lower bound estimate of gas phase concentration of 7-8 x 10^{16} m^{-3} at 50 mm from the plasma, while literature reports of experimental measurements in RF He/H_2O plasmas suggest densities around 10^{20} – 10^{21} m^{-3} [60], i.e. a similar order of magnitude to the H_2O_2 gas phase densities. For mM levels of H_2O_2, Gorbanev *et al* [57] observed $^{\bullet}OH$ concentration in liquid of ~20 µM and also that oxygen content was derived primarily from added O_2 in the gas feed rather than water dissociation. On this basis there is a unique opportunity to create a selective $^{\bullet}OH$ radical source and in Chapter 5, the potential for delivering $^{\bullet}OH$ activated media over a relatively long distance was demonstrated. $^{\bullet}OH$ radicals dissolved into the liquid will rapidly decay to other products over approximately 2.7 µs [94] and in that time will travel a few microns into the liquid [5]. In standard plasma-liquid studies it is accepted that direct interaction with the radical does not occur but that secondary interactions e.g. via Fenton-like reactions are responsible for $^{\bullet}OH$-related damage [80].

These rapid kinetics prevent detailed study of the direct interaction of short-lived radicals with living cells yet it is understood that free radicals and other ROS (as well as RNS, RSS and CO) are produced in numerous physiological processes and are implicated in many significant diseases [156], [157], [158]. Biological research shows ever diverse and complex interactions with underlying mechanisms that are unclear and a greater mechanistic understanding is required. The challenges however of isolating physiologically relevant reactions and of ROS measurement are considerable. Most medical interventions targeting ROS have failed [157] which strongly suggests a significant lack of understanding of ROS biochemistry and biology. The ability to create a radical or ROS source and also deliver the active species right to the cell could lead to an invaluable experimental investigative technique. With regard to the $^{\bullet}OH$ radical itself, it is considered to be the most reactive. It has the highest reduction potential (apart from that of the solvated electron) and is known to be a dominant

factor in DNA, lipid and protein damage. In fact recent evidence suggests a common cell death pathway, shared by all classes of bacterial antibiotics, whereby the production of hydroxyl radicals is promoted as an end product [159]. However despite the central role played by $^{\bullet}OH$, its interaction has not been measured directly [80]. Attri *et al* [94], using a plasma/UV-initiated source of $^{\bullet}OH$, estimated the radical density profile in liquid and compared it to the induced in-vitro cell death ratio. They estimate a threshold radical density of $0.3 \times 10^{16} cm^{-3}$ is required, for 60 s plasma exposure.

On this basis there is a unique opportunity to investigate the direct effects of $^{\bullet}OH$ on a living cell by using the plasma – droplet system. In principle, the $^{\bullet}OH$ gas phase density is measurable and its diffusion-reaction kinetics in a liquid sphere could be modelled to provide an estimate of density. In this chapter, individual *E. coli* cells are transported in droplets and exposed to the plasma for a short period. Since the droplets are a similar size to the bacteria (droplet radius = ~7 µm [100]; bacteria size ~ 3 µm [160]), $^{\bullet}OH$ radicals from the plasma, as well as H_2O_2 are likely to reach the cell. The plasma is ignited using only He and Ne, with H_2O added via evaporation. The absence of oxygen or nitrogen from the gas feed mainly excludes key RONS precursors and greatly simplifies the chemistry for this initial investigation. Within the size and velocity distribution of the droplets, each individual cell receives the same exposure and hence statistical analysis is valid since the droplet rate is $\sim 10^4 - 10^5\ s^{-1}$.

Non-plasma-generated ROS can induce biochemical pathways that renders the cell inactive [27]. H_2O_2 treatment caused inactivation of *E. coli* in a dose dependant manner [161]. Permanent inactivation is the desired outcome for many antibiotic interventions and is achieved by generating ROS, in particular OH [24]. Exposure to lethal concentrations of antibiotic generates $^{\bullet}OH$ via the initiation of a common cell death pathway as a response to oxidative alterations in the cells metabolism (i.e. TCA cycle and iron metabolism) [159]. Depending on the concentration x exposure time (CT) value, the inactivation state may be temporary and after sufficient time to recover from the treatment, exposed cells can re-establish viability. Sub-lethal exposure to ROS may allow the cell to build up resistance to the treatment and consequently reducing the treatment efficacy. Cells that survived the treatment experienced a lag phase prior to growth, the duration of which was proportional to H_2O_2 concentration and exposure time [161]. This study focusses on exposing isolated

cells contained within plasma-treated droplets for a definite time, with particular attention towards the biological effect of the chemical species that were detected in Chapter 4 i.e. H_2O_2 and $^{\bullet}OH$.

This is the first reported attempt to transport bacteria-loaded droplets through a steady-state atmospheric-pressure plasma. Catalase was added to the collection liquid to scavenge any plasma-produced H_2O_2, thereby eliminating long-term H_2O_2 exposure from any observed cell effect. Plasma-generated $^{\bullet}OH$ can act independently of H_2O_2, since $^{\bullet}OH$ formation is not reliant on H_2O_2 degradation unlike in the Fenton Reaction. The plasma-droplet system employed in this study could directly deliver a known concentration of $^{\bullet}OH$ to the cell without any intermediary molecules, which would not be possible using other treatment techniques. Cell viability was assessed, as well as growth kinetics, lipid peroxidation and 'free' DNA contained in the droplet collection liquid, with and without catalase. In order to extract the effects of $^{\bullet}OH$ radicals alone, the impact of H_2O_2 was investigated via the generation of their concentration-time curves.

6.1.1. Aims and Objectives

6.1.1.1. Aims

- Examine the biological and chemical response of bacteria-loaded droplets to plasma treatment
- Investigate cell response to non-plasma-generated species

6.1.1.2. Objectives

- Measure cell viability, growth kinetics/metabolism, 'free' DNA, morphology, lipid peroxidation
- Attempt equivalence cell exposure studies to similar concentrations of the plasma-produced chemical

6.2. Methodology

A cell suspension was delivered to the tip of a nebuliser where it interacted with a gas flow (Q_{He} = 3.5 slm; Q_{Ne} = 1.0 slm), resulting in the generation of bacteria-loaded droplets that were transported through the plasma. For a more detailed description of bacteria cell preparation, please see Chapter 3: section 3.3.2. A single piece of quartz tubing was used to transport the droplets from the nebuliser tip, through the plasma and into the collection liquid (5 ml Ringer's solution (RS) or Ringer's solution with catalase (RCS). The plasma was ignited within the same quartz tube downstream from the nebuliser, creating a specific plasma treatment zone to minimise the influence of ambient air on the resultant chemistry (i.e. N_2 and/or O_2). The rf input power (13.56 MHz) was varied to assess the effect on the resultant chemistry and biology. Plasma-treated cells were recovered into collection liquid containing catalase to limit post-treatment effects of plasma-generated H_2O_2. The number of cells that remained viable after plasma treatment was estimated by performing decimal serial dilutions of the collection liquid and inoculating 100 µl of each dilution onto agar plates. Two agar types were used to encourage growth in petri dishes: an *E.coli*-specific agar (Chromocult®) and a generic bacteria growth agar (Nutrient). Selective media is typically used to differentiate bacteria in a mixed population of cells, however since only *E. coli* was used in this study then any significant difference in the number of viable cells between the two agars from the same sample could be as a result of contamination within the plasma-droplet system. The agar plates were inverted and incubated to encourage growth; plates with between 30-300 colonies were used for viable cell determination. Agar plates with no growth from conditions that were inoculated with undiluted collection liquid had a limit of detection of 10 cfu/ml. Liquid used to collect plasma-treated bacteria was also tested for H_2O_2 by the same technique used in Chapter 4.

The collection liquid was analysed for the presence of *E. coli* DNA as a possible indicator of extensive cellular damage. It is known that DNA absorbs light with a wavelength of 260 nm, therefore by measuring the collection liquids absorbance at this wavelength, an estimate of the concentration of DNA can be made. After processing, 2 µl of the collection liquid was added to the sensor on a UV-spectrometer (Nanodrop 1000) and the absorbance at 260 nm was measured. No absorbance values were detected from the collection liquid, however the DNA concentration could be below the limit of detection for the spectrometer. Therefore any DNA that was contained in the collection liquid required amplification via the polymerase chain reaction (PCR) technique using oligonucleotides from the

literature (see Chapter 3: section 3.6.4) for more information on the protocol used). It was hoped that the analysis could be quantitative, therefore thermal lysis was the preferred DNA extraction method since it involved minimal sample processing (99ºC for 10 min). Attempts were made to extract DNA using a kit (silica spin column, Sigma Aldrich) however the technique often retains some DNA in the column and the yield was too low for quantitative analysis. The solution used for cell collection had to be changed for DNA analysis, in order to preserve the molecule as best as possible. Tris-EDTA (TE) buffer is routinely used in molecular studies due to its chemistry. EDTA is a chelating agent which reacts with free iron (Fe) in solution, preventing any additional Fe-associated chemistry that may degrade the molecule e.g. $^{\bullet}OH$ generation via Fenton Reaction. Tris buffers the solution to a biologically tolerant pH ~ 8.0. A widely-used test for lipid peroxidation (TBARS assay) attempted to detect end products of the reaction cascade in the liquid used to collect plasma-treated cells. *E. coli* were also subjected to non-plasma-generated ROS i.e. $^{\bullet}OH$ via Fenton Reaction and short exposure to H_2O_2. The same analytical techniques that were previously discussed with reference to plasma-treated cells i.e. viability, growth kinetics, lipid peroxidation, were also used to investigate the impact of non-plasma-generated ROS on *E. coli* in suspension. More details on these protocols can be found in Chapter 3: section 3.6.2

The collection liquid was used for growth kinetics analysis by measuring the change in optical density of an incubated bacteria suspension as a function of time. It is assumed that the density is approximately proportional to the number of viable cells. A typical example of a bacteria growth curve is presented below.

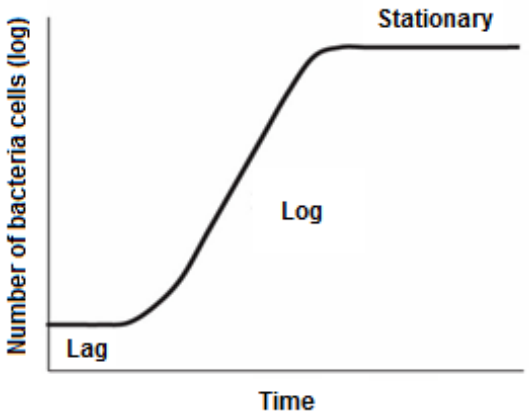

Figure 6.1 Schematic representation of a bacteria growth curve showing the three main phases: lag, log (exponential growth), and stationary phase

H_2O_2-induced damage is repaired in the lag phase [161]; therefore the length of time the cells remain in this phase can be used as an estimate the extent of cell damage by this species. The exposure time was equivalent to the total time of flight for the droplet exiting the plasma until collection (~10 ms), and [H_2O_2] measurements from chapter 4 can be used to estimate the plasma-generated H_2O_2 inactivation efficacy. When the cells have adjusted to their new environment, they begin growth and division at an exponential rate called the log phase (Figure 6.1). As the log phase progresses, the nutrient source becomes depleted and cytotoxic waste by-products of metabolism accumulate in the growth medium. The stationary phase is an unfavourable environment that results in the reduction in division rate and the net number of cells in the culture remains approximately equal i.e. rate of new cell production = rate of cell death. When the nutrient source is completely depleted, the cells die and the growth cycle ends.

6.3. Results

6.3.1. *E. coli* in droplets exposed to plasma-generated reactive species

6.3.1.1. Viable Cell Concentration

The concentration of viable cells was measured by directly inoculating the collection liquid, and decimal dilutions of the liquid, onto microbial growth agar and counting the number of colonies present after 24 h incubation at 37ºC. To nullify the sustained challenge from plasma-produced H_2O_2 on the collected bacteria cells, catalase was added to the collection liquid. The bar charts in Figure 6.2 show that the presence of catalase in the collection liquid was sufficient to prevent any inactivation from plasma-generated H_2O_2, regardless of input power (Figure 6.2 B). Without catalase, H_2O_2 accumulated in the collection liquid and resulted in a reduction in viability as a function of input power (Figure 6.2 A). Two different types of agar were used to grow the collected bacteria after plasma treatment: non-specific Nutrient agar (yellow) and selective Chromocult agar (blue), which only allows growth of undamaged coliform bacteria. Chromocult achieves this by actively suppressing growth of other bacteria through the inclusion of chemicals that make conditions unfavourable for growth. Negligible difference between the agar types suggests that the viability of plasma-treated *E. coli* are not affected by the treatment. Aerosolisation of the bacterial suspension results in ~ 3 log reduction in viability.

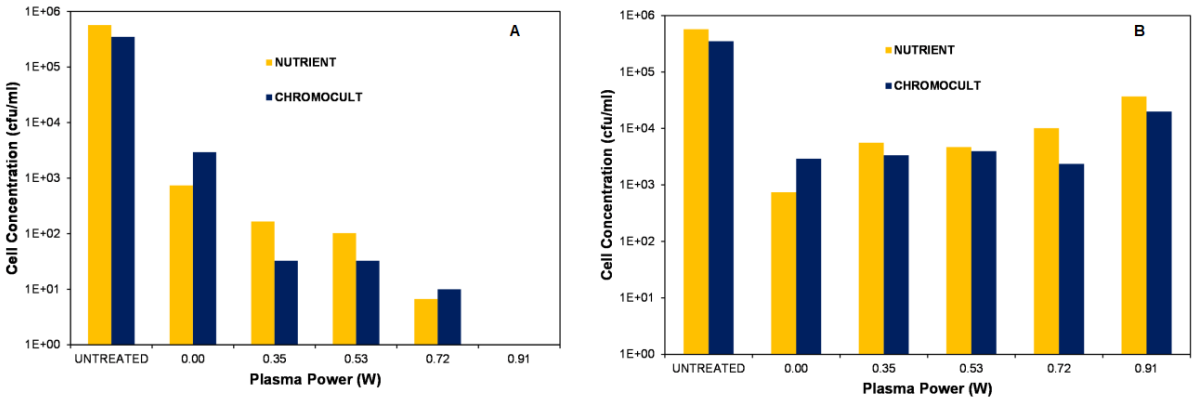

Figure 6.2 Graph A shows the viable cells that were recovered in the collection liquid (RS) after plasma exposure. Figure B demonstrates the effect of catalase in the collection liquid on viable cell recovery

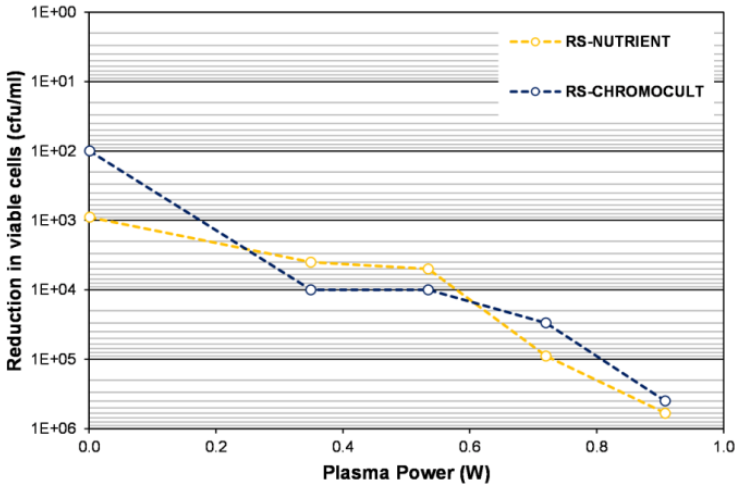

Figure 6.3 The graph shows the reduction in viable cell numbers as a function of plasma power. Cells were collected in Ringer's solution without catalase (RS) and two agar types were used for viable cell determination: nutrient and chromocult

The reduction in viable cell numbers after plasma treatment is shown in Figure 6.3 and the larger reductions in cell viability after treatment were observed for higher plasma powers. The calculated CT values for the treatment induced by the plasma-generated H_2O_2 are presented below (Figure 6.4). H_2O_2 concentration measurements were taken from Chapter 4, when droplets of Ringer's solution without bacteria were plasma-treated, and the exposure time was the total time-of-flight for the plasma-treated droplet until collection (10 ms).

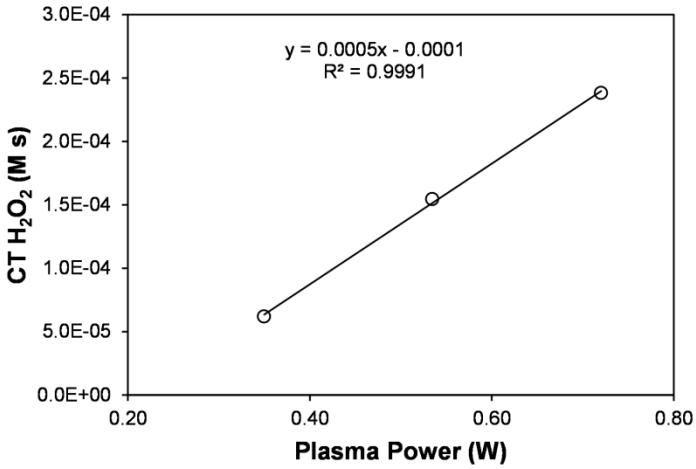

Figure 6.4 CT values calculated from the measured H_2O_2 concentration and the total time of flight for the plasma-treated droplet until collection, as a function of plasma power

Further analysis was undertaken to investigate the growth kinetics of the plasma-treated cells enclosed within droplets.

6.3.1.2. Growth Kinetic Profiles

Untreated cells were analysed alongside each set of plasma-exposed cells for comparison, since decimal dilutions *E. coli* cells showed a relationship between lag phase duration and initial cell density (Figure 6.5). Growth kinetics of incubated bacteria suspensions were assessed by measuring the optical density (n.b. spectrometer measures “absorbance”).

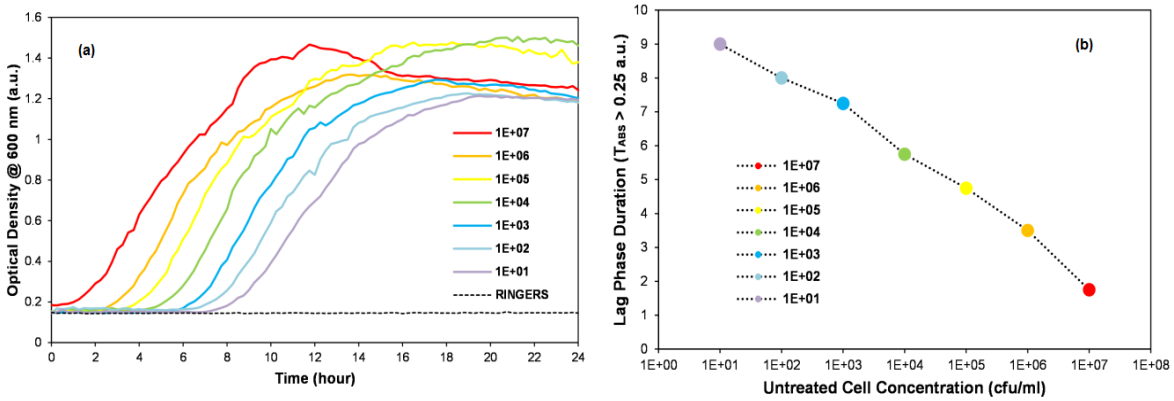

Figure 6.5 (a) shows the observed change in optical density of different concentrations of bacteria cells over an incubation time of 24 hours. Graph (b) shows the relationship between the initial cell concentration of a bacteria suspension and the observed duration of the lag growth phase (t_{abs} = 0.25 a.u.)

When Ringer’s solution with catalase (RCS) was used to collect plasma-exposed cells, the mean viable cell concentration in the collection liquid for all plasma powers was ~1 x 10^4 cfu/ml (Figure 6.2 (a)). Untreated cells of the same concentration generated a lag phase duration between 5-7 hours (Figure 6.5 ‘**O**’ = 1 x 10^3 cfu/ml and ‘**O**’ = 1 x 10^4 cfu/ml).

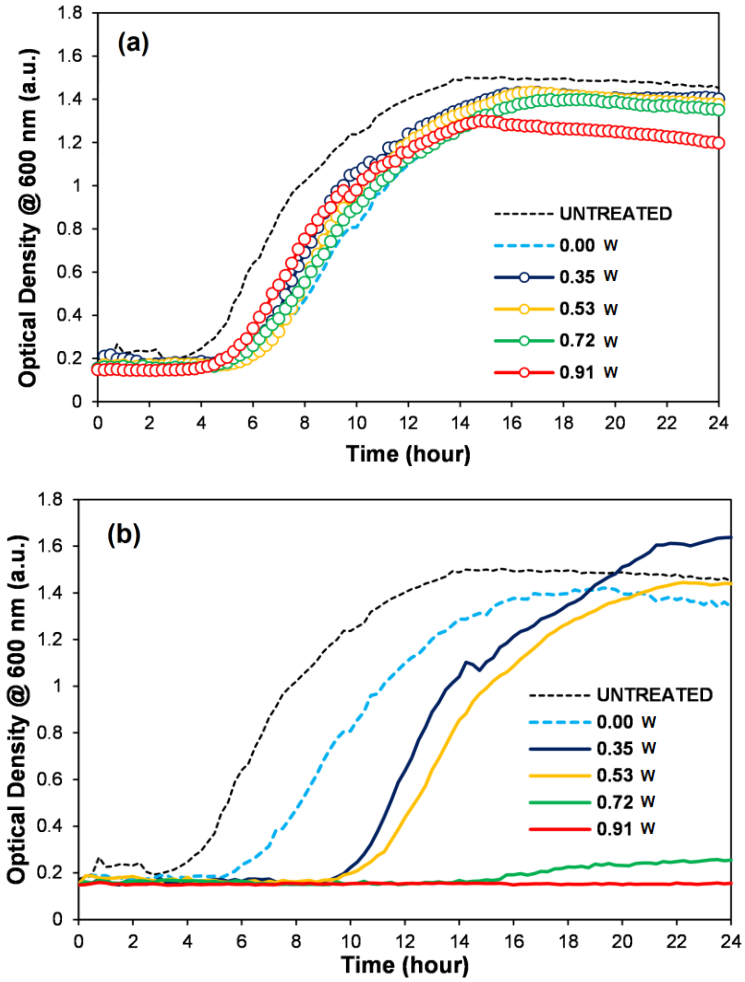

Figure 6.6 Growth curves of bacteria subjected treatments and collected with (a) and without (b) catalase. Untreated cells (dashed line) are cells in suspension, not aerosolised

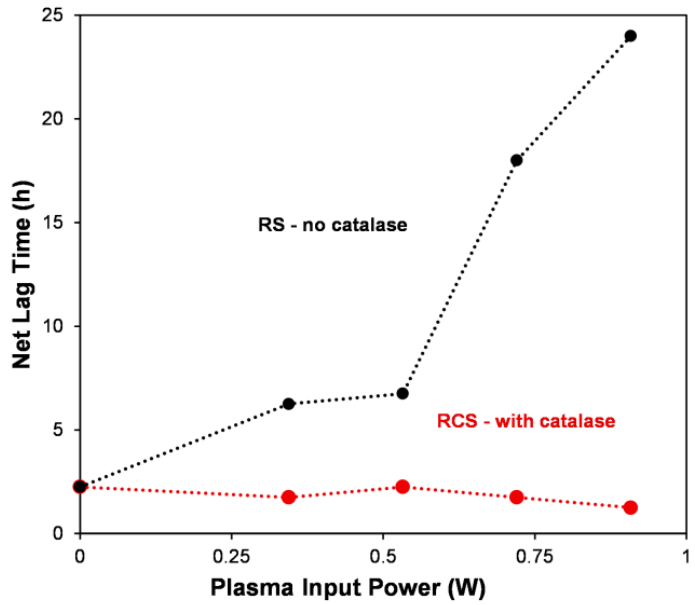

Figure 6.7 Graph showing the effect plasma power has on net lag phase duration i.e. untreated cell lag phase duration (~4.25 h) deducted from data

The observed lag phase duration for plasma-treated cells collected in RCS was ~ 5 hours (Figure 6.6 (a)), which is approximately equivalent to that of an untreated population of cells with a similar initial starting concentration. A graphical representation of the relationship between plasma power and net lag phase duration is given in Figure 6.7. Untreated cell lag phase duration of ~ 4.25 h has been deducted from these data. In the absence of catalase, plasma-treated cells are exposed to H_2O_2 throughout the growth measurement and the sustained challenge had a profound effect on lag phase duration (Figure 6.7 **RS**). The lag phase duration was largely unaffected in plasma-treated cell populations that were collected with catalase present, regardless of plasma power (Figure 6.7 **RCS**). However, the plasma-droplet interaction generates more than just H_2O_2 yet exposure to these additional radicals did not affect the lag duration. The lag phase allows cells to repair any damage before commencing division, therefore it is not known if exposure to these radicals caused damage that was repairable. It was assumed that an obvious target was the cell surface, therefore a stable end product of lipid peroxidation was chosen to assess the degree of surface interaction induced by the plasma-generated species.

6.3.1.3. Cell Surface Interaction

6.3.1.3.1. Lipid Peroxidation

Biomolecules on the cell surface, such as lipids, are the most susceptible to damage during exposure to an extra-cellular source of reactive species. In the phospholipid bilayer that composes the cell membrane, reactive species interaction with polyunsaturated fatty acids (PUFA) causes deterioration and triggers a degenerative chain reaction generally referred to as lipid peroxidation [27]. End products of the reaction cascade are stable in solution and can act as indicators of the damage induced by the species exposure e.g. malondialdehyde (MDA). MDA forms an adduct with thiobarbituric acid (TBA) which can be spectroscopically detected and has been used to assess plasma-induced lipid peroxidation [74], [78]. It must be noted that MDA may be generated due to damage incurred to other bio-molecules after exposure to reactive species (e.g. amino acids & DNA) and form MDA-TBA adducts that may overestimate lipid peroxidations involvement in human pathologies [162]. However, the detection of MDA-TBA adducts still offers a useful indication of the general state of oxidative stress that was caused by the plasma treatment of bacteria cells encapsulated within a droplet.

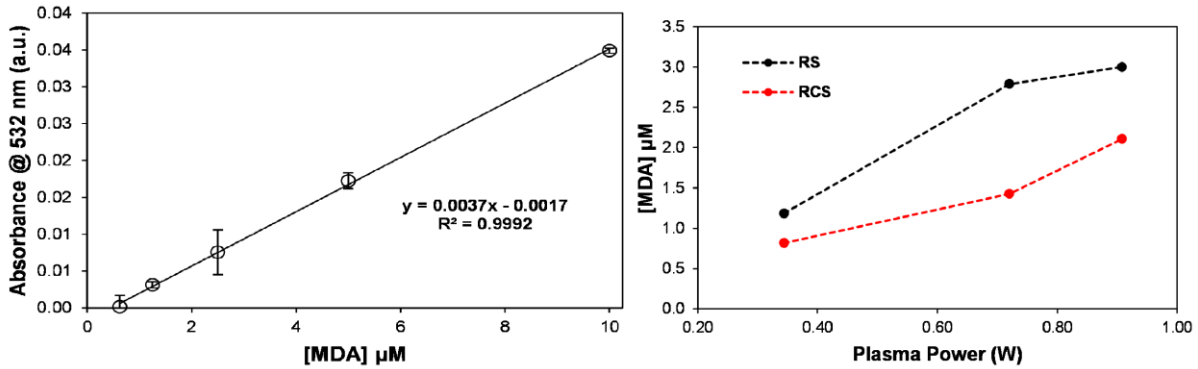

Figure 6.8 (a) TBARS assay calibration graph shows a linear relationship between the control solutions of known concentrations of MDA and the measured absorbance at 532 nm (Abs @ 532 nm). Figure 6.8 (b) is the concentration of MDA as a function of plasma power calculated from data from (a) when cells were collected in Ringer's solution with catalase (RCS) and without (RS)

TBARS assay was used to measure the amount of MDA from solutions that collected plasma-exposed bacteria-loaded droplets (Figure 6.8). MDA was detected independent of H_2O_2 scavenger presence in the collection liquid (i.e. catalase); therefore, MDA generation cannot be associated with cell exposure to plasma-produced H_2O_2 in the collection liquid (Figure 6.8). MDA could only have been generated during the total droplet time of flight (~10 ms) and H_2O_2 reduction potential is too low to induce an effect over these timescales. A species with a higher reduction potential must be responsible for the MDA detected in the collection liquid.

6.3.1.3.2. Intra-cellular biomolecule detection in the collection liquid: DNA analysis

The collection liquid will contain whole cells as well as DNA molecules released from cells with irreparable membrane damage after plasma exposure. A sample (1 ml) was filtered through a 0.25 µm membrane in order to remove the intact cells and subjected to amplification by PCR; unfiltered collection liquid was used for comparison. Both unfiltered solutions recorded a lower reading than the filtered solutions (Figure 6.9). Since the idea behind filtering the solutions was to recover any 'free' or released DNA only and to discard the DNA contained within whole cells, this appears to be an unusual result. The cause could lay with how the instrument detects the DNA; other substances or cell debris that absorb UV light could be interpreted as DNA.

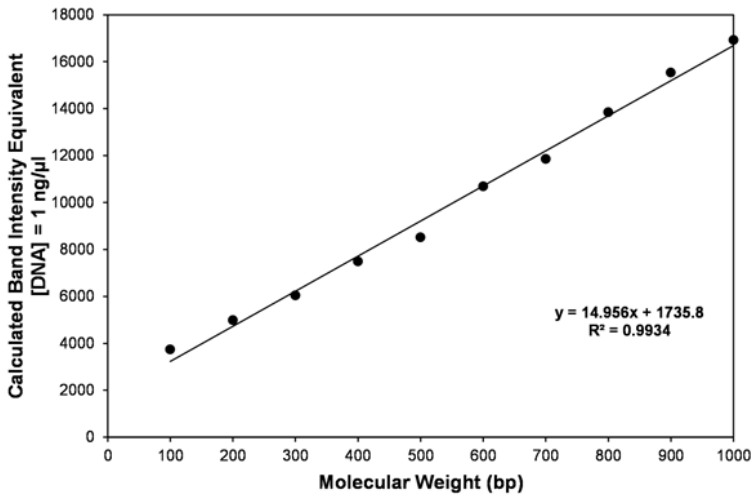

SAMPLE	DNA (ng/µl)
0 W (Unfiltered)	277
0 W (Filtered)	289
0.3 W (Unfiltered)	85
0.3 W (Filtered)	135

Figure 6.9 Calibration graph showing the measured band intensity of known DNA concentrations, as a function of the number of base pairs i.e. molecular weight. This data can be used to estimate [DNA] detected in the collection liquid

DNA in the collection liquid was amplified by the polymerase chain reaction (PCR) to increase the amount of DNA in the sample for analysis. The post-PCR product was subjected to gel electrophoresis through an agarose gel, and run alongside known molecular weights for quantification. Figure 6.9 shows the calculated band intensity for each standard molecular weight, and from this the amount of DNA in solutions used to collect DNA after plasma treatment could be estimated. The table inset shows that for cells only aerosolised (0 W), there was much more DNA after PCR than compared to the plasma-treated cells (0.3 W). This could be a result of there being less DNA available for amplification or the molecule has been damaged due to interaction with plasma-generated reactive species and/or UV radiation. However, it would be difficult to attribute plasma treatment with DNA damage using PCR due to the small nucleotide sequence that is targeted relative to the entire *E. coli* genome.

6.3.1.3.3. Morphology: Scanning Electron Microscopy

The following images show the morphology of *E. coli* that were recovered from the collection liquid after 30 min; 1 ml of the collection liquid was centrifuged in order to concentrate the cells, then re-suspended in 20 µl (x500 concentration) and deposited onto a glass coverslip. SEM images showed very little difference in morphology, regardless of treatment; plasma-exposed *E. coli* appeared similar to untreated cells (Figure 6.10).

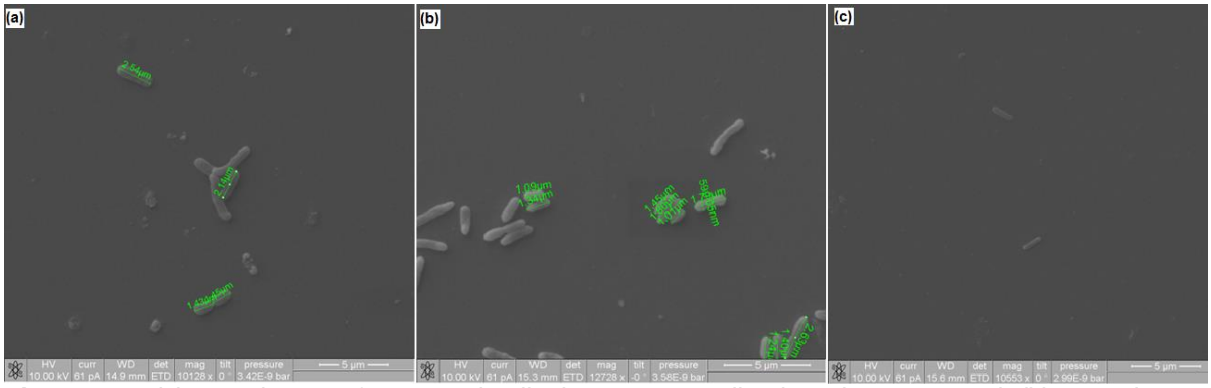

Figure 6.10 (a) SEM image of untreated cells, i.e. not aerosolised or plasma treated. (b) SEM image of aerosolised cells. (c) SEM image of aerosolised cells exposed to plasma; magnification ~x10 k

Experimentally, it was difficult to acquire a large enough sample size for SEM analysis. The viable cell concentration without aerosolisation, as determined by serial dilutions using agar plates, was ~6 x 10^5 cfu ml^{-1} (Figure 6.2). However, the total volume of bacteria suspension that was used to generate the droplets was 0.3 ml and the volume of collection liquid was 5 ml, a x15 dilution. The cells used in this chapter were collected over 30 min. but constraints on gas usage prevented longer collection times from being explored. Unsuccessful attempts were made to filter the collection liquid through a membrane, instead of centrifugation, to concentrate the cells prior to analysis. These preliminary results suggest that the surfaces of plasma-treated bacteria appear undamaged and are indistinguishable from cells not exposed to any external stress. Extensive optimisation of the cell-in-droplet collection and concentration technique would be required before any statistical analysis was possible. The following sections will explore the viability of the plasma-treated cells, as well as the growth kinetics.

6.3.2. *E. coli* exposed to non-plasma-generated reactive species

6.3.2.1. Hydrogen peroxide solution

E. coli in Ringer's solution (10^3 & 10^7 cfu/ml) and hydrogen peroxide solution was used for an equivalence study, in an attempt to mimic to a certain extent, the post-plasma intra-droplet environment. The cell suspension was adequately mixed using a magnetic stirrer, and hydrogen peroxide solution was added. After 10 seconds, catalase solution was added to quench the H_2O_2 and stop the cell exposure. A 10 second treatment duration was chosen as it was experimentally difficult to replicate the exact exposure time from the plasma treatment of bacteria-loaded droplets i.e. 10 ms. The amount of hydrogen peroxide in the solution was determined after catalase addition by the same method used in Chapter 4 (Ti-S assay) [104] and found to be negligible. Figure 6.11 displays the net lag time observed after *E. coli* were subjected to a number of separate H_2O_2 doses, i.e. concentration x exposure time (CT). Only the highest H_2O_2 CT (10 M s) had any significant effect on the net lag phase. There was no difference in the net lag durations calculated when both 10^3 cfu/ml (red circle) and 10^7 cfu/ml (black square) for the same H_2O_2 CT (Figure 6.11). The optical density graph for the highest H_2O_2 CTs investigated using 10^7 cfu/ml are shown in Figure 6.12.

6.3.2.1.1. Lag-phase duration

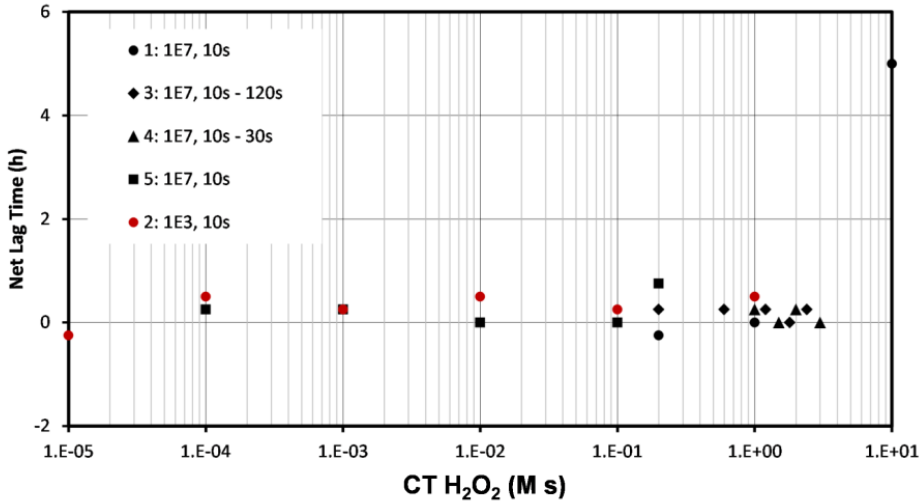

Figure 6.11 Composite graph showing the net lag time of an incubated bacteria suspension as a function of H_2O_2 CT value. Two concentrations of cells were used (1E3 cfu/ml & 1E7 cfu/ml) with varying exposure times to different concentrations of stock H_2O_2 solutions

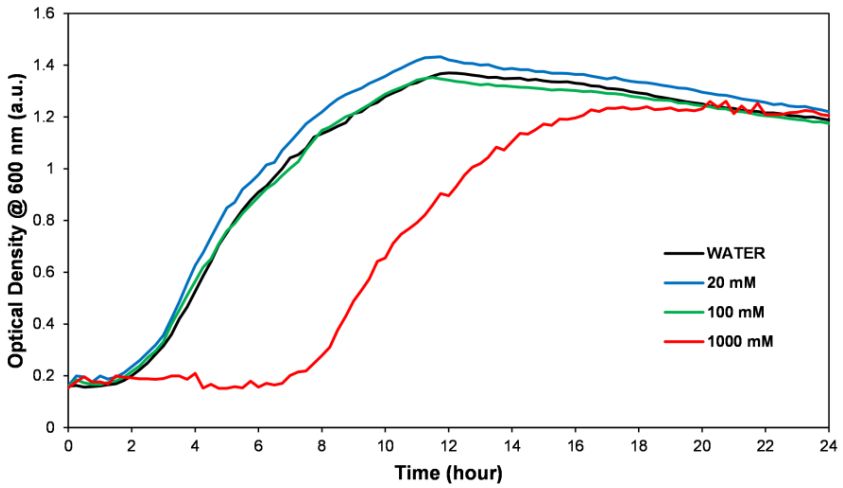

Figure 6.12 Graph showing *E. coli* [10^7 cfu/ml] exposed to 0 mM (i.e. water) 20 mM, 100 mM and 1000 mM H_2O_2 for 10 s

Figure 6.12 shows the growth curves of a bacteria suspension (10^7 cfu/ml) after exposure to different concentrations of H_2O_2 (exposure time = 10 seconds). The only observed effect on bacterial growth was for 1 M H_2O_2 exposure, which is nearly 3 orders of magnitude greater than what was measured from the plasma-droplet system.

6.3.2.1.2. Lipid peroxidation

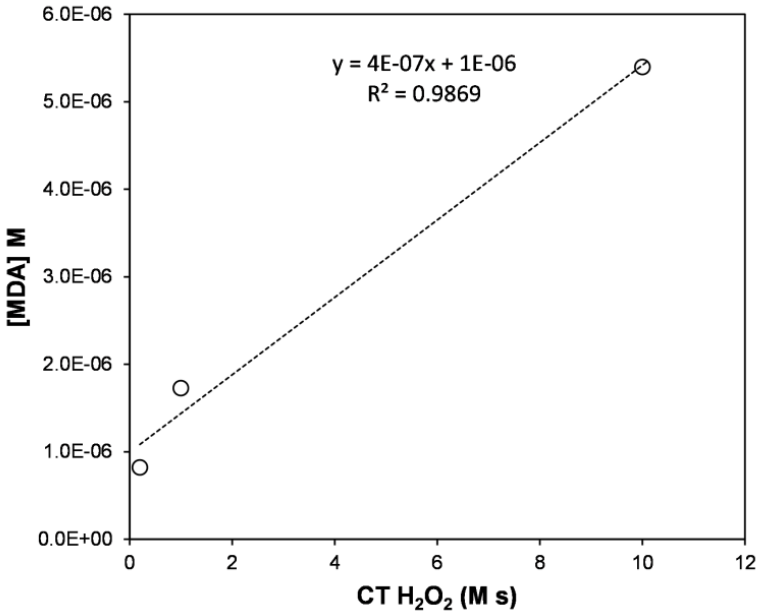

Figure 6.13 Graph showing the generated [MDA] as a function of [H_2O_2] exposure for 10 s for a cell suspension (10^7 cfu/ml) (see Figure 6.12 for associated growth curves).

Figure 6.13 displays the concentration of MDA measured from a cell suspension of 10^7 cfu/ml as a function of the H_2O_2 concentration x exposure time (CT) values. As the CT value increases, so

too does the amount of MDA detected, up to a maximum possible CT value of 10 M s i.e. [H_2O_2] = 1 M for 10 s duration. The reaction was stopped with the addition of catalase to the suspension contained in a beaker with magnetic stirrer.

6.3.2.2. Hydroxyl radical via Fenton reaction

6.3.2.2.1. Growth Kinetics

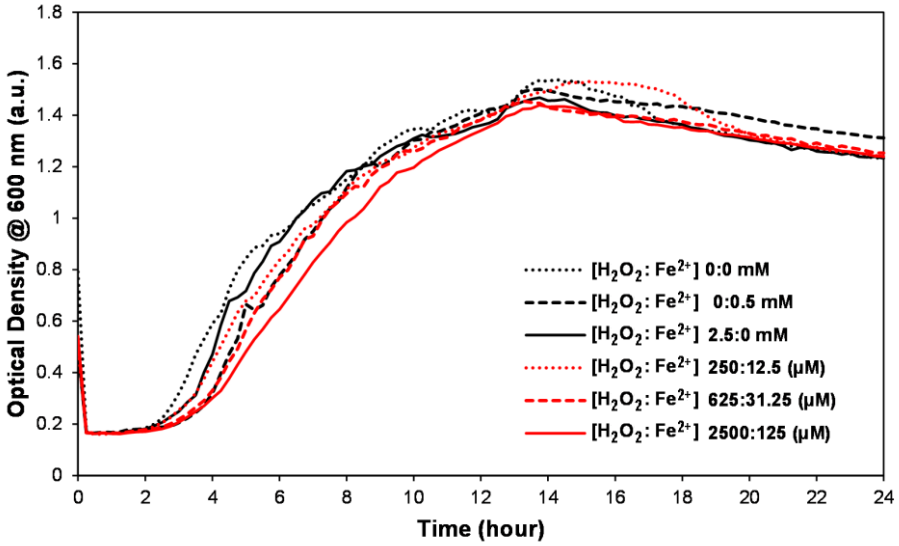

Figure 6.14 Graph showing the optical density change of incubated bacteria suspensions from cells that were exposed to the Fenton Reaction. Lines in BLACK lack 1 component of the Fenton Reaction; lines in RED vary [H_2O_2: Fe^{2+}] maintaining 20:1 composition

Bacterial cells in suspension were subjected to the Fenton Reaction. Fe^{2+} was added to cells in Ringer's solution (Figure 6.14). After 10 s H_2O_2 was added to generate OH* and after another 10 s interval, catalase was added to stop the reaction. Reaction solution was used for growth curve and lipid peroxidation analysis. All samples have lag phase duration similar to untreated cells at a concentration of 1 x 10^7 cfu/ml from first graph, and all experimental samples have a lag phase duration (i.e. Abs = 0.2 a.u.) between 2 ¼ - 2 ¾ hours i.e. no variation in lag phase duration between cells that were subjected to the Fenton Reaction, compared to those that were only exposed to each component separately.

6.3.2.2.2. Lipid Peroxidation

FENTON CONTROL SAMPLE	MEAN (zero-corrected) ABS @ 532 nm
[H_2O_2: Fe^{2+}] 0:0 mM	0.0048
[H_2O_2: Fe^{2+}] 2.5:0 mM	0.0046
[H_2O_2: Fe^{2+}] 0:0.5 mM	0.0059
FENTON SAMPLE	**MEAN (zero-corrected) ABS @ 532 nm**
[H_2O_2: Fe^{2+}] 250:12.5 (µM)	-0.0019
[H_2O_2: Fe^{2+}] 625:31.25 (µM)	0.0009
[H_2O_2: Fe^{2+}] 2500:125 (µM)	0.0028

Table 2 Table showing the analysis of the cell suspensions that were subjected to Fenton's Reaction and assessed for MDA content (TBARS assay)

Table 2 shows the sample matrix for the Fenton-generated $^{\bullet}OH$ equivalence study. All control samples, which omit 1 component of the reaction, generated a higher absorbance value than any of the samples that were subjected to the complete Fenton reaction. [H_2O_2] was the same for MB experiments; MB degradation rate was shown to be associated with [H_2O_2] i.e. generation of ROS. MB degradation using Fenton Reaction [H_2O_2] 250, 625 and 2500 µM confirms the generation of chemically-active, short-lived radicals (t_{exp} = 10 s) in a concentration-dependant manner. *E. coli* exposed to the same Fenton Reaction [H_2O_2] does not induce lipid peroxidation, as measured using TBARS assay (MDA). MDA was detected after *E. coli* exposure to [H_2O_2] 20 mM, 100 mM and 1000 mM (t_{exp} = 10 s), an increase in [H_2O_2] by a factor of 3. Whilst indirect $^{\bullet}OH$ (ROS) generation has been observed by measuring MB degradation, similar [$^{\bullet}OH$]/[ROS] does not produce a detectable lipid peroxidation product (MDA).

6.4. Discussion

There was very little difference in the number of cells recovered between the two agar types after each treatment condition, therefore ensuring adequate aseptic techniques were being followed throughout the study and the absence of bacteria other than *E. coli* could be reasonably assumed. There was no reduction in the number of viable cells after plasma treatment when the cells were collected in Ringer's solution with catalase (RCS). In the absence of catalase (RS), cell viability reduced in relation to increasing plasma power (Figure 6.3). This can be related to the result from chapter 4, where a positive relationship was observed between plasma power and [H_2O_2] measurement in the collection liquid. In the absence of catalase, the lag phase duration increased as a function of plasma power and could be attributed to prolonged exposure to plasma-produced H_2O_2. Cells collected in RCS were still exposed to plasma-generated species in-flight (~ 10 ms); however, no effect was observed in relation to cell viability or lag phase duration. This suggests that catalase successfully scavenged plasma-produced H_2O_2 before the molecule could interact with the cell and trigger inactivation modes. Observed higher levels of lipid peroxidation implies bacteria cell surface biomolecule interaction with plasma-generated species over short timescales (< 10 ms, Figure 6.8). *E. coli* DNA was also detected in the collection liquid and was measured in lower concentrations from the plasma-exposed cell sample (Figure 6.9). This evidence suggests that a reactive species generated by plasma-droplet interaction is responsible for the observed biological response, and yet has no observed long-term effect on morphology, viability or growth kinetics. SEM images from plasma-treated *E. coli* appear similar to unexposed cells.

H_2O_2 treatment caused inactivation of *E. coli* in a dose dependant manner [161]. Lower H_2O_2 concentrations resulted in a faster initial inactivation rates than higher concentrations. Cells deficient in DNA repair pathways (i.e. CM5409 (*polA*)) were the most sensitive to H_2O_2 challenge and experienced the quickest inactivation rate after only 90 s exposure to 1.25 mM H_2O_2 [161]. The inactivation pathway for low concentrations of H_2O_2 (<2 mM) was designated mode-1 while mode-2 inactivation occurs at higher H_2O_2 concentrations [161]. Mode-2 inactivation results from failure to repair H_2O_2-induced damage. Mode 2-killed cells permanently remain a standard size, on both plates and in liquid, and elongation is not observed. When the damage is repairable, growth can be initiated however the cells enter a filamentous growth phase without dividing (mode-1 inactivation). This inability to divide was presumed a consequence of damage to DNA, specifically the genes

responsible for septation [161]. The observation of two distinct kinetics of inactivation suggests different oxidation species are responsible. *E. coli* that were defective in DNA-repair mechanisms were predominantly inactivated by the mode-1 pathway [163]. The SOS response is induced upon exposure to H_2O_2, and protects against mode-1 inactivation due to an enhanced ability to repair DNA damage. The SOS response is a global DNA repair mechanism that becomes active upon detection of single-strand breaks (SSB). Damage to DNA in-vitro after exposure to H_2O_2 was attributed, in part, to the interaction with $^{\bullet}OH$ generated from a Fenton-like Reaction [164]. Metal cations (Me^{N+}) can react with H_2O_2 to generate $^{\bullet}OH$:

$$Me^{N+} + H_2O_2 \rightarrow Me^{(N+1)} + {}^{\bullet}OH + OH^- \qquad \textbf{(6.1)}$$

Formation of DNA SSBs requires H abstraction and only a strong reducing agent, such as $^{\bullet}OH$, could initiate the reaction. Degradation of H_2O_2 by DNA-bound iron could generate $^{\bullet}OH$ in close proximity to the DNA molecule and ferryl radicals generated in the same reaction may also be involved in damaging DNA [165]. An active inhibitor of metallic cations (i.e. chelator) can suppress $^{\bullet}OH$ generation via this pathway. DNA-repair deficient cells in the presence of a chelator prevented mode-1 inactivation after H_2O_2 treatment [163]. This suggests that transition metal-catalysed reduction of H_2O_2 (e.g. via Fe^{2+}) and formation of $^{\bullet}OH$ is involved in mode-1 inactivation of cells exposed to H_2O_2. H_2O_2 scavengers, such as iron-containing catalase, form part of the cells oxidative defence machinery and protect the cell by efficiently degrading the molecule into non-toxic products. In this study, *E. coli* in suspension were exposed to H_2O_2 and $^{\bullet}OH$ via Fenton reaction for 10 s to try to assess their involvement in bacteria inactivation. The exposure was stopped with the addition of catalase. No change in the growth kinetic profiles was observed when the cells were exposed to a similar concentration of H_2O_2 that was measured in chapter 4. The same H_2O_2 concentrations were used to generate $^{\bullet}OH$ via Fenton reaction (10 s) but this also had no effect on the growth profiles or lipid peroxidation (Figure 6.14 and Table 2). However, when the cells were exposed to much higher (x500) H_2O_2 concentrations (1 M), the lag phase duration increased and MDA was detected and increased as a function of $[H_2O_2]$ (Figure 6.12 and Figure 6.13). Since it required a much higher concentration of H_2O_2 than what was measured in chapter 4 to induce an effect, it can be stated that the plasma-droplet system generates too low a concentration of H_2O_2 to have an effect on growth

kinetics or lipid peroxidation. Figure 6.15 shows that the plasma-generated H_2O_2 would not be sufficient to generate the measured MDA since it requires a much larger (~ 5 orders of magnitude) CT value for H_2O_2 solution to generate the equivalent MDA concentration. CT values for plasma-generated H_2O_2 were calculated from the concentrations reported in Chapter 4 (actual not measured) and the total droplet time of flight (10 ms). A species other than H_2O_2 is therefore responsible for the lipid peroxidation caused by plasma exposure. Experimental evidence from Chapter 4 section 4.3.3.1 suggests that gas-phase $^{\bullet}OH$ generated by the plasma-droplet system can be transported away and retain its chemical reactivity up to 100 mm from the core plasma region. It is possible that the bacterium contained inside the droplet could interact with the plasma-generated $^{\bullet}OH$, however this would require radical diffusion from the gas phase into the liquid phase over the total droplet time of flight (~10 ms) and more experimental work would be required to fully verify this hypothesis.

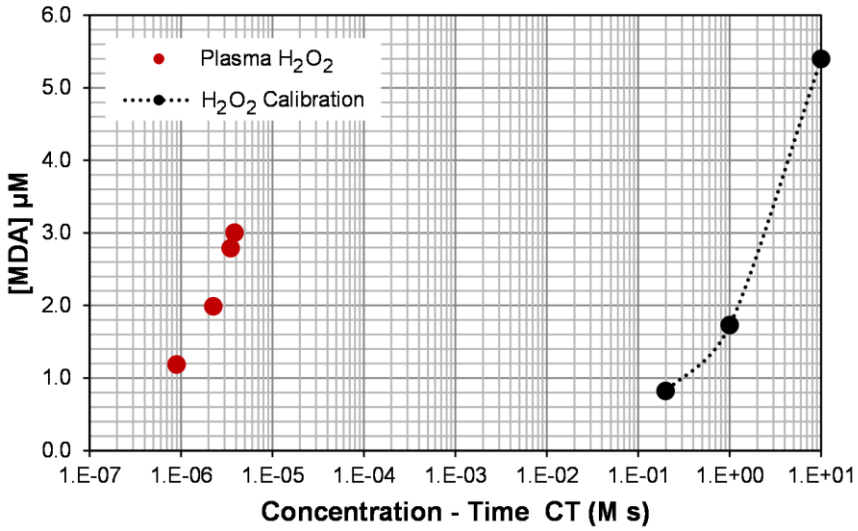

Figure 6.15 MDA generated from *E. coli* as a function of CT values for H_2O_2 generated by the plasma (red dot) and by H_2O_2 solution (black dot). In order to achieve the equivalent concentration of MDA measured after plasma treatment, a much higher CT value is required when exposing *E. coli* to H_2O_2 solution

Biocidal treatment efficacy (i.e. rate of log viable cell reduction) can be categorised, based on the concentration of an antibacterial substance and the length of time the cells are exposed to it. The Chick-Watson Model calculates the inactivation kinetics of a treatment, where the surviving ratio of cells ($\ln(N/N_o)$) is equal to the product of the concentration of the antibacterial substance (C) and exposure time (t):

$$\ln\left(\frac{N}{N_0}\right) = kCt \qquad \textbf{(6.2)} \quad [155]$$

Concentration-time (CT) values are an important measurement in water disinfection. It is typically used to estimate dosages for chlorination and the recommended CT value for *E. coli* inactivation is 5.4 x 10^{-6} M s^{-1} [166], CT values can be calculated for any chemical species that exhibits a biocidal effect e.g. ROS. Oxygen-containing radicals are known to damage cell components and sufficient exposure causes irreparable damage that can lead to inactivation. Estimates for ozone vary from 9.8 x 10^{-7} M s^{-1} [167] to 4.4 x 10^{-8} M s^{-1} to inactivate *E. coli* [166]. $^{\bullet}$OH, generated from UV-irradiated TiO_2 solution, had a CT value of 3.9 x 10^{-12} M s^{-1} to achieve a 2-log reduction in *E. coli* [155]. Steady-state $^{\bullet}$OH concentration was calculated from the measurement of the degradation rate of an $^{\bullet}$OH-specific probe, p-chlorobenzoic acid. Another study reported enhanced inactivation of *E. coli* with UV radiation in combination with H_2O_2 treatment, compared to UV exposure only [168]. $^{\bullet}$OH was again identified as a species responsible for the inactivation and expressed the highest disinfection efficacy. The CT values suggest that bacteria suspended in liquid can be inactivated by exposure to ROS generated in the liquid phase and $^{\bullet}$OH has a much lower CT value than ozone i.e. $^{\bullet}$OH is much more effective. Species' reactivity can be categorised by their affinity to interact with otherwise stable molecules i.e. reduction potential. $^{\bullet}$OH has the highest reduction potential (~2 V), and consequently the shortest half-life (~10^{-9} s), of the reactive species that can interact with biomolecules [169],[170]. MB exposed to Fenton-generated $^{\bullet}$OH degraded as a function of the concentration of the reactants and exposure time yet. *E. coli* in suspension were subjected to the same reaction and no increase in lag phase or MDA was observed. Although the cells were suspended in RS (buffered) and MB was diluted in dH_2O (non-buffered), $^{\bullet}$OH generation via Fenton reaction can occur using buffered solutions [171]. MDA was detected in both RS and RCS collection liquids, which suggests that the bacteria-loaded droplet was subjected to oxidative stress in-flight, regardless of the presence of an H_2O_2-scavenger in the collection liquid. A summary of the calculated MDA production rates from relevant literature are presented in Table 3. For a much lower concentration of cells, the MDA levels produced in the plasma – droplet system were much higher than observed in other plasma configurations.

First Author	Year	Plasma Type	MDA Production Rate (M s-1)	Cell (cfu/ml)	Liquid (vol)
Rutherford	2016	rf glow (0.35 W)	1.4 – 3.0 E-04	*E. coli* (10^5)	RCS (0.3 ml)
Dolezalova [74]	2015	Jet (rf-kINPen)	1.7E-11	*E. coli* (10^7)	NaCl (1 ml)
Dolezalova [3]	2016	DBD	1.6E-10	*E. coli* (10^6)	NaCl (10 ml)
Alkawareek [79]	2014	Jet (20 kHz)	2.7E-07	*E. coli* (10^7)	PBS (20 µl)
Colagar [86]	2013	Jet (18.56 kHz)	2.00E-02	*E. coli* (10^8)	LB broth (5 ml)

Table 3 Calculated MDA production rates (M s^{-1}) from plasma treatment of *E. coli* in the literature

The quantity of MDA in other plasma – liquid studies was observed with an associated reduction in cell survival. The production of MDA as described in the literature appears to rely on the presence of O_2 [27], [172]. However in this work, the amount of oxygen will be limited due to the noble gases feed even though the MDA production was much higher than other plasma – liquid studies. Yusporov *et al* [56] simulated the reaction of $^{\bullet}OH$, HO_2, and H_2O_2 reaction with Lipid A of *E. coli* and give estimates of bond breaks per radical molecule impact which implies that MDA can be formed without O_2. Hong *et al* [173] showed that *E. coli* were inactivated due to the generation of $^{\bullet}OH$ via a copper (Cu)-mediated Fenton-like reaction. Low concentrations of Cu did not affect cell survival, however MDA was still detected for treatment times up to 60 min. As the concentration of Cu-generated $^{\bullet}OH$ increased, so too did the amount of MDA as a function of both initial Cu concentration and exposure time. The authors proposed that the mechanism of inactivation was oxidation, not peroxidation, of lipids in the *E. coli* cell membrane, in particular monounsaturated fatty acids (UFA) and not the previously reported polyunsaturated fatty acids (PUFA) [173]. Detection of MDA with minimal *E. coli* inactivation suggests sub-lethal damage occurred but any damage was repaired and had no long-term effect on cell survival. This corresponds well with the results from the current study, where MDA was measured in the liquid used to collect the plasma-treated bacteria-loaded droplets, without any reduction in cell numbers. Attempts to understand the complex biochemical pathways involved in cell inactivation by radicals generated in the liquid phase is of considerable relevance to Plasma Medicine, especially when the aim is to safely treat human tissue whilst inactivating bacteria.

6.5. Conclusion

The plasma-droplet system can enclose isolated bacteria cells within liquid carrier vessels and be transported through a confined discharge zone without affecting viability. Equivalence studies that were carried out *on E. coli* using similar concentrations generated from the plasma-droplet system had no effect on viability, growth kinetics or lipid (per)oxidation. Figure 6.15 compares the concentration of MDA generated after exposure to plasma–generated H_2O_2 and an H_2O_2 solution. For an equivalent concentration of MDA to be produced, a much larger H_2O_2 concentration was required compared to the plasma exposure. From the literature, it is expected that $^{\bullet}OH$ to be generated at the plasma-droplet interface and due to the confinement of the cell within a low volume droplet, plasma-generated $^{\bullet}OH$ could interact with the cell surface and initiate biochemical pathways. The detection of MDA without an associated effect on viability has not been reported in plasma-bacteria investigations. A similar effect has been reported for Cu-mediated $^{\bullet}OH$ generation in low Cu concentrations [173]. How MDA is produced without loss of viability is not known but recent reports suggest oxidation of monounsaturated fatty acids as a possible mechanism for MDA generation.

Using the plasma – droplet system the plasma-activated chemistry in the droplet, which is likely to include the $^{\bullet}OH$ radical, caused sub-lethal damage to the bacterial cell as detected by the presence of MDA. This is normally an indicator of lipid peroxidation. However the limited oxygen availability for the reaction suggests that other chemical reactions may be involved. The amount of MDA generated was much larger than reported for other plasma – liquid studies. Overall this suggests that the plasma–droplet system can provide evidence of direct $^{\bullet}OH$ radical damage to a living cell. A more detailed analysis or simulation of the droplet chemistry would be very useful in support of this work.

7. CONCLUSIONS AND FUTURE INVESTIGATIONS

7.1 Plasma-droplet system: concluding remarks

Atmospheric-pressure non-thermal plasma treatment of liquid droplets in-flight allowed for the generation of short-lived reactive species and transport away from the source without complete evaporation of the liquid. This unique system configuration allowed for a single pass exposure through a confined plasma in the absence of O_2 and N_2 from the feed gas. Droplets were entrained in the gas flow and transported through the plasma in a short time (transit time ~ 120 μs), much shorter than possible in other plasma configurations under steady-state conditions. The custom plasma-droplet system used in the current study has shown versatility with regards to the liquid type that can be plasma-treated. The plasma-generated species interacted with droplets produced from dH_2O, Ringer's solution, bacterial suspension and gold nanoparticle precursor solution. Each droplet becomes its own micro-reactor during and after plasma exposure, where gas-phase species interact with the liquid and diffuse into the liquid phase, initiating secondary chemical pathways. The droplets acquired chemical reactivity properties which were not present in untreated droplets. Droplets-in-flight allowed for the delivery of short-lived reactive species well beyond the plasma region. An enhanced effect between short-lived reactive species and a bacteria-loaded droplet was observed, due to the cell confinement within the droplet. The liquid used to collect the plasma-treated droplets became chemically active, due to the presence of H_2O_2 which remained stable 4 weeks after the initial treatment. The plasma-droplet system can generate and deliver short-lived reactive species to an isolated cell without affecting viability whilst simultaneously producing a chemically stable solution containing a potent biocidal agent i.e. H_2O_2. The ability to deliver uniform concentrations of reactive species to isolated cells could advance the current knowledge bottleneck regarding the gas-phase species generated by plasma and how they influence cells. By removing complexities associated with the plasma treatment, such as liquid volume which surrounds a cell and simplification of chemistry, the plasma-droplet system could provide new information, or more detail on current knowledge, of the direct qualitative and quantitative effects of plasmas on biological systems.

7.2 Key findings from this thesis

This investigation is the first report of micron-sized liquid droplet transport through a non-thermal He/Ne plasma. The measured H_2O_2 production rate from the plasma-droplet system far exceeds anything currently reported in the literature and was detectable and stable in the collection liquid weeks after the experiment. The highly-reactive $^{\bullet}OH$ could be transported from the plasma and induce a chemical effect up to 115 mm away from the source. Bacteria in droplets exposed to plasma suffered no observable loss in viable cell concentration when collected in the presence of an H_2O_2 scavenger. Plasma-generated $^{\bullet}OH$ activity associated with the droplet suggests that bacteria contained within the droplet could interact with the $^{\bullet}OH$ over the total droplet time of flight until collection (~ 10 ms). Lipid peroxidation as a result of bacteria-loaded droplet exposure to plasma was observed but the same degree of damage was not achieved when the bacteria were exposed to Fenton-generated $^{\bullet}OH$. From H_2O_2 solution bench tests, the high concentration-time requirements for lipid peroxidation by H_2O_2 alone indicate conclusively that species other than H_2O_2 are responsible in the plasma-droplet. The conclusion of this investigation is that the plasma-droplet system can generate significant amounts of $^{\bullet}OH$ to interact with bacteria in droplets post plasma exposure lipid peroxidation in-flight before collection. The system could be used to deliver $^{\bullet}OH$ to remotely induce chemistry in other applications that would otherwise only be possible through direct plasma treatment of liquid.

7.3 Future investigations

The plasma-droplet system was established using a gas mixture of neon to generate the droplets and helium to transport the droplets through the plasma. During the current study it has become uneconomical to use neon due to political circumstances in the region where the gas is extracted from the Earth i.e. Ukraine. Argon could be an appropriate replacement, although the metastable species produced from argon plasmas complicate the chemistry which could make elucidation of the plasma-induced biochemical response more difficult. A novel and much more accurate droplet generator and plasma interface has been constructed by other researchers in NIBEC. This only requires a single gas to operate. It generates monosize droplets with a very narrow distribution and a fixed/selectable velocity.

It has been reported that droplet flow through a discharge region alters flow direction and generates turbulence which has a direct influence on the reactive species concentration profile at a downstream target. The plasma-droplet system offers an opportunity to investigate the potential effect on turbulent flow post-plasma exposure, and the use of droplets could prolong any effect which may make the elucidation of the effect more experimentally possible. Dye-loaded droplets could be plasma-treated and collected via impaction, and the deposition profile could be compared to results from this thesis that reported dye-loaded droplets not exposed to plasma. The target could be loaded with a chemical indicator specific to a particular reactive species to investigate individual species reaction profiles.

Other gases and compositions could be added to the feed gas to compare the droplet chemistry and antibacterial effect with the He/Ne plasma reported in Chapter 5. Examples include O_2 and N_2 in different ratios as well as H_2O vapour. Measurement of the humidity within the quartz tube of the plasma-droplet system would give a better indication of the water content in the plasma and the influence this has on the chemistry. There is also the potential to heat the gas prior to delivery into the plasma region to encourage droplet evaporation. This could expose the bacteria cell to direct plasma without the protection of the liquid droplet, and real-time monitoring of the plasma emission using OES might offer a novel technique to detect bacteria-in-flight using plasma.

The plasma-droplet system can inactivate bacteria cells on agar and when an additional tube was attached to the quartz tube, the zone of inhibition was relatively consistent at various distances from the plasma. The maximum distance that could be tested was limited due to the vertical orientation of the shroud and the available space within the PCR workstation. It is not known at what distance the plasma-droplet system does not have an antibacterial effect but this would require redesigning the shroud and attempt to make the system more compact. The UV emission from the plasma alone was not sufficient to inactivate *E. coli* on agar, however further studies investigating the sub-lethal exposure to UV is possible with the plasma-droplet system, and comprehensive DNA analysis post-plasma-generated UV exposure could yield some interesting results that would be applicable across a number of research areas.

Chapter 4 reported on the measurement of plasma-generated H_2O_2 from the droplet collection liquid. Bacteria growth curves from Chapter 6 showed the effect of prolonged exposure to plasma-

produced H_2O_2 when the aerosolised cells were collected in the absence of catalase. A further equivalence study would be to expose non-aerosolised cells to the plasma-generated H_2O_2 and compare with results when non-aerosolised cells were exposed to different concentrations of a H_2O_2 solution (see section 6.3.2.1). By comparing any effects the plasma-generated H_2O_2 has on bacterial growth compared to a H_2O_2 solution could offer an opportunity to investigate the effects of additional, as yet unmeasured, plasma-generated reactive species.

The low volume liquid droplet and transport away from the plasma could allow for charge measurements of the droplet surface in flight. Solvated electrons are the most highly-reducing species in chemistry but are often experimentally ignored due to the difficulty in detection and quantification. The plasma-droplet system could allow for detection of plasma-induced surface charge measurement before quenching, due to the nature of the droplet being in-flight. It may also be worthwhile investigating the effect the droplet charge may have on the cell enclosed within the droplet, due to possible electroporative effects. Gene transfection by electroporation manipulates cell membranes by electrical pulses in liquid but is inefficient and relatively time-consuming process. Literature on plasma-induced charge effects on cells in liquid is scarce and the plasma-droplet system could advance knowledge in this particular research area. It would be interesting to see if gene transfection would occur. One possible way to investigate this would be to perform a gene transfection experiment using the plasma-droplet system in parallel with a conventional electroporation protocol and equipment, and compare the efficiency, quality and yield of the cloned product between the two techniques.

The chemical analysis of the plasma-droplet system focussed on the detection and quantification two biologically-relevant species, namely $^{\bullet}OH$ and H_2O_2. The confinement of the plasma removed the influence of O_2 and N_2 from the resultant plasma chemistry, however a comprehensive study involving the addition of a range of antioxidants to the liquid used to generate and collect the droplets would be required to establish a more complete characterisation of the species generated and their influence on biological systems. 1-butanol was added to a solution of MB in Chapter 4 and successfully prevented degradation due to $^{\bullet}OH$; catalase was added to the droplet collection liquid in Chapter 6 in order to degrade plasma-produced H_2O_2. In order to progress the experimental findings from this current study, other selective scavengers could be added to the droplet collection liquid to

further investigate the chemistry initiated by the plasma droplet system e.g. superoxide dismutase for $^{\bullet}O_2^-$, sodium azide for $^1O_2$, D-mannitol or coumarin as a biologically tolerant scavenger of $^{\bullet}OH$. Selective anti-oxidants could be added to the nebuliser liquid to generate scavenger-loaded droplets and transport through the plasma-droplet system. The resultant chemistry in the absence of that particular radical species could be assessed and compared to conditions without the scavenger. This technique might be problematic for enzymatic-based anti-oxidants due to the protein denaturation temperature around 60 ºC and the gas temperature of the plasma is ~ 80ºC. The protein structure may not remain intact after plasma exposure and an ineffective scavenging of the specific radical species could be incomplete. It is not known whether a solution containing an enzyme would remain chemically active after transport through the plasma-droplet system and could offer another investigation. Enzyme activity could be assessed by oxidant challenge post plasma-treatment or by detecting markers of protein oxidation e.g. Protein Carbonyl assay.

The above scavengers would help in understanding the chemical and biological mechanisms. Other additives to the liquid could be the subject of study themselves. For examples the rapid synthesis of nanoparticles has been achieved. Since these are known to have strong biocidal properties, the inclusion of nanoparticle synthesis and delivery protocols for the technique developed in chapter 5 may enhance the effectiveness, provided the precursor is sufficiently converted. Also synthesis of the nanoparticles, or simply their inclusion, in the same droplet as the bacteria may help improve understanding of mechanisms. This could be further developed by the inclusion of free DNA in the droplet, without bacteria. Electron bombardment and $^{\bullet}OH$ interaction with DNA is known to be critical with regard to damage and an important element in radiotherapy / chemotherapy. Nanoparticles and chemotherapy agents e.g. platinum add very strong synergistic effects. Traditional studies have mostly used dry DNA under vacuum exposed to high energy electrons or photons. The plasma – droplet system would allow for the study of these effects at atmospheric pressure and low energy in liquid and hence the DNA is in a more realistic environment.

8. APPENDIX

8.1. Chapter 3

8.1.1. Appendix 1: Equipment List

8.1.1.1. General

- PCR Workstation (VWR, Code: UV/PCR2-UK, https://uk.vwr.com/store/product/13475788/pcr-workstation-vwr-material-stainless-steel-vwr-pcr-workstation-worksurface-wd-720540-mm-eu-plug-wdh-ext-750620780-mm-weight-kg-48-lighting-2-uv-tubes-internal-254-nm-25-w-each-1-uv-tube-in-uv-air-recirculator-254-nm-8-w-1-white-light-tube-internal-15-w-shelves-removable)
- Standardised brass weights (Oertling)
- Ultrasound bath (U 95, Ultrawave, http://www.ultrawave.co.uk/u95-new-reduced-pricing.html)
- Vernier calipers (Mitutoyo Absolute Digimatic, 500-196-30, http://www.mitutoyo.co.uk/hometabs/top-rated/500-196-30)

8.1.1.2. Gas and Electrical Components

- Radio frequency (13.56 MHz) power generator (Cesar RF Power Supplies http://www.advanced-energy.com/en/Cesar_RF_Generators.html)
- Roller Inductor Antenna Tuner (Matching network) MFJ-989D (MFJ Enterprises http://www.mfjenterprises.com/Product.php?productid=MFJ-989D)
- High frequency ‘spark’ generator BD-10AS (Electro-Technic Products Inc http://www.electrotechnicproducts.com/bd-10as-high-frequency-generator/)
- Radio frequency (13.56 MHz) current-voltage probe (Impedans Octiv VI probe, https://www.impedans.com/octiv-vi)
- Multi-gas Controller (MKS Instruments UK Ltd. http://www.mksinst.com/intl/UK1.aspx)
- Mass Flow Controller (MFC) – helium (MKS Instruments UK Ltd. http://www.mksinst.com/intl/UK1.aspx Serial # 021570023)
- MFC – neon (MKS Instruments UK Ltd. http://www.mksinst.com/intl/UK1.aspx Serial # 132379223)
- ¼’’ swagelock connection from MFC to (in-house gas tubing)

- ¼'' swagelock bulkhead adapter (SS Swagelok Tube Fitting, Bulkhead Union, 1/4 in. http://www.swagelok.com/search/find_products_home.aspx?part=SS-400-61-4AN)
- Swagelock Stainless Steel All-Welded In-Line Filter, 1/4 in. Swagelok Tube Fitting, 0.5 Micron Pore Size (http://www.swagelok.com/search-results/search-results.aspx?qs=SS-4FWS-05)
- Nebuliser gas capillary tubing (2.0 mm OD/1.0 mm ID. BRC 115 Burgener Research http://www.burgener.co.uk/Prices.html)
- UpChurch fingertight fittings (One-Piece Fingertight Male Nut, 10-32 Coned, black single for 2.0 mm OD https://www.idex-hs.com/fluidic-connections/fittings/coned-fittings/one-piece-fingertight-fittings.html)
- Round Quartz tubing (2.4 mm OD/2.0 mm ID #CV2024Q-100 and 2.6 mm OD/2.0 mm ID #CV2024Q-300, CM Scientific Ltd./ www.vitrotubes.com)

8.1.1.3. Optical Components

- Fibre-optic cable (Ocean Optics)
- Spectrometer (199-299 nm) (Ocean Optics)
- Spectrometer (QE65000: 350 – 1100 nm, Ocean Optics)
- LED light source (Schott)
- Cuvette holder (Ocean Optics: https://oceanoptics.com/product/cuv-uv-cuvette-holder/)

8.1.1.4. Aerosol Generation and Collection Apparatus

- Syringe Pump AL1000-220 (World Precision Instruments: http://www.wpi-europe.com/products/pumps-and-microinjection/laboratory-syringe-pumps/al1000-220.aspx)
- Enhanced Parallel Path Nebuliser X-175 (Serial # 24830, Burgener Research International: http://burgenerresearch.com/)

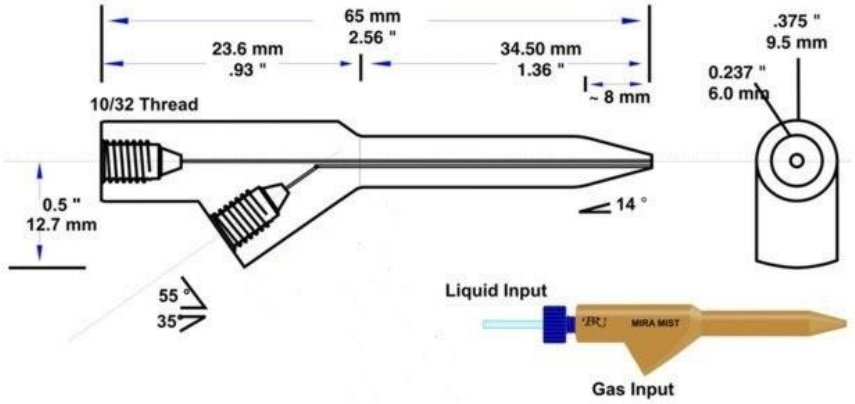

Figure 8.1 Cross-sectional view of the nebuliser employed in this study (Mira Mist X-175 Enhanced Parallel Path, http://burgenerresearch.com/NebSpecs.html

- Gas Washing Bottle Apparatus (VWR, https://ie.vwr.com/store/catalog/product.jsp?catalog_number=201-0381)
- 5 ml Luer-Lock tip Syringe (Terumo, https://www.terumotmp.com/ProductDetails.aspx?categoryId=1&productId=208)
- UpChurch fingertight fittings (One-Piece Fingertight Male Nut, 10-32 Coned, for 1/16" OD https://www.idex-hs.com/fluidic-connections/fittings/coned-fittings/one-piece-fingertight-fittings.html)
- Nebuliser liquid capillary tubing (2.0 mm OD/1.0 mm ID. BRC 115 Burgener Research http://www.burgener.co.uk/Prices.html)
- Transparent flexible tubing (4.0 mm OD/2.4 mm ID'Tygon®' http://www.plastics.saint-gobain.com/)
- Syringe filter membranes (0.22 µm pore size, Nalgene) http://www.thermoscientific.com/content/tfs/en/product/nalgene-25mm-syringe-filters.html)
- 15 ml sterile conical tube (Fisher Scientific https://www.fishersci.com/shop/products/falcon-15ml-conical-centrifuge-tubes/p-193301)
- P.V.C. Grommet kit (RS Components, Stock no.6664584, http://uk.rs-online.com/web/p/cable-grommet-kits/6664584/)
- 70 % Ethanol solution (Sigma Aldrich, UK http://www.sigmaaldrich.com/catalog/product/fluka/02877?lang=en&region=GB)

8.1.1.5. Bacteria Culture and Analytical Equipment

- Orbital Incubator (S150 – Stuart Scientific http://www.stuart-equipment.com/category.asp?dsl=119&mnu=24)
- Microcentrifuge (Eppendorf 5415r)
- 1.5 ml Eppendorf tubes (SSI Bio http://www.ssibio.com/microcentrifuge-tubes)
- Microwell plate Spectrophotometer (BMG LabTech FLUOStar Omega http://www.bmglabtech.com/en/products/microplate-readers/fluostar-omega-obj-42-743.html)
- 96-well sterile microwell plates (Nunc http://www.thermoscientific.com/en/product/nunc-96-well-polypropylene-microwell-plates.html)
- UV-spectrophotometer (Nanodrop 1000 http://www.nanodrop.com/Download.aspx?Type=Software&Cat=NanoDrop%201000)
- Bacteria DNA Extraction kit (GenElute, Sigma, http://www.sigmaaldrich.com/technical-documents/protocols/biology/genelute-bacterial-genomic-dna-kit.html)

8.1.1.5.1. Microbial Growth Media

8.1.1.5.1.1. Nutrient broth (Oxoid Limited, Basingstoke, Hampshire, UK: CM0001- Lot. 1034072, Exp. 2017/04 *http://www.oxoid.com/UK/blue/prod_detail/prod_detail.asp?pr=CM0001&c=UK&lang=EN)*

A single-strength formulation was prepared by dissolving 13 g in 1000 ml dH_2O and dispensing into 10 x 100 ml Schott bottles. The growth media must be sterilised before use by autoclaving at 121°C for 15 minutes. Nutrient broth is noted by the supplier of the bacteria as the preferred liquid growth medium to use (NCTC)

8.1.1.5.1.2. Nutrient agar (Oxoid Limited, Basingstoke, Hampshire, UK: CM0003 - Lot. 1503396, Exp. 2019/05 *http://www.oxoid.com/UK/blue/prod_detail/prod_detail.asp?pr=CM0004&c=UK&lang=EN)*

Nutrient agar is noted by the supplier of the bacteria as the preferred solid growth medium to use (NCTC). 28 g was added to 1000 ml dH2O and heated on a magnetic hot-plate to aid dissolving. The solution was sterilised by autoclaving at 121°C for 15 minutes then allowed to cool before pouring into sterile petri dishes.

8.1.1.5.1.3. Chromocult agar (Merck, Germany: 1.10426.500)

Chromocult is a coliform-specific growth medium that actively supresses growth of most other microorganisms. It contains “Tergitol®-7” (sodium heptadecyl sulphate) which suppresses the growth of gram-positive bacteria and some non-enteric gram-negative bacteria. It also contains a unique chromogenic mix that includes two specific substrates associated with characteristic coliform enzymes, aiding easy visual differentiation between *E. coli* and other members of the coliform species. β-D-galactosidase cleaves the Salmon-GAL substrate, resulting in the colonies being a salmon-red colour. β-D-glucouronidase is only found in *E. coli* strains and cleaves the second substrate, X-glucouronide, producing dark blue/violet colonies.

It is important not to boil the mixture during preparation. 26.5 g was added to 100 ml dH2O and placed on a magnetic hot-plate. Continually mix the contents with a magnetic stirrer to aide complete dissolution (approx. 35 min.). Some turbidity may exist but this doesn’t affect the agars performance. The solution was poured into sterile petri dishes and allowed to solidify.

n.b.

8.1.1.5.1.4. Ringer’s Solution (Oxoid Limited, Basingstoke, Hampshire, UK: CM0003 - Lot. 1503396, Exp. 2019/05 *http://www.oxoid.com/UK/blue/prod_detail/prod_detail.asp?pr=CM0004&c=UK&lang=EN)*

A standard ¼ strength solution was prepared by dissolving 1 tablet in 500 ml dH2O. This was subsequently dispensed into 5 x 100 ml Schott bottles and sterilised by autoclaving at 121°C for 15 minutes. Each 100 ml Ringer’s solution was filtered using 0.25 µm syringe filters (Nalgene) and aliquoted into 2 x 50 ml sterile conical tubes. 900 µl was dispensed into sterile 1.5 ml Eppendorf tubes and 9 ml was dispensed into sterile 30 ml universal tubes for decimal serial dilutions.

8.2. Chapter 5

8.2.1. Untreated bacteria growth on agar: colony size

When inoculated onto agar, cells compete with each other for the finite nutrients contained within the microbial growth media. This competition for growth is often the main factor that influences the size and shape of a colony. Different cell concentrations were inoculated onto agar and incubated and the diameter of the colonies that were produced after incubation was measured and compared (Figure 8.2).

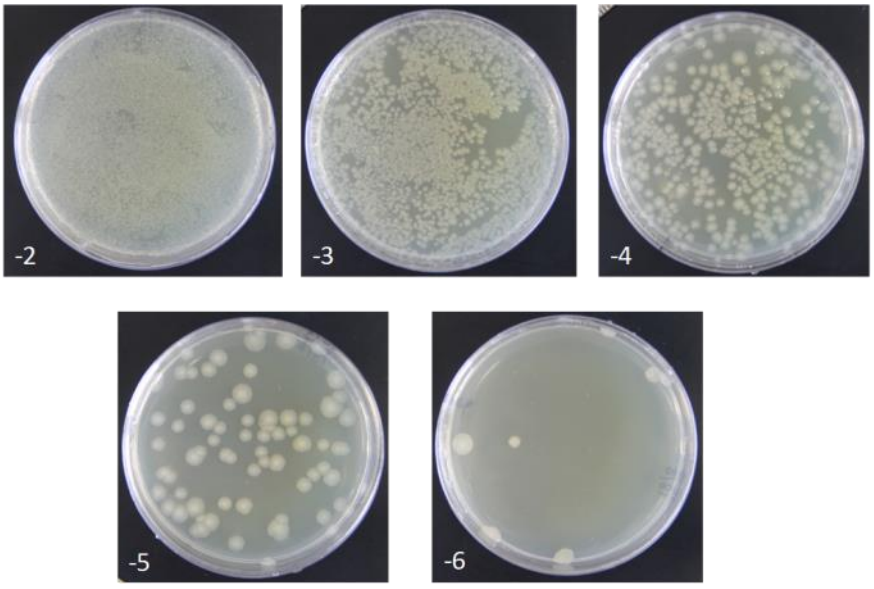

Figure 8.2 Images showing bacteria growth on agar plates after 24 h at 37 ºC with varying initial cell density of the inoculum (number inset). The colony size increases as the cell density decreases

Agar plates were inoculated with the same volume of different serial dilutions from the initial culture (10^8 cfu/ml) to observe the size of colonies. These agar plates were not exposed to plasma. As expected, the size of colonies increased when the cell density of the inoculum decreased. At low cell densities, there was less competition for the available nutrients and so larger colonies were observed for a given incubation time. This information should be considered when assessing the microbial growth after plasma treatment.

8.2.2. Droplet flow visualisation

8.2.2.1. Diameter v distance

Green food dye solution was used to generate droplets under the same gas and liquid flows used for the plasma studies. The plasma was not ignited during food dye droplet transport through the

system. Distances between the end of quartz tube and the agar surface varied from 5 mm to 110 mm; treatment time was 3 minutes. Images were taken after agar plates were placed at all distances; total time from start to finish = 45 min, starting at the closest distance (5 mm).

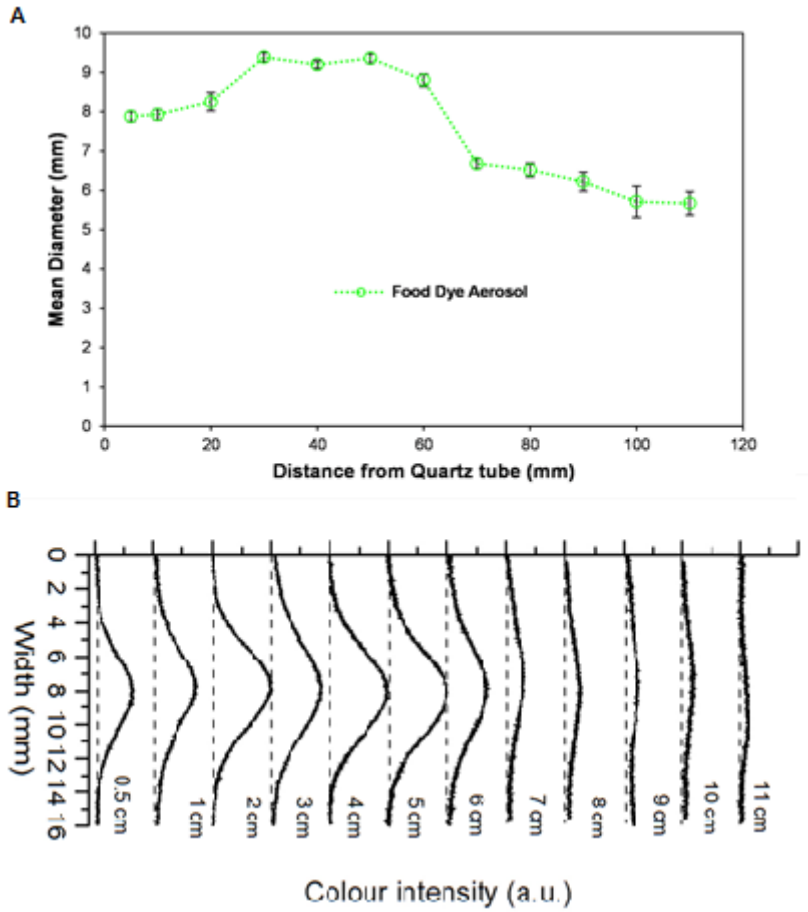

Figure 8.3 Graph (a) shows the diameter of the area of the agar which was coloured as a result of the aerosolised food dye impacting at different distances from the quartz tube end. Representation of the colour intensity of the food dye aerosol on the agar surface as a function of distance from the quartz tube end shown in (b)

The colour produced from the aerosolised dye on the agar surface was observed up to 110 mm from the end of the quartz tube, but the colour change was difficult to observe by eye from 70 mm onwards (Figure 8.3). At the closest distance (5 mm), the diameter was greater than the I.D. of the quartz tube (i.e. < 2 mm) which implies some divergence of the droplet flow upon exiting the quartz tube. Droplets were previously imaged at 1.5 and 4 mm from the end of the tube and flow profile was laminar [100], however, the distances assessed here are much greater and droplet flow dynamics at these distances in unknown. The colour intensity from the food dye aerosol was higher in the middle of the area treated where the central portion of the gas/aerosol stream was concentrated.

8.2.2.2. Diffusion v distance/time

Aerosolised food dye was used to determine how the aerosol flow diffuses into an agar surface at different distances. Conditions that were investigated were:

1= 0.5 cm, time = 20sec

2= 2 cm, time= 20sec

3= 2 cm, time= 3 min

4= 4 cm, time= 3 min

Images were taken immediately after each treatment for 3 min (approx. 80 pictures in these 3 min). Two more photos were taken at 30 and 60 min after finishing the treatment. To analyse the diameter of the coloured areas on the agar, 5 time points were used: 1, 45, 90, 135 & 180 sec. The intensity of the colour deposited onto the agar surface decreased after aerosolisation had ceased for all conditions. For the shortest distance, the diameter was similar for the first 3 min after treatment, but at 30 and 60 min the diameter increased and the colour became fainter. Higher colour intensity was observed in the middle of the coloured area but this intensity decreased with the time. This could be explained by the aerosolised dye diffusing into the agar.

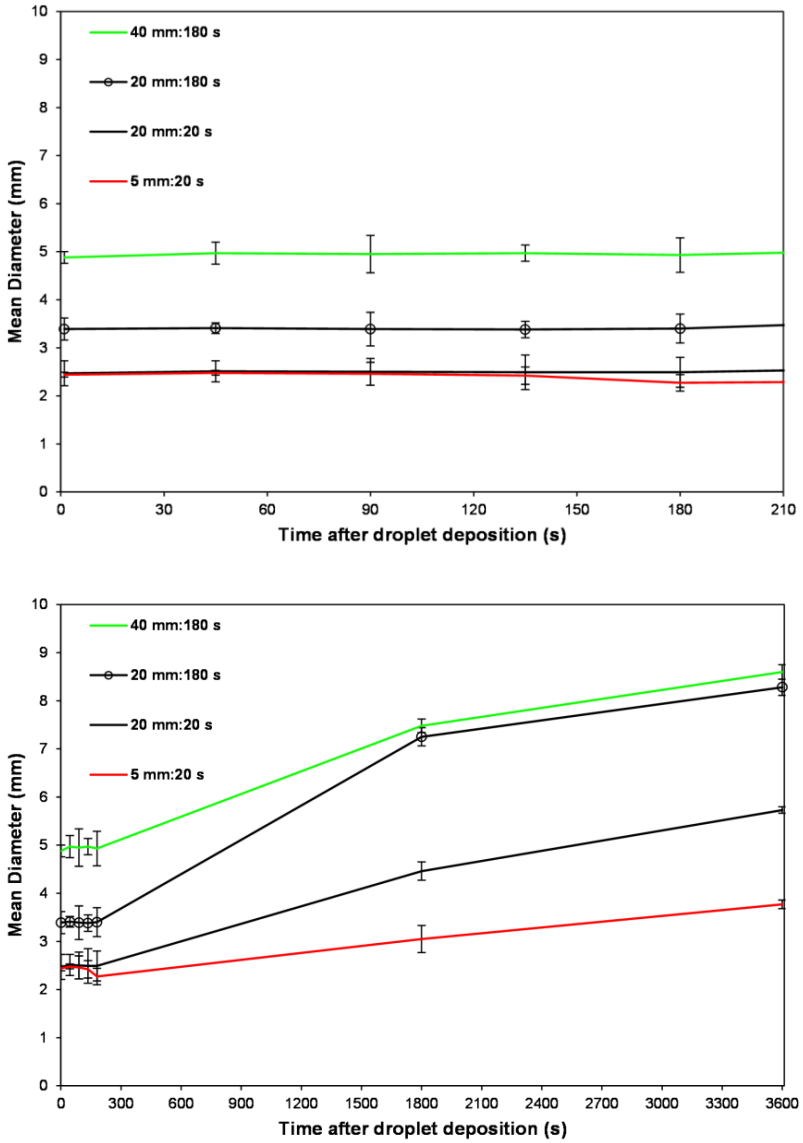

Figure 8.4 Graphs showing the measured diameter of the coloured region on the agar surface resulting from the impaction of aerosolised dye

The internal diameter of the quartz tube that entrains the gas and droplet flow is 2 mm; any measured diameter greater than 2 mm implies flow divergence, either from quartz tube end or agar surface turbulence. The closest distance between quartz tube end and agar surface (5 mm) had a diameter > 2 mm, imaged within 1 s of droplet impaction ending. This implies flow divergence when interacting with ambient air from the smallest distance (5 mm). The diameter was larger at a distance of 40 mm (green line) from the quartz tube end compared to 20 mm (black line, circle marker) for 180 s treatment (Figure 8.5).

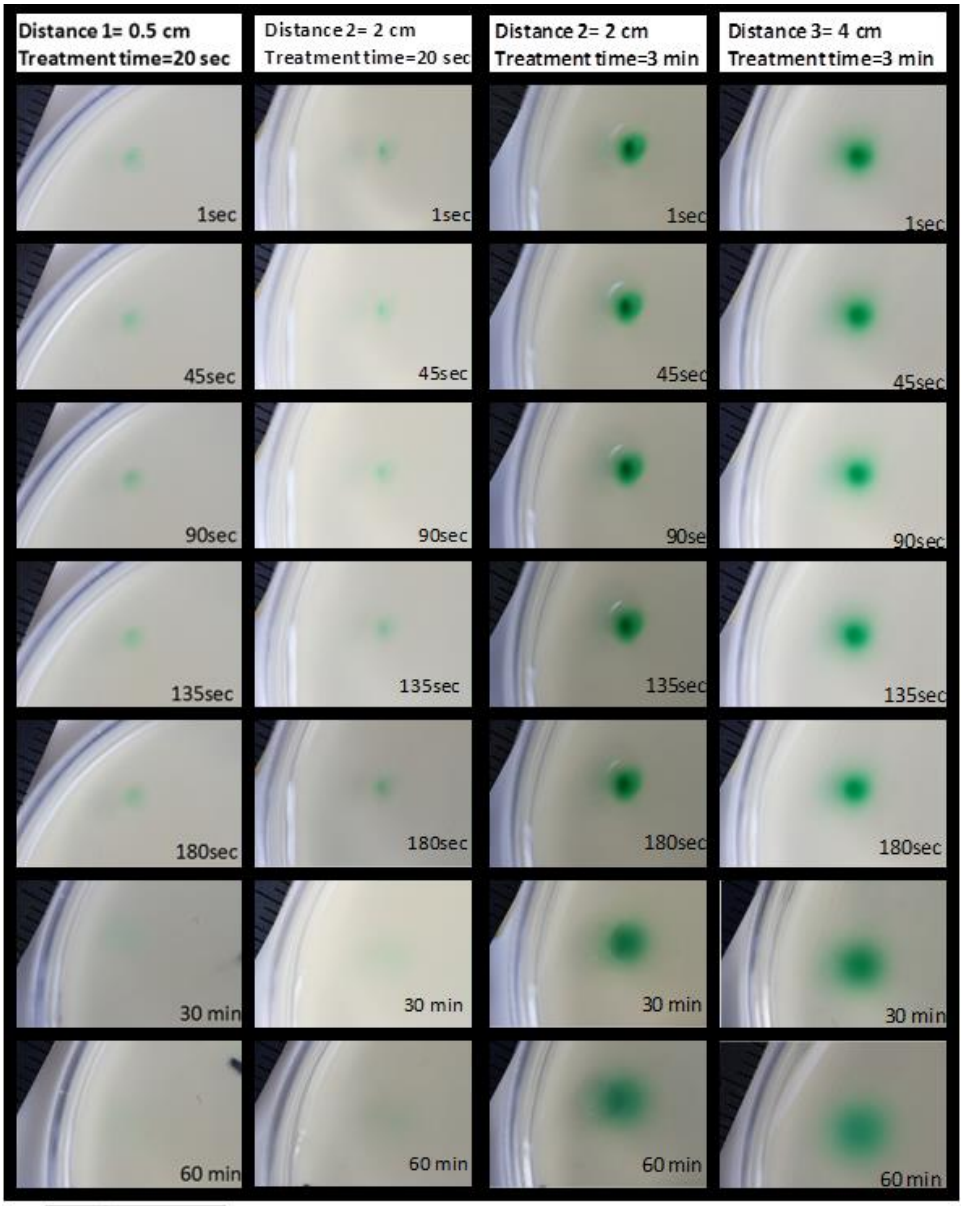

Time photos	DIAMETER (mm) d1-20sec AVERAGE	SD
1sec	2.44	0.05
45sec	2.48	0.05
90sec	2.46	0.24
135sec	2.42	0.18
180sec	2.27	0.17
30min	3.05	0.28
60min	3.77	0.09

Time photos	DIAMETER (mm) d2-20sec AVERAGE	SD
1sec	2.47	0.26
45sec	2.54	0.22
90sec	2.50	0.28
135sec	2.48	0.36
180sec	2.48	0.31
30min	4.48	0.15
60min	5.78	0.07

Time photos	DIAMETER (mm) d2-3min AVERAGE	SD
1sec	3.99	0.23
45sec	3.41	0.11
90sec	3.39	0.35
135sec	3.38	0.17
180sec	3.40	0.30
30min	7.25	0.19
60min	8.28	0.17

Time photos	DIAMETER (mm) d3-min AVERAGE	SD
1sec	4.88	0.12
45sec	4.97	0.23
90sec	4.95	0.39
135sec	4.97	0.17
180sec	4.93	0.36
30min	7.48	0.14
60min	8.60	0.15

Figure 8.5 Composite images showing the area of the agar that becomes coloured as a result of droplet interaction, measured at 0.5 cm for 10 s exposure, 2 cm for 10 s and 180 s exposure, and at 4 cm for 180 s treatment time. Inset is the measured diameter data as a function of time after droplet impaction

8.2.3. Gas Indentation

The impact of the gas flow on the agar surface was evaluated by performing analysis on agar plates that were exposed to the same gas flows as used for bacteria treatment. Conditions that were analysed: 2 cm between the agar surface and the quartz tube end, exposed for 3 min, and a distance

of 4.3 cm, exposed for 3 & 9 min. Indentation on the agar surface as a result of the gas flow could have an effect on the image contrast analysis. Agar plates without bacteria were exposed to a similar gas flow to that used during the plasma treatments. Three treatments were carried out at different distances and exposure times.

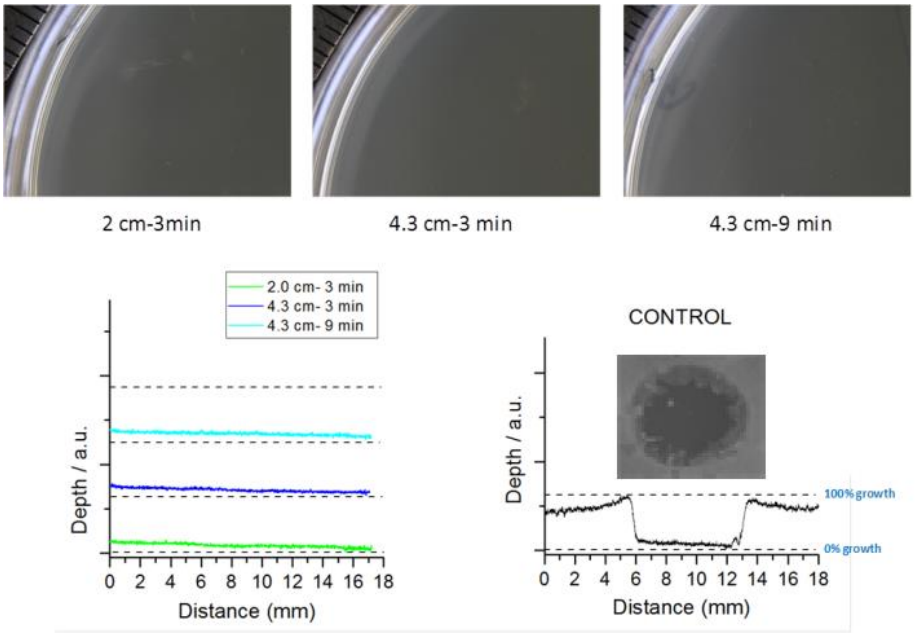

Figure 8.6 Images show areas of agar treated with gas flow (no plasma) and no bacteria present on the surface. Contrast analysis of the exposed area showed no difference when compared to an area of agar not exposed to the gas flow.

Results from the image contrast analysis show there is no difference across the area exposed to the effluent from the system (Q_{gas} = 4.5 slm, Figure 8.6). Bacteria were inoculated onto an agar surface and ethanol solution was added to induce inhibition of growth (see 'CONTROL'). A difference in contrast was observed across the treated area (see picture inset). These results validate the image analysis technique is suitable to use for assessing a treatments microbial growth inhibition efficacy, such as plasma-generated species entrained within a high velocity gas flow.

8.2.4. pH

Preliminary studies were conducted to ascertain whether there was any inhibitory growth effect caused by the gas flow. The pH of deionised water was adjusted using 1 M NaOH and HCl and was added to agar to determine the pH range that *E. coli* can grow. Each agar plate inoculated with 100 µl of *E. coli* 1e8 cfu/ml and allowed to dry (30 min air dry and 15 min incubator at 37ºC). Standard pH solutions (pH 1-pH 13) were prepared using 0.1 M HCl and 0.1M NaOH to adjust the required pH. 2 µl of each solution was added to the plate, allowed to dry (5 min) and the plate was incubated at

37ºC for 24 hours. Ethanol was used for the positive control and deionised water for the negative control. Solutions of varying pH were added to the agar surface inoculated with bacteria, to observe whether the zone of inhibition could be explained in part by pH. Growth inhibition was only observed with pH 13 (100% inhibition) and pH 1 (less than 100%).

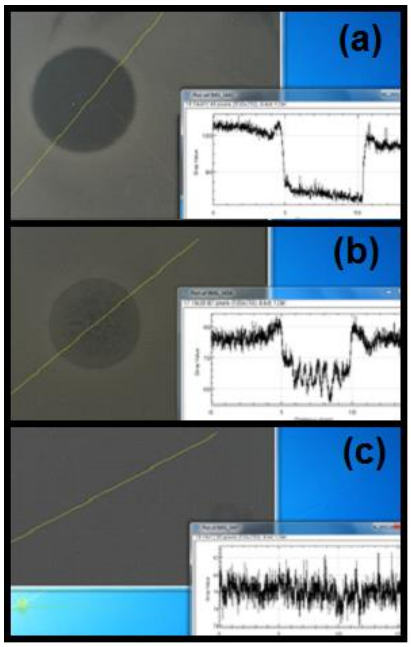

Figure 8.7 Images of the zones of inhibition and inset the contrast profiles for 3 different pH values: (a) pH 13, (b) pH 1, (c) pH 10

The results indicate that only extreme pH values (pH 1 & 13) inhibit bacteria growth on agar surface (Figure 8.7). It was difficult to experimentally verify what pH the droplets were as they exited the quartz tube using indicator strips due to droplet evaporation before colour change developed. However, it has been shown that only extremely acidic and basic bulk solutions have an inhibitory effect on bacteria growth on agar. It is unlikely that the plasma-exposed droplets would reach such extremes and as a result, any inhibitory growth effect from pH variation is negated.

9. REFERENCES

[1] Kong, M. G., Kroesen, G., Morfill, G., Nosenko, T., Shimizu, S., van Dijk, J. and Zimmermann, J. L. Plasma medicine: an introductory review. New Journal of Physics. 2009;11(11):115012.

[2] Laroussi, M. From Killing Bacteria to Destroying Cancer Cells: 20 Years of Plasma Medicine. Plasma Processes and Polymers. 2014;11(12):1138-41.

[3] Doležalová, E., Prukner, V., Lukeš, P. and Šimek, M. Stress response of *Escherichia coli* induced by surface streamer discharge in humid air. Journal of Physics D: Applied Physics. 2016;49(7):075401.

[4] Takamatsu, T., Kawano, H., Sasaki, Y., Uehara, K., Miyahara, H., Matsumura, Y., Iwasawa, A., Azuma, T. and Okino, A. Imaging of the *Staphylococcus aureus* Inactivation Process Induced by a Multigas Plasma Jet. Current microbiology. 2016;73(6):766-72.

[5] Lindsay, A., Anderson, C., Slikboer, E., Shannon, S. and Graves, D. B. Momentum, heat, and neutral mass transport in convective atmospheric pressure plasma-liquid systems and implications for aqueous targets. Journal of Physics D: Applied Physics. 2015;48(42):424007.

[6] Graves, D. B. The emerging role of reactive oxygen and nitrogen species in redox biology and some implications for plasma applications to medicine and biology. Journal of Physics D: Applied Physics. 2012;45(26):263001.

[7] Lu, X., Naidis, G. V., Laroussi, M., Reuter, S., Graves, D. B. and Ostrikov, K. Reactive species in non-equilibrium atmospheric-pressure plasmas: Generation, transport, and biological effects. Physics Reports. 2016 5/4;630:1-84.

[8] Bruggeman, P. J., Kushner, M. J., Locke, B. R., Gardeniers, J. G. E., Graham, W. G., Graves, D. B., Hofman-Caris, R. C. H. M., Maric, D., Reid, J. P., Ceriani, E., Fernandez Rivas, D., Foster, J. E., Garrick, S. C., Gorbanev, Y., Hamaguchi, S., Iza, F., Jablonowski, H., Klimova, E., Kolb, J., Krcma, F., Lukeš, P., Machala, Z., Marinov, I., Mariotti, D., Mededovic Thagard, S., Minakata, D., 22, N., E. C.,

Pawlat, J., Petrovic, Z. L. J., Pflieger, R., Reuter, S., Schram, D. C., Schröter, S., Shiraiwa, M., Tarabová, B., Tsai, P. A., Verlet, J. R. R., von Woedtke, T., Wilson, K. R., Yasui, K. and Zvereva, G. Plasma-liquid interactions: a review and roadmap. Plasma Sources Science and Technology. 2016;25(5):053002.

[9] Boehm, D., Heslin, C., Cullen, P. J. and Bourke, P. Cytotoxic and mutagenic potential of solutions exposed to cold atmospheric plasma. Scientific Reports. 2016 Feb 24;6:21464.

[10] Gallagher, M. J., Vaze, N., Gangoli, S., Vasilets, V. N., Gutsol, A. F., Milovanova, T. N., Anandan, S., Murasko, D. M. and Fridman, A. Rapid Inactivation of Airborne Bacteria Using Atmospheric Pressure Dielectric Barrier Grating Discharge. IEEE Transactions on Plasma Science. 2007;35(5):1501-10.

[11] Romero-Mangado, J., Nordlund, D., Soberon, F., Deane, G., Maughan, K., Sainio, S., Singh, G., Daniels, S., Saunders, I. T., Loftus, D., Meyyappan, M., Koehne, J. and Gandhiraman, R. P. Morphological and chemical changes of aerosolized *E. coli* treated with a dielectric barrier discharge. Biointerphases. 2016 03/01; 2017/05;11(1):011009.

[12] Shimizu, K., Yamada, M., Kanamori, M. and Blajan, M. Basic Study of Bacteria Inactivation at Low Discharge Voltage by Using Microplasmas. IEEE Transactions on Industry Applications. 2010;46(2):641-9.

[13] Vaze, N. D., Gallagher, M. J., Park, S., Fridman, G., Vasilets, V. N., Gutsol, A. F., Anandan, S., Friedman, G. and Fridman, A. A. Inactivation of Bacteria in Flight by Direct Exposure to Nonthermal Plasma. IEEE Transactions on Plasma Science. 2010;38(11):3234-40.

[14] Vaze, N. D., Park, S., Brooks, A. D., Fridman, A. and Joshi, S. G. Involvement of multiple stressors induced by non-thermal plasma-charged aerosols during inactivation of airborne bacteria. PLOS ONE. 2017 02/06;12(2):e0171434.

[15] Beveridge, T. J. and Graham, L. L. Surface layers of bacteria. Microbiological Reviews. 1991 12;55(4):684-705.

[16] Tripathi, P., Beaussart, A., Andre, G., Rolain, T., Lebeer, S., Vanderleyden, J., Hols, P. and Dufrêne, Y. F. Towards a nanoscale view of lactic acid bacteria. Micron. 2012 12;43(12):1323-30.

[17] Poortinga, A. T., Bos, R., Norde, W. and Busscher, H. J. Electric double layer interactions in bacterial adhesion to surfaces. Surface Science Reports. 2002 6;47(1):1-32.

[18] Yusupov, M., Neyts, E. C., Verlackt, C. C., Khalilov, U., van Duin, Adri C. T. and Bogaerts, A. Inactivation of the Endotoxic Biomolecule Lipid A by Oxygen Plasma Species: A Reactive Molecular Dynamics Study. Plasma Processes and Polymers. 2015 02/01;12(2):162-71.

[19] Singer, S. J. and Nicolson, G. L. The Fluid Mosaic Model of the Structure of Cell Membranes. Science. 1972 02/18;175(4023):720.

[20] Alberts, B., Johnson, A. and Lewis, J. The Lipid Bilayer. In: Molecular Biology of the Cell. 4th ed. https://www.ncbi.nlm.nih.gov/books/NBK26871/: New York: Garland Science; 2002.

[21] Reece, J. B., Urry, L. A., Cain, M. L., Wasserman, S. A., Minorsky, P. V. and Jackson, R. B. Campbell Biology. 9th ed. U.S.A.: Pearson Education, Inc; 2011.

[22] Betteridge DJ. What is oxidative stress? Metabolism. 2000 February 2000;49(2):3-8.

[23] Baez, A. and Shiloach, J. *Escherichia coli* avoids high dissolved oxygen stress by activation of SoxRS and manganese-superoxide dismutase. Microbial Cell Factories. 2013 02/21;12:23-.

[24] Fang, F. C. Antimicrobial Actions of Reactive Oxygen Species. mBio. 2011 09/06;2(5):e00141-11.

[25] Niki, E., Yoshida, Y., Saito, Y. and Noguchi, N. Lipid peroxidation: Mechanisms, inhibition, and biological effects. Biochemical and biophysical research communications. 2005 12/9;338(1):668-76.

[26] Gaunt, L. F., Beggs, C. B. and Georghiou, G. E. Bactericidal Action of the Reactive Species Produced by Gas-Discharge Nonthermal Plasma at Atmospheric Pressure: A Review. IEEE Transactions on Plasma Science. 2006;34(4):1257-69.

[27] Ayala, A., Muñoz, M. F. and Argüelles, S. Lipid Peroxidation: Production, Metabolism, and Signaling Mechanisms of Malondialdehyde and 4-Hydroxy-2-Nonenal. Oxidative Medicine and Cellular Longevity. 2014;2014:31.

[28] Griswold, A. Genome Packaging in Prokaryotes: the Circular Chromosome of *E. coli*. Nature Education. 2008;1(1):57.

[29] Sinha, R. P. and Häder, D. P. UV-induced DNA damage and repair: a review. Photochem Photobiol Sci. 2002;1(4):225-36.

[30] Vink AA, Roza L. Biological consequences of cyclobutane pyrimidine dimers. Journal of Photochemistry and Photobiology B: Biology. 2001 31 December 2001;65(2):101-4.

[31] Schenk, M., Raffellini, S., Guerrero, S., Blanco, G. A. and Alzamora, S. M. Inactivation of *Escherichia coli*, *Listeria innocua* and *Saccharomyces cerevisiae* by UV-C light: Study of cell injury by flow cytometry. LWT - Food Science and Technology. 2011 1;44(1):191-8.

[32] Marnett, L. J. Lipid peroxidation—DNA damage by malondialdehyde. Mutation Research/Fundamental and Molecular Mechanisms of Mutagenesis. 1999 3/8;424(1–2):83-95.

[33] Cadet, J., Douki, T. and Ravanat, J. Oxidatively generated base damage to cellular DNA. Free Radical Biology and Medicine. 2010 7/1;49(1):9-21.

[34] Duesterberg, C. K., Mylon, S. E. and Waite, T. D. pH Effects on Iron-Catalyzed Oxidation using Fenton's Reagent. Environmental science & technology. 2008 11/15;42(22):8522-7.

[35] Mendis, D. A., Rosenberg, M. and Azam, F. A note on the possible electrostatic disruption of bacteria. IEEE Transactions on Plasma Science. 2000;28(4):1304-6.

[36] Weaver, J. C. Electroporation of cells and tissues. Plasma Science, IEEE Transactions on. 2000;28(1):24-33.

[37] Vernier, P. T., Levine, Z. A. and Gundersen, M. A. Water Bridges in Electropermeabilized Phospholipid Bilayers. Proceedings of the IEEE. 2013;101(2):494-504.

[38] Rems, L. and Miklavčič, D. Tutorial: Electroporation of cells in complex materials and tissue. Journal of Applied Physics. 2016 05/28; 2017/05;119(20):201101.

[39] Simon, X., Duquenne, P., Koehler, V., Piernot, C., Coulais, C. and Faure, M. Aerosolisation of *Escherichia coli* and associated endotoxin using an improved bubbling bioaerosol generator. Journal of Aerosol Science. 2011 8;42(8):517-31.

[40] Burgener JA, inventor; Enhanced parallel path nebulizer with a large range of flow rates. U.S. Patent number 6,634,572 B1. U.S.A. 2003 .

[41] Juozaitis, A., Willeke, K., Grinshpun, S. A. and Donnelly, J. Appl Environ Microbiol. 1994;60(3):861-70.

[42] Grinshpun, S. A., Willeke, K., Ulevicius, V., Juozaitis, A., Terzieva, S., Donnelly, J., Stelma, G. N. and Brenner, K. P. Effect of Impaction, Bounce and Reaerosolization on the Collection Efficiency of Impingers. Aerosol Science and Technology. 1997 01/01;26(4):326-42.

[43] Braithwaite, N. S. J. Introduction to gas discharges. Plasma Sources Science and Technology. 2000;9(4):517.

[44] Fridman, A. and Kennedy, L. A. Plasma in Nature in the Laboratory and in Industry. In: Plasma Physics and Engineering. 1st ed. CRC Press; 2004. p. 3.

[45] Moreau, M., Orange, N. and Feuilloley, M. G. J. Non-thermal plasma technologies: New tools for bio-decontamination. Biotechnology Advances. 2008 0;26(6):610-7.

[46] Conrads, H. and Schmidt, M. Plasma generation and plasma sources. Plasma Sources Science and Technology. 2000;9(4):441.

[47] Bruggeman, P. J. and Brandenburg, R. Atmospheric pressure discharge filaments and microplasmas: physics, chemistry and diagnostics. Journal of Physics D: Applied Physics. 2013;46(46):464001.

[48] Hofmann, S., van Gessel, A. F. H., Verreycken, T. and Bruggeman, P. J. Power dissipation, gas temperatures and electron densities of cold atmospheric pressure helium and argon RF plasma jets. Plasma Sources Science and Technology. 2011;20(6):065010.

[49] Iza, F., Kim, G. J., Lee, S. M., Lee, J. K., Walsh, J. L., Zhang, Y. T. and Kong, M. G. Microplasmas: Sources, Particle Kinetics, and Biomedical Applications. Plasma Processes and Polymers. 2008;5(4):322-44.

[50] Mariotti, D. Nonequilibrium and effect of gas mixtures in an atmospheric microplasma. Applied Physics Letters. 2008 04/14; 2017/05;92(15):151505.

[51] Tendero, C., Tixier, C., Tristant, P., Desmaison, J. and Leprince, P. Atmospheric pressure plasmas: A review. Spectrochimica Acta Part B: Atomic Spectroscopy. 2006 1;61(1):2-30.

[52] Whalley, R. D. and Walsh, J. L. Turbulent jet flow generated downstream of a low temperature dielectric barrier atmospheric pressure plasma device. Scientific Reports. 2016 08/26;6:31756.

[53] Winter, J., Wende, K., Masur, K., Iseni, S., Dünnbier, M., Hammer, M. U., Tresp, H., Weltmann, K. and Reuter, S. Feed gas humidity: a vital parameter affecting a cold atmospheric-pressure plasma jet and plasma-treated human skin cells. Journal of Physics D: Applied Physics. 2013;46(29):295401.

[54] Hänsch, M. A. C., Mann, M., Weltmann, K. and von Woedtke, T. Analysis of antibacterial efficacy of plasma-treated sodium chloride solutions. Journal of Physics D: Applied Physics. 2015;48(45):454001.

[55] Liu DX, Bruggeman PJ, Iza F, Rong MZ, Kong MG. Global model of low-temperature atmospheric-pressure He + H_2O plasmas. - Plasma Sources Science and Technology. (- 2):- 025018.

[56] Yusupov, M., Neyts, E. C., Simon, P., Berdiyorov, G., Snoeckx, R., van Duin, A. C. T. and Bogaerts, A. Reactive molecular dynamics simulations of oxygen species in a liquid water layer of interest for plasma medicine. Journal of Physics D: Applied Physics. 2014;47(2):025205.

[57] Gorbanev, Y., O'Connell, D. and Chechik, V. Non-Thermal Plasma in Contact with Water: The Origin of Species. Chemistry – A European Journal. 2016;22(10):3496-505.

[58] Vasko, C. A., Liu, D. X., van Veldhuizen, E. M., Iza, F. and Bruggeman, P. J. Hydrogen Peroxide Production in an Atmospheric Pressure RF Glow Discharge: Comparison of Models and Experiments. Plasma Chemistry and Plasma Processing. 2014;34(5):1081-99.

[59] Benedikt, J., Schröder, D., Schneider, S., Willems, G., Pajdarová, A., Vlček, J. and Schulz-von der Gathen, V. Absolute OH and O radical densities in effluent of a He/H_2O micro-scaled atmospheric pressure plasma jet. Plasma Sources Science and Technology. 2016;25(4):045013.

[60] Bruggeman, P. J., Cunge, G. and Sadeghi, N. Absolute OH density measurements by broadband UV absorption in diffuse atmospheric-pressure He/H_2O RF glow discharges. Plasma Sources Science and Technology. 2012;21(3):035019.

[61] Xiong, Q., Yang, Z. and Bruggeman, P. J. Absolute OH density measurements in an atmospheric pressure dc glow discharge in air with water electrode by broadband UV absorption spectroscopy. Journal of Physics D: Applied Physics. 2015;48(42):424008.

[62] Laroussi, M. and Leipold, F. Evaluation of the roles of reactive species, heat, and UV radiation in the inactivation of bacterial cells by air plasmas at atmospheric pressure. International Journal of Mass Spectrometry. 2004 4/15;233(1–3):81-6.

[63] Zhang, Q., Zhuang, J., von Woedtke, T., Kolb, J. F., Zhang, J., Fang, J. and Weltmann, K. Synergistic antibacterial effects of treatments with low temperature plasma jet and pulsed electric fields. Applied Physics Letters. 2014 09/08; 2017/05;105(10):104103.

[64] Perni, S., Shama, G., Hobman, J. L., Lund, P. A., Kershaw, C. J., Hidalgo-Arroyo, G., Penn, C. W., Deng, X. T., Walsh, J. L. and Kong, M. G. Probing bactericidal mechanisms induced by cold atmospheric plasmas with *Escherichia coli* mutants. Applied Physics Letters. 2007 02/12; 2017/05;90(7):073902.

[65] Daeschlein, G. Antimicrobial and antiseptic strategies in wound management. International Wound Journal. 2013;10(s1):9-14.

[66] Wang, M., Holmes, B., Cheng, X., Zhu, W., Keidar, M. and Zhang, L. G. Cold Atmospheric Plasma for Selectively Ablating Metastatic Breast Cancer Cells. PLOS ONE. 2013 09/11;8(9):e73741.

[67] Laroussi, M., Mendis, D. A. and Rosenberg, M. Plasma interaction with microbes. New Journal of Physics. 2003;5(1):41.

[68] Alkawareek, M. Y., Algwari, Q. T., Gorman, S. P., Graham, W. G., O'Connell, D. and Gilmore, B. F. Application of atmospheric pressure nonthermal plasma for the in vitro eradication of bacterial biofilms. FEMS Immunology & Medical Microbiology. 2012 07/01;65(2):381-4.

[69] Edelblute, C. M., Malik, M. A. and Heller, L. C. Surface-dependent inactivation of model microorganisms with shielded sliding plasma discharges and applied air flow. Bioelectrochemistry. 2015 6;103:22-7.

[70] Mai-Prochnow, A., Clauson, M., Hong, J. and Murphy, A. B. Gram positive and Gram negative bacteria differ in their sensitivity to cold plasma. Scientific Reports. 2016 12/09;6:38610.

[71] Fernández, A., Shearer, N., Wilson, D. R. and Thompson, A. Effect of microbial loading on the efficiency of cold atmospheric gas plasma inactivation of *Salmonella enterica serovar* Typhimurium. International journal of food microbiology. 2012 1/16;152(3):175-80.

[72] Mai-Prochnow, A., Murphy, A. B., McLean, K. M., Kong, M. G. and Ostrikov, K. (. Atmospheric pressure plasmas: Infection control and bacterial responses. International journal of antimicrobial agents. 2014 6;43(6):508-17.

[73] Jia Li, Sakai, N., Watanabe, M., Hotta, E. and Wachi, M. Study on Plasma Agent Effect of a Direct-Current Atmospheric Pressure Oxygen-Plasma Jet on Inactivation of *E. coli* Using Bacterial Mutants. Plasma Science, IEEE Transactions on. 2013;41(4):935-41.

[74] Doležalová, E. and Lukeš, P. Membrane damage and active but nonculturable state in liquid cultures of *Escherichia coli* treated with an atmospheric pressure plasma jet. Bioelectrochemistry. 2015 6;103:7-14.

[75] Oliver, J. D. Recent findings on the viable but nonculturable state in pathogenic bacteria. FEMS microbiology reviews. 2010 07/01;34(4):415-25.

[76] Sasaki, S., Honda, R., Hokari, Y., Takashima, K., Kanzaki, M. and Kaneko, T. Characterization of plasma-induced cell membrane permeabilization: focus on OH radical distribution. Journal of Physics D: Applied Physics. 2016;49(33):334002.

[77] Bartis, E. A. J., Graves, D. B., Seog, J. and Oehrlein, G. S. Atmospheric pressure plasma treatment of lipopolysaccharide in a controlled environment. Journal of Physics D: Applied Physics. 2013;46(31):312002.

[78] Joshi, S. G., Cooper, M., Yost, A., Paff, M., Ercan, U. K., Fridman, G., Friedman, G., Fridman, A. and Brooks, A. D. Nonthermal Dielectric-Barrier Discharge Plasma-Induced Inactivation Involves Oxidative DNA Damage and Membrane Lipid Peroxidation in *Escherichia coli*. Antimicrobial Agents and Chemotherapy. 2010 12/28;55(3):1053-62.

[79] Alkawareek, M. Y., Gorman, S. P., Graham, W. G. and Gilmore, B. F. Potential cellular targets and antibacterial efficacy of atmospheric pressure non-thermal plasma. International Journal of Antimicrobial Agents. 2014 2;43(2):154-60.

[80] Xu, D., Liu, D., Wang, B., Chen, C., Chen, Z., Li, D., Yang, Y., Chen, H. and Kong, M. G. *In Situ* OH Generation from O_2^- and H_2O_2 Plays a Critical Role in Plasma-Induced Cell Death. PLoS ONE. 2015 06/05;10(6):e0128205.

[81] Lazović, S., Maletić, D., Leskovac, A., Filipović, J., Puač, N., Malović, G., Joksić, G. and Petrović, Z. L. Plasma induced DNA damage: Comparison with the effects of ionizing radiation. Applied Physics Letters. 2014 09/22; 2017/05;105(12):124101.

[82] Hirst, A. M., Simms, M. S., Mann, V. M., Maitland, N. J., O'Connell, D. and Frame, F. M. Low-temperature plasma treatment induces DNA damage leading to necrotic cell death in primary prostate epithelial cells. British journal of cancer. 2015 04/28;112(9):1536-45.

[83] O'Connell, D., Cox, L. J., Hyland, W. B., McMahon, S. J., Reuter, S., Graham, W. G., Gans, T. and Currell, F. J. Cold atmospheric pressure plasma jet interactions with plasmid DNA. Applied Physics Letters. 2011 01/24; 2017/05;98(4):043701.

[84] Kurita, H., Nakajima, T., Yasuda, H., Takashima, K., Mizuno, A., Wilson, J. I. B. and Cunningham, S. Single-molecule measurement of strand breaks on large DNA induced by atmospheric pressure plasma jet. Applied Physics Letters. 2011 11/07; 2017/05;99(19):191504.

[85] Lu, H., Patil, S., Keener, K. M., Cullen, P. J. and Bourke, P. Bacterial inactivation by high-voltage atmospheric cold plasma: influence of process parameters and effects on cell leakage and DNA. Journal of applied microbiology. 2014;116(4):784-94.

[86] Hosseinzadeh Colagar, A., Memariani, H., Sohbatzadeh, F. and Valinataj Omran, A. Nonthermal Atmospheric Argon Plasma Jet Effects on *Escherichia coli* Biomacromolecules. Applied Biochemistry and Biotechnology. 2013;171(7):1617-29.

[87] Lackmann, J., Schneider, S., Edengeiser, E., Jarzina, F., Brinckmann, S., Steinborn, E., Havenith, M., Benedikt, J. and Bandow, J. E. Photons and particles emitted from cold atmospheric-pressure plasma inactivate bacteria and biomolecules independently and synergistically. J R Soc Interface. 2013 09/25;10(89).

[88] Han, X., Cantrell, W. A., Escobar, E. E. and Ptasinska, S. Plasmid DNA damage induced by helium atmospheric pressure plasma jet. The European Physical Journal D. 2014;68(3):46.

[89] Deng, X. T., Shi, J. J. and Kong, M. G. Protein destruction by a helium atmospheric pressure glow discharge: Capability and mechanisms. Journal of Applied Physics. 2007 04/01; 2017/05;101(7):074701.

[90] Zhou, R., Zhou, R., Zhuang, J., Zong, Z., Zhang, X., Liu, D., Bazaka, K. and Ostrikov, K. Interaction of Atmospheric-Pressure Air Microplasmas with Amino Acids as Fundamental Processes in Aqueous Solution. PLOS ONE. 2016 05/16;11(5):e0155584.

[91] Lackmann, J., Baldus, S., Steinborn, E., Edengeiser, E., Kogelheide, F., Langklotz, S., Schneider, S., Leichert, L. I. O., Benedikt, J., Awakowicz, P. and Bandow, J. E. A dielectric barrier discharge terminally inactivates RNase A by oxidizing sulfur-containing amino acids and breaking structural disulfide bonds. Journal of Physics D: Applied Physics. 2015;48(49):494003.

[92] Tanaka, H., Nakamura, K., Mizuno, M., Ishikawa, K., Takeda, K., Kajiyama, H., Utsumi, F., Kikkawa, F. and Hori, M. Non-thermal atmospheric pressure plasma activates lactate in Ringer's solution for anti-tumor effects. Scientific Reports. 2016 11/08;6:36282.

[93] Judée, F., Fongia, C., Ducommun, B., Yousfi, M., Lobjois, V. and Merbahi, N. Short and long time effects of low temperature Plasma Activated Media on 3D multicellular tumor spheroids. Scientific Reports. 2016 02/22;6:21421.

[94] Attri, P., Kim, Y. H., Park, D. H., Park, J. H., Hong, Y. J., Uhm, H. S., Kim, K., Fridman, A. and Choi, E. H. Generation mechanism of hydroxyl radical species and its lifetime prediction during the plasma-initiated ultraviolet (UV) photolysis. Scientific Reports. 2015 03/20;5:9332.

[95] Locke, B. R. and Shih, K. Review of the methods to form hydrogen peroxide in electrical discharge plasma with liquid water. Plasma Sources Science and Technology. 2011;20(3):034006.

[96] Burlica, R. and Locke, B. R. Pulsed Plasma Gliding-Arc Discharges With Water Spray. IEEE Transactions on Industry Applications. 2008;44(2):482-9.

[97] Ono, R. and Oda, T. Dynamics and density estimation of hydroxyl radicals in a pulsed corona discharge. Journal of Physics D: Applied Physics. 2002;35(17):2133.

[98] Graves, D. B., Hamaguchi, S. and O'Connell, D. In Focus: Plasma Medicine. Biointerphases. 2015 06/01; 2017/05;10(2):029301.

[99] von Woedtke, T., Metelmann, H. -. and Weltmann, K. -. Clinical Plasma Medicine: State and Perspectives of in Vivo Application of Cold Atmospheric Plasma. Contributions to Plasma Physics. 2014;54(2):104-17.

[100] Maguire, P. D., Mahony, C. M. O., Kelsey, C. P., Bingham, A. J., Montgomery, E. P., Bennet, E. D., Potts, H. E., Rutherford, D. C. E., McDowell, D. A., Diver, D. A. and Mariotti, D. Controlled microdroplet transport in an atmospheric pressure microplasma. Applied Physics Letters. 2015;106(22).

[101] Zheng, Y. and Yao, M. Liquid impinger BioSampler's performance for size-resolved viable bioaerosol particles. Journal of Aerosol Science. 2017 4;106:34-42.

[102] Miles, A. A., Misra, S. S. and Irwin, J. O. The estimation of the bactericidal power of the blood. The Journal of hygiene. 1938 11;38(6):732-49.

[103] Kanazawa, S., Kawano, H., Watanabe, S., Furuki, T., Akamine, S., Ichiki, R., Ohkubo, T., Kocik, M. and Mizeraczyk, J. Observation of OH radicals produced by pulsed discharges on the surface of a liquid. Plasma Sources Science and Technology. 2011;20(3):034010.

[104] Eisenberg, G. Colorimetric Determination of Hydrogen Peroxide. Industrial & Engineering Chemistry Analytical Edition. 1943 05/18;15(5):327-8.

[105] Lukeš, P., Doležalová, E., Sisrova, I. and Clupek, M. Aqueous-phase chemistry and bactericidal effects from an air discharge plasma in contact with water: evidence for the formation of peroxynitrite through a pseudo-second-order post-discharge reaction of H_2O_2 and HNO_2. - Plasma Sources Science and Technology(- 1):- 015019.

[106] Heijnen, L. and Medema, G. Quantitative detection of *E. coli*, *E. coli* O157 and other shiga toxin producing *E. coli* in water samples using a culture method combined with real-time PCR. J Water Health. 2006 12/01;4(4):487.

[107] Bruggeman, P. J. and Leys, C. Non-thermal plasmas in and in contact with liquids. Journal of Physics D: Applied Physics. 2009;42(5):053001.

[108] Bruggeman, P. J., Verreycken, T., González, M. Á., Walsh, J. L., Kong, M. G., Leys, C. and Schram, D.,C. Optical emission spectroscopy as a diagnostic for plasmas in liquids: opportunities and pitfalls. Journal of Physics D: Applied Physics. 2010;43(12):124005.

[109] Machala, Z., Tarabová, B., Hensel, K., Doležalová, E., Šikurová, L. and Lukeš, P. Formation of ROS and RNS in Water Electro-Sprayed through Transient Spark Discharge in Air and their Bactericidal Effects. Plasma Processes and Polymers. 2013;10(7):649-59.

[110] Wandell, R. J. and Locke, B. R. Hydrogen Peroxide Generation in Low Power Pulsed Water Spray Plasma Reactors. Industrial & Engineering Chemistry Research. 2014 01/15;53(2):609-18.

[111] Askari, S., Levchenko, I., Ostrikov, K., Maguire, P. D. and Mariotti, D. Crystalline Si nanoparticles below crystallization threshold: Effects of collisional heating in non-thermal atmospheric-pressure microplasmas. Applied Physics Letters. 2014;104(16).

[112] Bruggeman, P. J. and Schram, D.,C. On OH production in water containing atmospheric pressure plasmas. Plasma Sources Science and Technology. 2010;19(4):045025.

[113] Brandenburg, R., Lange, H., von Woedtke, T., Stieber, M., Kindel, E., Ehlbeck, J. and Weltmann, K. Antimicrobial Effects of UV and VUV Radiation of Nonthermal Plasma Jets. IEEE Transactions on Plasma Science. 2009;37(6):877-83.

[114] Huang, F., Chen, L., Wang, H. and Yan, Z. Analysis of the degradation mechanism of methylene blue by atmospheric pressure dielectric barrier discharge plasma. Chemical Engineering Journal. 2010 8/1;162(1):250-6.

[115] Manoj Kumar Reddy, P., Rama Raju, B., Karuppiah, J., Linga Reddy, E. and Subrahmanyam, C. Degradation and mineralization of methylene blue by dielectric barrier discharge non-thermal plasma reactor. Chemical Engineering Journal. 2013 2/1;217:41-7.

[116] Cantão, F.,de Oliveira, Melo, W. d. C., Oliveira, L. C. A., Passos, A. R. and Silva, A. C. d. Utilization of Sn/Nb2O5 composite for the removal of methylene blue. QuÃmica Nova. 2010;33:528-31.

[117] Medien, H. A. A. and Khalil, S. M. E. Kinetics of the oxidative decolorization of some organic dyes utilizing Fenton-like reaction in water. Journal of King Saud University - Science. 2010 7;22(3):147-53.

[118] Mizuta, Y., Masumizu, T., Kohno, M., Mori, A. and Packer, L. Biochem Mol Biol Int. 1997;43(5):1107-20.

[119] Satoh, A. Y., Trosko, J. E. and Masten, S. J. Methylene Blue Dye Test for Rapid Qualitative Detection of Hydroxyl Radicals Formed in a Fenton's Reaction Aqueous Solution. Environmental science & technology. 2007 04/01;41(8):2881-7.

[120] Schneider, N. M., Norton, M. M., Mendel, B. J., Grogan, J. M., Ross, F. M. and Bau, H. H. Electron-Water interactions and implications for liquid cell electron microscopy. Journal of Physical Chemistry C. 2014;118(38):22373-82.

[121] Winter, J., Tresp, H., Hammer, M. U., Iseni, S., Kupsch, S., Schmidt-Bleker, A., Wende, K., Dünnbier, M., Masur1, K., Weltmann, K. and Reuter, S. Tracking plasma generated H_2O_2 from gas into liquid phase and revealing its dominant impact on human skin cells. - Journal of Physics D: Applied Physics(- 28):- 285401.

[122] Maguire, P. D., Rutherford, D. C. E., Macias-Montero, M., Mahony, C. M. O., Kelsey, C. P., Tweedie, M., Pérez-Martin, F., McQuaid, H., Diver, D. A. and Mariotti, D. Continuous In-Flight Synthesis for On-Demand Delivery of Ligand-Free Colloidal Gold Nanoparticles. Nano Letters. 2017 03/08;17(3):1336-43.

[123] Burlica, R., Grim, R. G., Shih, K., Balkwill, D. and Locke, B. R. Bacteria Inactivation Using Low Power Pulsed Gliding Arc Discharges with Water Spray. Plasma Processes and Polymers. 2010;7(8):640-9.

[124] Zhao, J., Zhou, J., Su, J., Guo, H., Wang, X. and Gong, W. Propene epoxidation with in-site H_2O_2 produced by H_2/O_2 non-equilibrium plasma. AIChE Journal. 2007;53(12):3204-9.

[125] Burlica, R., Shih, K. and Locke, B. R. Formation of H_2 and H_2O_2 in a Water-Spray Gliding Arc Nonthermal Plasma Reactor. Industrial & Engineering Chemistry Research. 2013 09/18;52(37):13516-.

[126] Shih, K. and Locke, B. R. Optical and Electrical Diagnostics of the Effects of Conductivity on Liquid Phase Electrical Discharge. IEEE Transactions on Plasma Science. 2011;39(3):883-92.

[127] Wende, K., Williams, P., Dalluge, J., Gaens, W. V., Aboubakr, H., Bischof, J., von Woedtke, T., Goyal, S. M., Weltmann, K. D., Bogaerts, A., Masur, K. and Bruggeman, P. J. Identification of the biologically active liquid chemistry induced by a nonthermal atmospheric pressure plasma jet. Biointerphases. 2015 Jun 6;10(2):029518.

[128] Girard, P., Arbabian, A., Fleury, M., Bauville, G., Puech, V., Dutreix, M. and Sousa, J. S. Synergistic Effect of H_2O_2 and NO_2 in Cell Death Induced by Cold Atmospheric He Plasma. Scientific Reports. 2016 07/01;6:29098.

[129] Porter, D., Poplin, M. D., Holzer, F., Finney, W. C. and Locke, B. R. Formation of Hydrogen Peroxide, Hydrogen, and Oxygen in Gliding Arc Electrical Discharge Reactors With Water Spray. IEEE Transactions on Industry Applications. 2009;45(2):623-9.

[130] Laurita, R., Barbieri, D., Gherardi, M., Colombo, V. and Lukeš, P. Chemical analysis of reactive species and antimicrobial activity of water treated by nanosecond pulsed DBD air plasma. Clinical Plasma Medicine. 2015 12;3(2):53-61.

[131] Kirkpatrick, M. J. and Locke, B. R. Hydrogen, Oxygen, and Hydrogen Peroxide Formation in Aqueous Phase Pulsed Corona Electrical Discharge. Industrial & Engineering Chemistry Research. 2005 06/01;44(12):4243-8.

[132] Hsieh, K. C., Wang, H. and Locke, B. R. Analysis of Electrical Discharge Plasma in a Gas-Liquid Flow Reactor Using Optical Emission Spectroscopy and the Formation of Hydrogen Peroxide. Plasma Processes and Polymers. 2016;13(9):908-17.

[133] Mann, M. S., Tiede, R., Gavenis, K., Daeschlein, G., Bussiahn, R., Weltmann, K., Emmert, S., Woedtke, T. v. and Ahmed, R. Introduction to DIN-specification 91315 based on the characterization of the plasma jet kINPen® MED. Clinical Plasma Medicine. 2016 12;4(2):35-45.

[134] Ding, K., Liebermanm, M. A. and Lichtenberg, A. J. Hybrid model of neutral diffusion, sheaths, and the *α* to *γ* transition in an atmospheric pressure He/H_2O bounded rf discharge. Journal of Physics D: Applied Physics. 2014;47(30):305203.

[135] Liang, C. J. and Huang, S. C. Kinetic model for sulfate/hydroxyl radical oxidation of methylene blue in a thermally-activated persulfate system at various pH and temperatures. Sustain Environ Res. 2012;22(4):199-208.

[136] Kishore K, Guha SN, Mahadevan J, Moorthy PN, Mittal JP. Redox reactions of methylene blue: A pulse radiolysis study. International Journal of Radiation Applications and Instrumentation. Part C. Radiation Physics and Chemistry. 1989 1989;34(4):721-7.

[137] Schröter, S., Foucher, M., Niemi, K., Dedrick, J. P., de Oliveira, N., Joyeux, D., Nahon, L., Wagenaars, E., Gans, T., Booth, J. and O'Connell, D. Atomic oxygen and hydroxyl density measurements in an atmospheric pressure RF-plasma with water admixtures using UV and synchrotron VUV absorption spectroscopy. In: Proc 22nd ISPC. ; 2015.

[138] Verreycken, T., Mensink, R., van der Horst, R., Sadeghi, N. and Bruggeman, P. J. Absolute OH density measurements in the effluent of a cold atmospheric-pressure Ar/H_2O RF plasma jet in air. Plasma Sources Science and Technology. 2013;22(5):055014.

[139] Srivastava, N. and Wang, C. Effects of water addition on OH radical generation and plasma properties in an atmospheric argon microwave plasma jet. Journal of Applied Physics. 2011 09/01; 2017/05;110(5):053304.

[140] Yonemori, S., Nakagawa, Y., Ono, R. and Oda, T. Measurement of OH density and air/helium mixture ratio in an atmospheric-pressure helium plasma jet. Journal of Physics D: Applied Physics. 2012;45(22):225202.

[141] Li, L., Nikiforov, A., Xiong, Q., Britun, N., Snyders, R., Lu, X. and Leys, C. OH radicals distribution in an Ar-H_2O atmospheric plasma jet. Physics of Plasmas. 2013 09/01; 2017/05;20(9):093502.

[142] Kim, Y. H., Hong, Y. J., Baik, K. Y., Kwon, G. C., Choi, J. J., Cho, G. S., Uhm, H. S., Kim, D. Y. and Choi, E. H. Measurement of Reactive Hydroxyl Radical Species Inside the Biosolutions During Non-thermal Atmospheric Pressure Plasma Jet Bombardment onto the Solution. Plasma Chemistry and Plasma Processing. 2014;34(3):457-72.

[143] Isaksen, I. S. A. and Dalsøren, S. B. Getting a Better Estimate of an Atmospheric Radical. Science. 2011 01/06;331(6013):38.

[144] Vaida, V. Perspective: Water cluster mediated atmospheric chemistry. The Journal of Chemical Physics. 2011;135(020901).

[145] Lindsey, M. E. and Tarr, M. A. Quantitation of hydroxyl radical during Fenton oxidation following a single addition of iron and peroxide. Chemosphere. 2000 8;41(3):409-17.

[146] Maezono, T., Tokumura, M., Sekine, M. and Kawase, Y. Hydroxyl radical concentration profile in photo-Fenton oxidation process: Generation and consumption of hydroxyl radicals during the discoloration of azo-dye Orange II. Chemosphere. 2011 3;82(10):1422-30.

[147] Daeschlein, G., Napp, M., von Podewils, S., Lutze, S., Emmert, S., Lange, A., Klare, I., Haase, H., Gümbel, D., von Woedtke, T. and Jünger, M. In Vitro Susceptibility of Multidrug Resistant Skin and Wound Pathogens Against Low Temperature Atmospheric Pressure Plasma Jet (APPJ) and Dielectric Barrier Discharge Plasma (DBD). Plasma Processes and Polymers. 2014;11(2):175-83.

[148] The International Commission on Non-Ionizing,Radiation Protection. GUIDELINES ON LIMITS OF EXPOSURE TO ULTRAVIOLET RADIATION OF WAVELENGTHS BETWEEN 180 nm AND 400 nm (INCOHERENT OPTICAL RADIATION). Health physics. 2004;87(2).

[149] Bekeschus, S., Schmidt, A., Weltmann, K. and von Woedtke, T. The plasma jet kINPen – A powerful tool for wound healing. Clinical Plasma Medicine. 2016 7;4(1):19-28.

[150] Ikawa, S., Kitano, K. and Hamaguchi, S. Effects of pH on Bacterial Inactivation in Aqueous Solutions due to Low-Temperature Atmospheric Pressure Plasma Application. Plasma Processes and Polymers. 2010;7(1):33-42.

[151] Laroussi, M., Tendero, C., Lu, X., Alla, S. and Hynes, W. L. Inactivation of Bacteria by the Plasma Pencil. Plasma Processes and Polymers. 2006;3(6-7):470-3.

[152] Oehmigen, K., Hähnel, M., Brandenburg, R., Wilke, C., Weltmann, K. -. and von Woedtke, T. The Role of Acidification for Antimicrobial Activity of Atmospheric Pressure Plasma in Liquids. Plasma Processes and Polymers. 2010;7(3-4):250-7.

[153] Kovalova, Z., Leroy, M., Jacobs, C., Kirkpatrick, M. J., Machala, Z., Lopes, F., Laux, C. O., DuBow, M. S. and Odic, E. Atmospheric pressure argon surface discharges propagated in long tubes: physical characterization and application to bio-decontamination. Journal of Physics D: Applied Physics. 2015;48(46):464003.

[154] Robert, E., Sarron, V., Darny, T., Riès, d., Dozias, S., Fontane, J., Joly, L. and Pouvesle, J. Rare gas flow structuration in plasma jet experiments. Plasma Sources Science and Technology. 2014;23(1):012003.

[155] Cho, M., Chung, H., Choi, W. and Yoon, J. Linear correlation between inactivation of *E. coli* and OH radical concentration in TiO_2 photocatalytic disinfection. Water research. 2004 2;38(4):1069-77.

[156] Winterbourn, C. C. Reconciling the chemistry and biology of reactive oxygen species. Nat Chem Biol. 2008 print;4(5):278-86.

[157] Nathan, C. and Cunningham-Bussel, A. Beyond oxidative stress: an immunologist's guide to reactive oxygen species. Nat Rev Immunol. 2013 print;13(5):349-61.

[158] Witting, P. K. Measuring redox-active species in cells and tissues. Focus on "A case of mistaken identity: are reactive oxygen species actually reactive sulfide species?". Am J Physiol Regul Integr Comp Physiol. 2016 04/01;310(7):R547.

[159] Kohanski, M. A., Dwyer, D. J. and Collins, J. J. How antibiotics kill bacteria: from targets to networks. Nat Rev Micro. 2010 print;8(6):423-35.

[160] Reshes, G., Vanounou, S., Fishov, I. and Feingold, M. Cell Shape Dynamics in *Escherichia coli*. Biophysical journal. 2007 07/06;94(1):251-64.

[161] Imlay, J. A. and Linn, S. Bimodal pattern of killing of DNA-repair-defective or anoxically grown *Escherichia coli* by hydrogen peroxide. Journal of Bacteriology. 1986 05;166(2):519-27.

[162] Knight, J. A., Pieper, R. K. and McClellan, L. Specificity of the thiobarbituric acid reaction: its use in studies of lipid peroxidation. Clinical chemistry. 1988 12/01;34(12):2433.

[163] Imlay, J. A. and Linn, S. DNA damage and oxygen radical toxicity. Science. 1988 06/03;240(4857):1302.

[164] Imlay, J. A., Chin, S. M. and Linn, S. Toxic DNA damage by hydrogen peroxide through the Fenton reaction in vivo and in vitro. Science. 1988 04/29;240(4852):640.

[165] Imlay, J. A. and Linn, S. Mutagenesis and stress responses induced in *Escherichia coli* by hydrogen peroxide. Journal of Bacteriology. 1987 07;169(7):2967-76.

[166] Baker, K. H., Hegarty, J. P., Redmond, B., Reed, N. A. and Herson, D. S. Effect of Oxidizing Disinfectants (Chlorine, Monochloramine, and Ozone) on *Helicobacter pylori*. Applied and Environmental Microbiology. 2001 11/29;68(2):981-4.

[167] Gamage, S., Gerrity, D., Pisarenko, A. N., Wert, E. C. and Snyder, S. A. Evaluation of Process Control Alternatives for the Inactivation of *Escherichia coli*, MS2 Bacteriophage, and *Bacillus subtilis* Spores during Wastewater Ozonation. Ozone: Science & Engineering. 2013 11/01;35(6):501-13.

[168] Sun, P., Tyree, C. and Huang, C. Inactivation of *Escherichia coli*, Bacteriophage MS2, and *Bacillus* Spores under UV/H_2O_2 and UV/Peroxydisulfate Advanced Disinfection Conditions. Environmental science & technology. 2016 04/19;50(8):4448-58.

[169] Buxton, G. V., Greenstock, C. L., Helman, W. P. and Ross, A. B. Critical Review of rate constants for reactions of hydrated electrons, hydrogen atoms and hydroxyl radicals (·OH/·O−) in Aqueous Solution. Journal of Physical and Chemical Reference Data. 1988;17(2):513-886.

[170] Giorgio, M., Trinei, M., Migliaccio, E. and Pelicci, P. G. Hydrogen peroxide: a metabolic by-product or a common mediator of ageing signals? Nature reviews. Molecular cell biology. 2007 print;8(9):722-8.

[171] Cheeseman, K. H., Beavis, A. and Esterbauer, H. Hydroxyl-radical-induced iron-catalysed degradation of 2-deoxyribose. Biochemical Journal. 1988;252(3):649-53.

[172] Onyango, A. N. and Baba, N. New hypotheses on the pathways of formation of malondialdehyde and isofurans. Free Radical Biology and Medicine. 2010 11/30;49(10):1594-600.

[173] Hong, R., Kang, T. Y., Michels, C. A. and Gadura, N. Membrane Lipid Peroxidation in Copper Alloy-Mediated Contact Killing of *Escherichia coli*. Applied and Environmental Microbiology. 2012 01/02;78(6):1776-84.